THREE-DIMENSIONAL ECHOCARDIOGRAPHY
IN THE PREOPERATIVE ASSESSMENT
OF CONGENITAL HEART DISEASE

Cover illustration:
Background: Teatro anatomico (Anatomical theatre), situated in Palazzo del Bo' in Padova (Italy). It is the first of this type constructed in Europe (XVII century). *Above: (left)* "*en face*" three-dimensional reconstruction of an atrial septum defect type 2; *(center)* three-dimensional volumetric data set, from which any two-dimensional computer-generated cross-section can be derived; *(right)* anatomical specimen of an atrial septum defect type 2.

THREE-DIMENSIONAL ECHOCARDIOGRAPHY IN THE PREOPERATIVE ASSESSMENT OF CONGENITAL HEART DISEASE

Drie-dimensionale echocardiografie in het preoperatieve onderzoek van aangeboren hartafwijkingen

Proefschrift

ter verkrijging van de graad van doctor aan de Erasmus Universiteit van Rotterdam op gezag van de Rector Magnificus

Prof. dr. ir. J.H. van Bemmel

en volgens besluit van het College voor Promoties

De openbare verdediging zal plaatsvinden op woensdag 29 november 2000 om 9:45 uur

door

Anita Dall' Agata

geboren te Basel, Zwitserland

Promotiecommissie

Promotores: **Prof. dr. A.J.J.C. Bogers**
                                              Prof. dr. J.R.T.C. Roelandt

Overige leden: **Prof. dr. ir. N. Bom**
                                              Dr. W.A. Helbing
                                              Prof. dr. P.M.T. Pattynama

To my mother

CONTENTS

CHAPTER 1

INTRODUCTION

Echocardiography is an important non-invasive diagnostic tool in the clinical management of congenital heart disease. It allows an early and rapid diagnosis of most congenital heart anomalies and it is widely used for clinical follow-up.[1-2] In many patients the anatomical and functional assessment of congenital pathology is sufficient for the planning of surgical repair and other imaging techniques or cardiac catheterization can be avoided.[3] However, an accurate assessment of the pathology is necessary before cardiac surgery is considered, in order to reduce the time for exploration, to be able to decide on the most appropriate surgical repair and to minimise myocardial damage. Furthermore the ongoing evolution and improvement of surgical techniques demands for more detailed and accurate diagnostic techniques.

Nowadays, echocardiography of patients with congenital heart disease requires investigators with high skills and experience. Images, especially in grown-up patients, often have to be acquired in modified echocardiographic views. Furthermore, the anatomy and spatial relations of pathologic structures can be highly complex especially after primary surgical repair and a correct diagnosis is frequently made from a mental integration of sequentially obtained two-dimensional images in order to build up a three-dimensional (3D) objective image.

In the past years there has been a considerable engineering effort to produce a 3D reconstruction from cardiac ultrasound images.[4-8] While more refined, faster and user friendly software became available the technique has increasingly been used for testing.[9-11]

So far, it has been demonstrated that 3D echocardiography is an accurate method for quantification of ventricular volumes and systolic function as well as for assessment of mitral and aortic valvular disease.[12-14]

Some studies have shown its usefulness in assessment of congenital heart disease, particularly in atrial septal defects.[15-17] However, systematic application in this field is not completed yet.

The purpose of this study was to investigate the feasibility, accuracy and diagnostic potential of 3D echocardiography in the common congenital cardiac anomalies in a preoperative setting.

The accuracy of the diagnosis was evaluated by comparing the pathology with the intraoperative findings. Its additional value over current echocardiographic methods was also studied.

OUTLINE OF THE THESIS

The segmental approach, commonly used for the anatomical classification, was applied both in the introductory overview of the applicability of 3D echocardiography in various congenital heart disease (**Chapter 2**) and in the arrangement of the further chapters.[18]

Since 3D echocardiography allows *"en face"* views of cardiac structures and more particularly the septa, in **Chapter 3** the feasibility and accuracy of this technique in the assessment of the anatomy of the secundum atrial septal defect is described. A comparison is made with 2D echocardiography and intra-operatory findings. Special attention has been paid in quantifying the size of the defect, in order to identify its potential role in catheter-based device closure of the secundum atrial septal defect. The search of the optimal acquisition

method for adequate morphological and accurate quantitative assessment of atrial septal defect is presented in **Chapter 4.**

On the other hand the feasibility and accuracy of 3D echocardiography in the identification and classification of ventricular septal defects is described in **Chapter 5.** The ventricular septal defects are studied as either an isolated defect or as part of a more complex congenital anomaly.

The right ventricular function is an important factor in the clinical evaluation and follow-up of a patient with congenital heart disease. Accurate quantification is still difficult with the actual techniques, due to its peculiar anatomical morphology, and absence of a "gold-standard". Since 3D echocardiography allows quantification of left ventricular volumes without need for geometrical assumptions, we analysed the feasibility and accuracy of this technique by using three different methods for measuring the right ventricular volume and ejection fraction. We compare the results with magnetic resonance imaging as the reference method (**Chapter 6**).

Another group of lesions encountered during preoperative screening is the obstruction of the ventricular outflow tract, either left or right, isolated or associated with other malformations. These may be located at sub-valvular, valvular and supra-valvular level and may have different shape and extension. In **Chapter 7** the feasibility and accuracy of 3D echocardiography in the assessment of obstructive lesions of both the left and the right ventricular outflow tracts are described. The clinical potential of the information is discussed. Among the more complex congenital pathologies, which are associated with some of the lesions described in previous chapters, we analysed a serie of patients with tetralogy of Fallot (**Chapter 8**). The morphological characteristics of surgical interest, such as the ventricular septal defect, the overriding of the aortic valve, the obstruction of the right ventricular

outflow tract and the anomaly of the coronary arteries are analysed with 3D echocardiography.

Finally in **Chapter 9** we evaluate the feasibility, reproducibility and accuracy of 3D echocardiography for calculating the aortic valve area in patients with aortic stenosis. Potential errors resulting from planimetry in suboptimally selected cross-sectional images are analysed.

REFERENCES

1. Davidson WR Jr, Cyran SE. Echocardiography in the adult with congenital heart disease. Echocardiography 1993;10:513-5

2. Rice MJ, Sahn DJ. Transesophageal echocardiography for congenital heart disease—who, what and when. Mayo Clin Proc. 1995;70:401-2

3. Sreeram N, Sutherland GR, Geuskens R. The role of transesophageal echocardiography in adolescents and adults with congenital heart defects. Eur Heart J 1991; 12:231-40

4. Feltes TF. Advances in transesophageal echocardiography: impact of a changing technology on children with congenital heart disease. J Am Coll Cardiol. 1991 18;1515-6

5. Belohlavek M, Foley DA, Gerber TC, Kinter TM, Greenleaf JF, Seward JB. Three- and four-dimensional cardiovascular ultrasound imaging: a new era for echocardiography. Mayo Clin Proc 1993;68:221-40

6. Levine RA, Weyman AE, Handschumacher MD. Three-dimensional echocardiography: techniques and applications. Am J Cardiol 1992;69:121H-131H

7. Pandian NG, Roelandt J Nanda NC, Sugeng L, Cao QL, Azevedo J, Scwartz SL, Vannan MA, Ludomirski A, Marx G, Vogel M. Dynamic three-dimensional echocardiography. Methods and clinical potential. Echocardiography 1994;11:237-59

8. Roelandt J, Salustri A, Vletter W, Nosir Y, Bruining N. Precordial multiplane echocardiography for dynamic anyplane, paraplane and three-dimensional imaging of the heart. Thoraxcentre J 1994;6/5:4-13

9. Wang XF, Li ZA, Cheng TO, et al. Clinical application of three-dimensional transesophageal echocardiography. Am Heart J 1994;128:380-8

10. Roelandt JRTC, ten Cate FJ, Vletter WB, Taams MA. Ultrasonic dynamic three-dimensional visualization of the heart with a multiplane transesophageal imaging transducer. J Am Soc Echocardiogr 1994; 7:217-29

11. Schwartz SL, Cao Q, Azevedo J, Pandian NG. Simulation of intraoperative visualisation of cardiac structures and study of dynamic surgical anatomy with real time three-dimensional echocardiography. Am J Cardiol 1994;73:501-7

12. Abraham TP, Warner JG, Kon ND. Feasibility, accuracy and incremental value of intraoperative three-dimensional transesophageal echocardiography in valve surgery. Am J Cardiology 1997;80:1577-82

13. Gopal AS, Shen Z, Sapin PM, Keller AM, Schnellbaecher MJ, Leibowitz DW, Akinboboye OO, Rodney RA, Blood DK, King DL. Assessment of cardiac function by three-dimensional echocardiography compared with conventional noninvasive methods. Circulation 1995;92:842-53

14. YFM Nosir. Three-dimensional echocardiography an accurate technique for cardiac quantification. PhD Thesis, Erasmus University Rotterdam , ISBN 90-73235-76-6, 1999

15. Vogel M, Losch S. Dynamic three-dimensional echocardiography with a computed tomography imaging probe: initial clinical experience with transthoracic application in infants and children with congenital heart defects. Br Heart J 1994; 71: 462-7

16. Salustri A, Spitaels S, McGhie J, Vletter W, Roelandt JRTC. Transthoracic three-dimensional echocardiography in adult patients with congenital heart disease. J Am Coll Cardiol 1995; 26:759-67

17. Hagler DJ. Echocardiographic segmental approach to complex congenital heart disease in the neonate. Echocardiography 1991;8:467-75

18. Van Praagh R, Durnin RE, Jockin H, Wagner HR, Korns M, Garabedian H, Ando M, Calder AL. Anatomically corrected malposition of the great arteries (S,D,L). Circulation 1975;51:20-31

CHAPTER 2

CONGENITAL HEART DISEASE

A. Dall'Agata, JRTC Roelandt, AJJC Bogers

CONGENITAL HEART DISEASE

A. DALL'AGATA, J.R.T.C ROELANDT, A.J.J.C. BOGERS

T he incidence of congenital heart defects is approximately 0.8%. Diagnosis is usually made immediately after birth or early in infancy and occasionally later in adulthood. Congenital cardiovascular anomalies may present as a simple and isolated malformation or have quite a complex anatomy. Cross-sectional imaging in combination with Doppler and colour-flow imaging allows the assessment of most congenital defects and planning of surgical repair.[1] Transoesophageal echocardiography is particularly useful for perioperative assessment.[2]

Three-dimensional echocardiography is a novel imaging technique, which provides a realistic depiction of the underlying pathology.[3] Several studies have demonstrated that the potential of 3D echocardiography is feasible for the assessment of congenital defects in both paediatric and adult populations.[4-6] Acquisition of the images is achieved using either a transthoracic or a transoesophageal rotational approach.[5,6]

Atrial septal defects

The most common types of atrial septal defects (ASD) are ASD type II (7% of all congenital defects) and type I. Sinus venosus defects and coronary sinus defects are less common.

Acquisition for 3D reconstruction can be performed from the subcostal or a foreshortened apical window using a transthoracic approach and from a mid-oesophageal window using transoesophageal echocardiography.

During 3D reconstruction, the ASD type II can be visualised *en face* from a right or left atrial viewpoint, as it can be seen from a surgical right or left atriotomy.[7-10] These views allow display of the location, shape and morphological characteristics of the defect in one single image.[10] The ASD type II may be located centrally or extend more dorsally and higher in the atrial septum (figure 1). It may be oval, circular or irregular and its margins may be smooth or indented. The defect usually appears as a simple hole, due to the absent fusion of the primitive septa. Sometimes remnants of a valvular foramen ovale may still be present and appear as a fenestration or a flail aneurysmatic membrane (figure 2). A striking finding of 3D echocardiography is the different morphology of the left and right side of the atrial septal surface.[10] The surface of the atrial septum on its left side is rather smooth. On its right side, it is folded and does not lie in one plane. It is a complex structure, in which the ASD type II is located. In the right atrium, the defect has a close
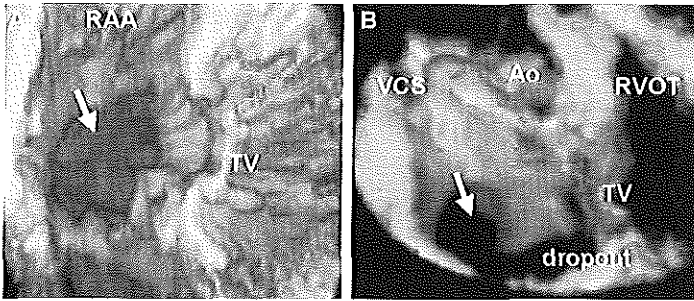
Figure 1

En face reconstruction from the right atrium of ASD2 (arrow) of different location. A = large central ASD2 (view); B = dorsal ASD2, a rim is present between the defect and the vena cava superior. RAA = right atrial appendage, TV = tricuspid valve, VCS = vena cava superior, Ao = aorta, RVOT = right ventricular outflow tract.
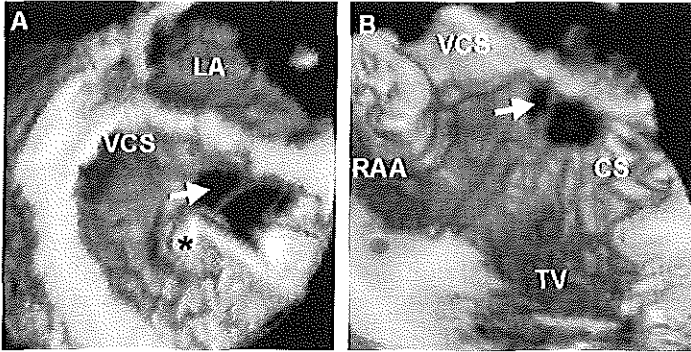
Figure 2

A = ASD2 (arrow) partially obliterated by an aneurysmatic membrane (*); B(fenestrated ASD2 (arrow). VCS = vena cava superior, RAA = right atrial appendage, TV = tricuspid valve, CS = coronary sinus.
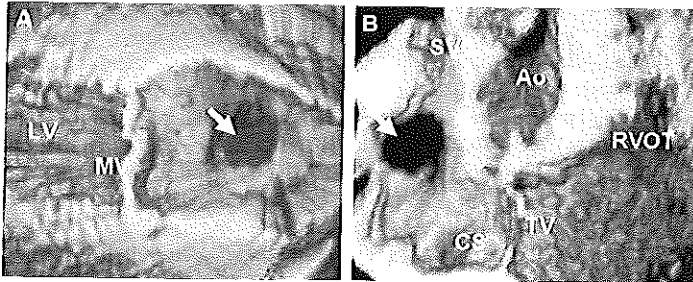
Figure 3

ASD2 (arrow) as seen from the left (A) and from the right (B) atrium. The atrial septum is smooth on its left side and folded and more complex on the right. The relationship with the other atrial structures is well displayed. LV = left ventricle, MV = mitral valve, Ao = aorta, RVOT = right ventricular outflow tract, TV = tricuspid valve, VCS = vena cava superior.

Figure 4

The size and the shape of the ASD2 (arrow) varies during the cardiac cycle. A = it reaches its maximal size during end-systole; B = its smallest size during mid/end-diastole. RV = right ventricle, TV = tricuspid valve.

Figure 5

3D imaging in a 7-year-old boy of a device (Cardiaseal) (arrow) implanted for ASD2 transcatheter closure, as seen from the right atrium (A) 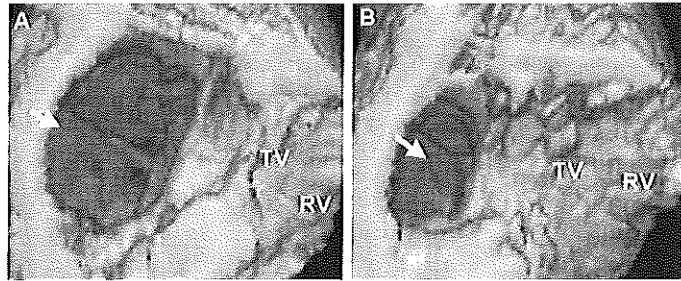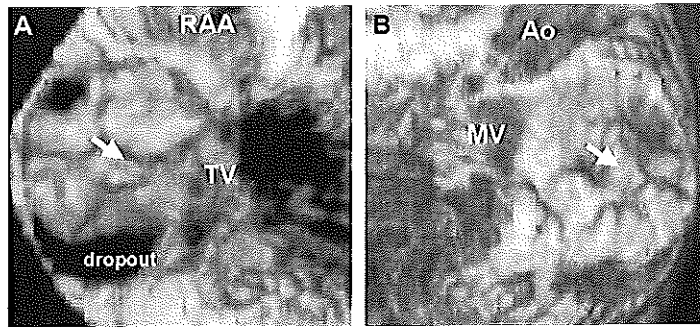and from the left atrium (B). The four arms constituting the device and the apposition on the interatrial septum are clearly visualised. RAA = right atrial appendage, TV = tricuspid valve, Ao = aortic valve, MV = mitral valve.

relationship with other anatomical structures, as the tricuspid valve, venae cavae, coronary sinus and aortic wall (figure 3). Another important finding disclosed by 3D echocardiography is that the ASD type II is a dynamic structure, which changes in size during the cardiac cycle (figure 4); 30 to 70% reduction of its size in mid- to end-systole has been reported.[9-11]

Three-dimensional echocardiography allows assessment of the shape and measurement of the major diameters of the defect in *en face* views, the amount of rim around it and the distances to the other structures of the right atrium. Quantification of the defects with 3D echocardiography has been validated on cardiac specimens and by measurements during open-heart surgery.[10-13] The measurements also compare well with those of other diagnostic and imaging techniques such as MRI.[12-14]

The measurement accuracy from 3D echocardiography provides useful information for planning and decision-making during implantation of catheter-based closure devices (figure 5). For successful placement, a rim of ≥ 5mm around the defect should be present.[14]
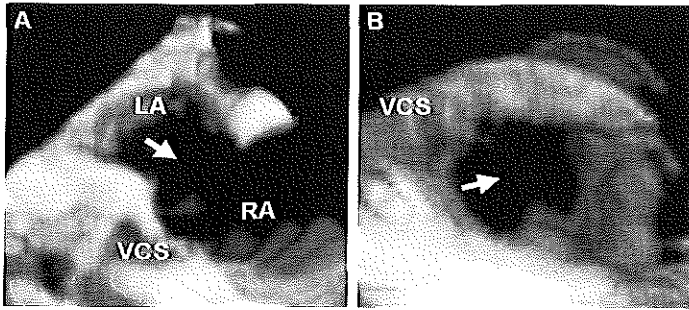
Figure 6

Sinus venosus defect (arrow). A = volume-rendered image showing a transverse cross-section of the defect, located high in the interatrial septum and closely related to the vena cava superior; B = *en face* view of the defect from the right atrium. RA = right atrium, LA = left atrium, VCS = vena cava superior.
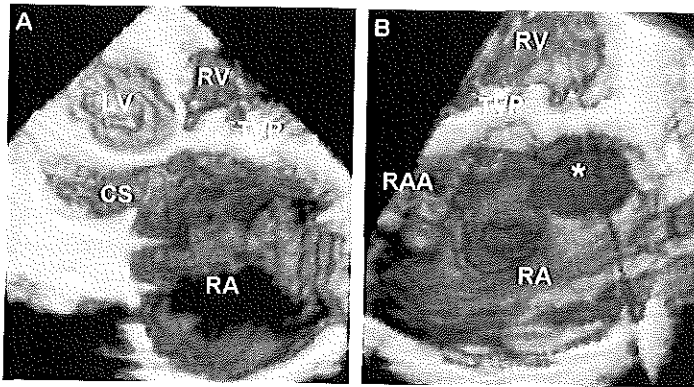
Figure 7

Volume-rendered imaging of a dilated coronary sinus (*) in a patient with enlarged right atrium secondary to tricuspid valve prosthesis insufficiency. A = representation of the right atrium in a modified transverse cross-section: the large coronary sinus is displayed along its long axis; B = view facing the coronary sinus (*). LV = left ventricle, RV = right ventricle, CS = coronary sinus, TVP = tricuspid valve prosthesis, RA = right atrium, RAA = right atrial appendage.

Few data are available on the feasibility and utility of 3D echocardiography for assessment of the other types of atrial septal defect. Visualisation of sinus venosus defect and the anomalous pulmonary vein connection associated with this pathology is difficult by transthoracic acquisition, due to its dorsal and high location (figure 6). Examples of 3D reconstruction of inferior vena cava ASD type or coronary sinus type have not been reported. However, 3D imaging of the mouth of the coronary sinus in the right atrium, either by transthoracic and transoesophageal echocardiography, is feasible (figure 7).
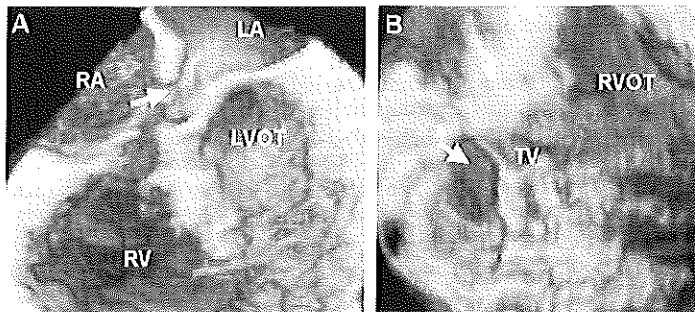
Figure 8

Partial atrioventricular septal defect (arrow). A = seen from a volume-rendered reconstructed 4-chamber view; B = looking to the septum from the right side: the defect lies just above the tricuspid valve leaflets. RA = right atrium, LA = left atrium, RV = right ventricle, LVOT = left ventricular outflow tract, TV = tricuspid valve, RVOT = right ventricular outflow tract.
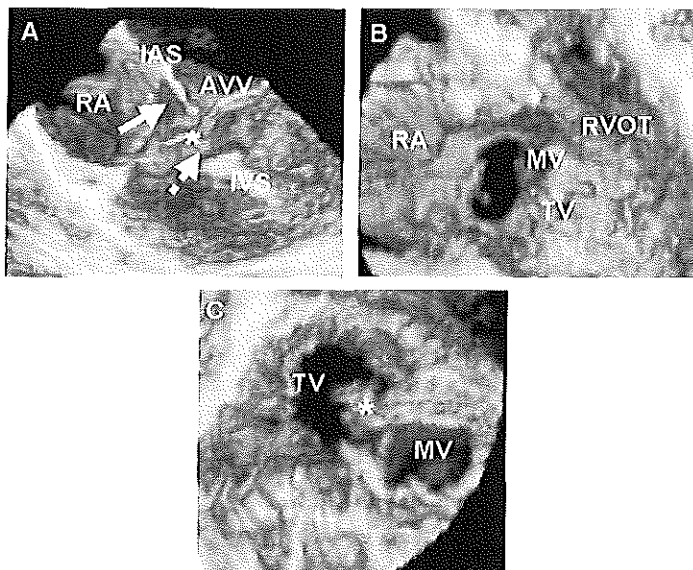
Figure 9

Complete atrioventricular septal defect. A = volume-rendered reconstructed 4 chamber view: the atrial (arrow) and the ventricular (dotted arrow) component of the defect and their different orientation in space are clearly visualised; B = view of the defect as seen from the right side: the atrial component is larger than the ventricular component; C = view from below the atrioventricular valves: the anterior leaflet (*) is bridging the interventricular septum. RA = right atrium, IAS = interatrial septum, AVV = atrioventricular valve, IVS = interventricular septum, RVOT = right ventricular outflow tract, TV = tricuspid valve, MV = mitral valve.

Atrioventricular septal defects

Atrioventricular septal defects comprise a range of malformations that may involve the atrial septum, atrioventricular valves and ventricular septum. These defects comprise ostium primum atrial septal defect or partial atrioventricular septal defect and complete atrioventricular defect. Three-dimensional echocardiography makes it possible to demonstrate the defect from the right and left side of the septal surface, providing information on the shape, size and extension of the lesion.[15]

Partial atrioventricular defect (ostium primum defect) is located immediately adjacent to the atrioventricular valves (figure 8). A cleft is usually present in the left atrioventricular valve.

Complete atrioventricular septal defect includes, in addition to the partial defect, a ventricular septal defect in the inlet part of the ventricular septum (figure 9).

Frequently the common atrioventricular valves present with a wide variation in chordae and papillary attachment. The anterior and posterior bridging leaflets often leave a cleft in the left and right atrioventricular valves. Evidence of a cleft may be difficult to find by 2D echocardiography. Three-dimensional reconstruction of the atrioventricular valves from an atrial or a ventricular perspective shows that the left atrioventricular valve is made up of three leaflets: the normally anterior leaflet is divided into an anterior or posterior portion by a cleft (figure 10).[15]
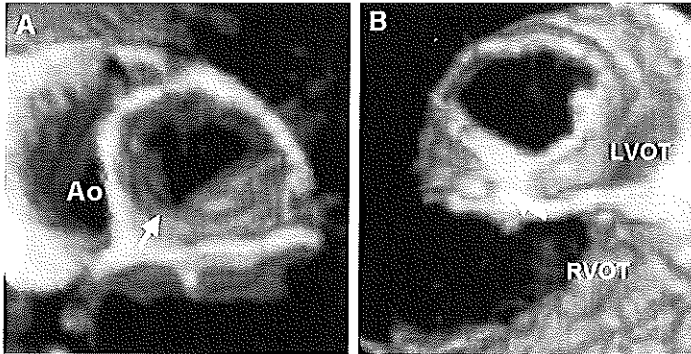
Figure 10

Left-sided atrioventricular valve of a patient with partial atrioventricular septal defect during diastole as seen from the left atrium (A) and from the left ventricle (B): the septal leaflet is divided in a superior and in an inferior component by a cleft (arrow). Ao = aorta, LVOT = left ventricular outflow tract, RVOT = right ventricular outflow tract.

Atrioventricular valve anomalies

Anomalies of the atrioventricular valves are frequently encountered in patients with congenital heart disease. They may be isolated or associated to other pathology.

Three-dimensional echocardiography allows a complete evaluation of the valves.[16,17]
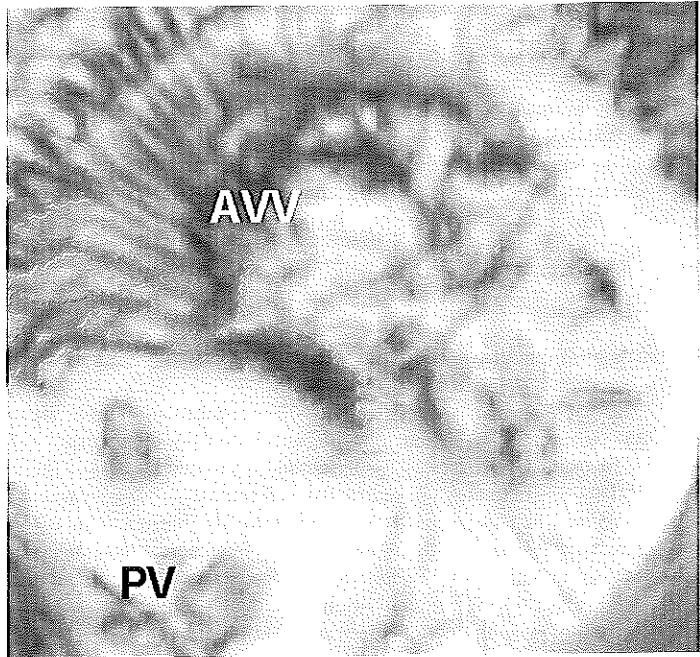
Figure 11

Complex morphology of a common atrioventricular valve in a child with monoatrium, hypoplastic right ventricle, transposition of the great arteries: looking to the valve from the atrium it is possible to identify four leaflets. PV = pulmonary valve.
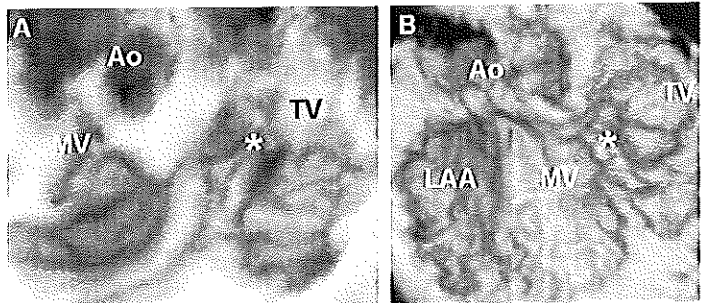
Figure 12

Cleft (*) of the septal leaflet of the tricuspid valve. A = in a patient with corrected transposition of the great arteries (L-loop). The septal leaflet of the tricuspid valve is rotated more anteriorly and medially. B = in a patient with mitral stenosis already operated for ASDI closure. Ao = aorta, MV = mitral valve, TV = tricuspid valve, LAA = left atrial appendage.

The atrioventricular valve may be a common atrioventricular valve, which drains both atrial chambers to two separate ventricles, as in complete atrioventricular defect, or to one single ventricle, as in univentricular connection (figure 11). The leaflets may be dysplastic, prolapsing or stenotic. There may be a double orifice or a cleft, isolated or associated to an atrioventricular septal defect (figures 10 and 12).

Dynamic volume-rendering imaging derived from a ventricular cutplane with a view of the valves gives detailed information on the structure of the mitral valve apparatus. Abnormal number, length and attachment of chordae or papillary muscle may be present. The tensor apparatus may arise from both sides of the interventricular septum (straddling) (figure 9). The atrioventricular valvular annulus may be committed to both ventricles, while the subvalvular apparatus maintains its normal conformation (overriding).

Ebstein's anomaly of the tricuspid valve

This pathology is characterised by a downward displacement of the tricuspid valve into the right ventricle, due to anomalous attachments of the tricuspid leaflets.

Tricuspid valve tissue is dysplastic and a variable portion of the septal and inferior leaflets adhere to the right ventricular wall some distance away from the atrioventricular junction. The anterior leaflet, although normally attached to the tricuspid annulus, may have a sail-like shape with various degrees of interchordal space obliteration and adherence to the ventricular wall. The abnormally situated tricuspid orifice produces a portion of the right ventricle lying between the atrioventricular ring and the origin of the valve, which is continuous with the right atrial chamber (figure 13).[8]
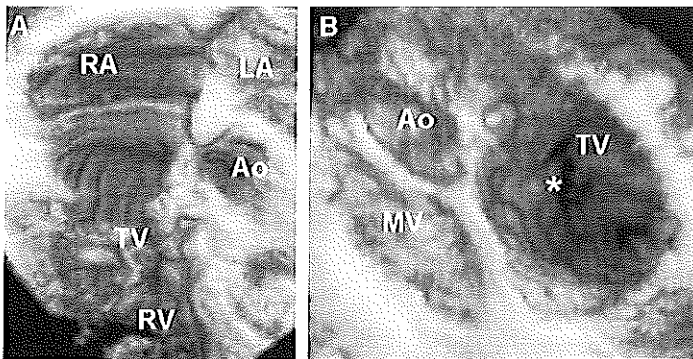
Figure 13

Ebstein's tricuspid valve. A = volume-rendered imaging of the right chambers: the large right atrium is divided into a section that derives from the original right atrium and in a so-called ventricularised part. The volume rendering displays a septation between the two parts that might represent the atrioventricular groove. The atrioventricular valve is displayed lower in the ventricle and it is possible to appreciate the large surface of the free wall leaflet and its chordal attachments to the parietal wall. B = view of the valve from the right atrium during diastole: the leaflets are not coaptating and a regurgitant orifice is visualised (*). RA = right atrium, LA = left atrium, TV = tricuspid valve, RV = right ventricle, Ao = aorta, MV = mitral valve.

Ventricular septal defect

The interventricular septum is a complex curvilinear structure of varied thickness and spatial orientation categorised in different components. Three-dimensional reconstruction of the ventricular septal defect (VSD) has shown to be feasible and accurate in vitro and in vivo studies.[19-23] A view from the right ventricle defines the location of the defect with respect to the inlet or outlet portion of the ventricle (figure 14). The defect may be covered completely by the tricuspid valve (inlet) and be visible only during closure of the valve or
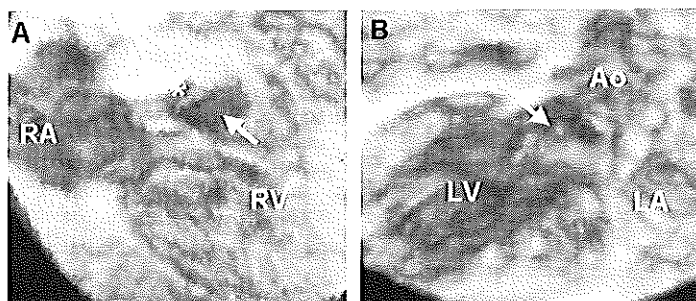
Figure 14

Perimembranous ventricular septal defect (arrow). A = seen from the right side: the aortic valve (*) lies behind it. B = seen from the left side. RA = right atrium, RV = right ventricle, Ao = aorta, LA = left atrium, LV = left ventricle.
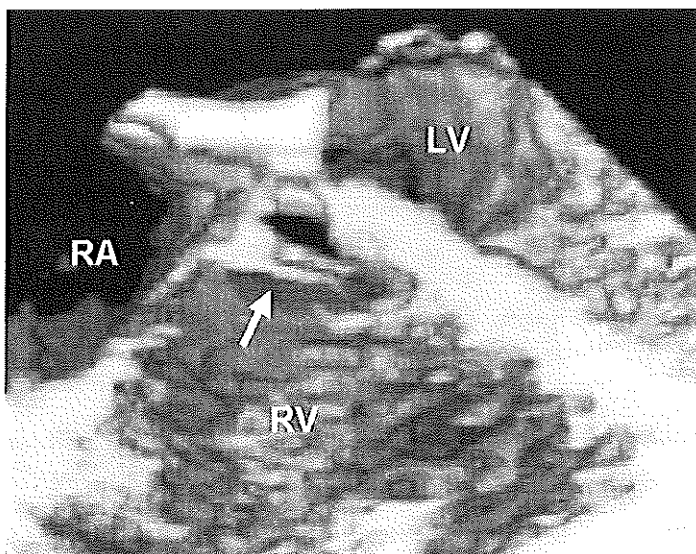
Figure 15

Chordal attachment of the tricuspid septal leaflet obstructing the VSD (arrow).

may be adjacent to the tricuspid valve extending into the outlet septum. Perimembranous defects are more easily displayed by 3D echocardiography, using oblique cutplanes. Accessory tissue derived from the septal tricuspid leaflet and remnants of the membranous septum may obstruct the defect (figure 15).

Furthermore, three-dimensional echocardiography allows accurate measurements of the maximal and minimal diameters of the VSD.[19,22,23] Limitations in visualisation of the VSD are those of two-dimensional echocardiography and are mainly related to the defect size.[19-23]

Three-dimensional display of the VSD could be of potential value in planning optimal approaches for defect repair.[24,25] Furthermore, the possibility of measuring the defect cross-sectional area could provide an alternative and direct method to calculate shunt flow by multiplying area by the continuous wave Doppler time-velocity integral.

Outflow tract anomalies

Obstructive outflow tract anomalies of both the left and right ventricle may lie at the sub-valvular, valvular or supravalvular level. They may occur contemporarily on multiple levels. Furthermore they may be associated with more complex congenital heart disease.

Three-dimensional-echocardiography gives an accurate visualisation of the diverse lesions.[26,27] After selection of a long-axis cutplane displaying the outflow tract lesion, views from above and below the lesion can be created. The application of rendering algorithms improves the comprehension of the lesion in relation to its position in the heart and the near structures.

Subvalvular aortic stenosis may vary from a discrete fibrous ridge to a fibromuscular shelf to a collar or tunnel-like shape. Views looking at the lesion from above, as in an aortotomy, deliver information on the shape of the lesion and on its distance from the semilunar valve. From views facing the obstruction from below, it is possible to evaluate its extension into the ventricle, to the interventricular septum and to the ventricular surface of the anterior mitral leaflet (figure 16).
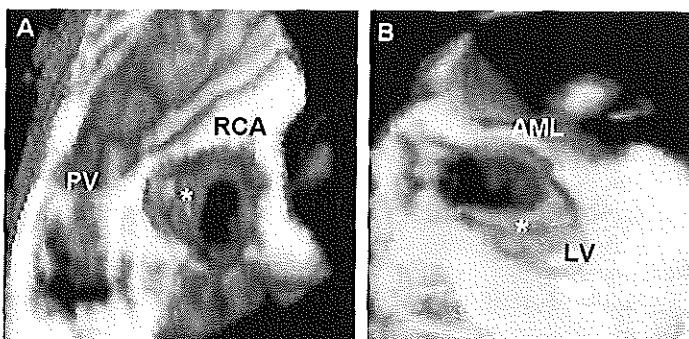
Figure 16

Discrete subaortic stenosis. A = view from above the valve as in an aortotomy: the obstruction appears as a circular membrane (*). B = view from the left ventricle: the membrane (*) extends to the inferior surface of the anterior mitral leaflet and to the interventricular septum. PV = pulmonary valve, RCA = right coronary artery, AML = anterior mitral leaflet, LV = left ventricle.
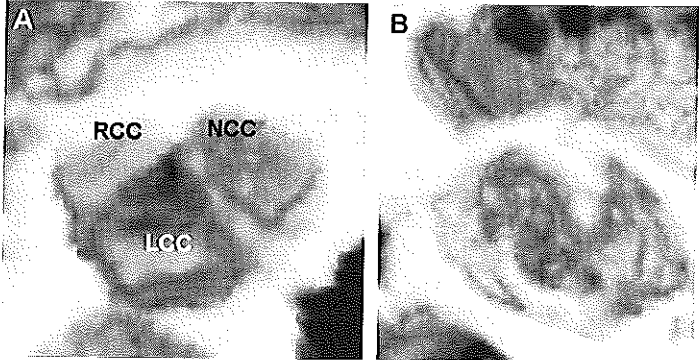
Figure 17

A = congenital aortic valve stenosis, viewed during systole looking from the aortic root: the valve is tricuspid, the right coronary cusp (RCC) and the non-coronary cusp (NCC) are thickened and immobile, while the left coronary cusps (LCC) look dysplastic, but still mobile; B = bicuspid aortic valve.
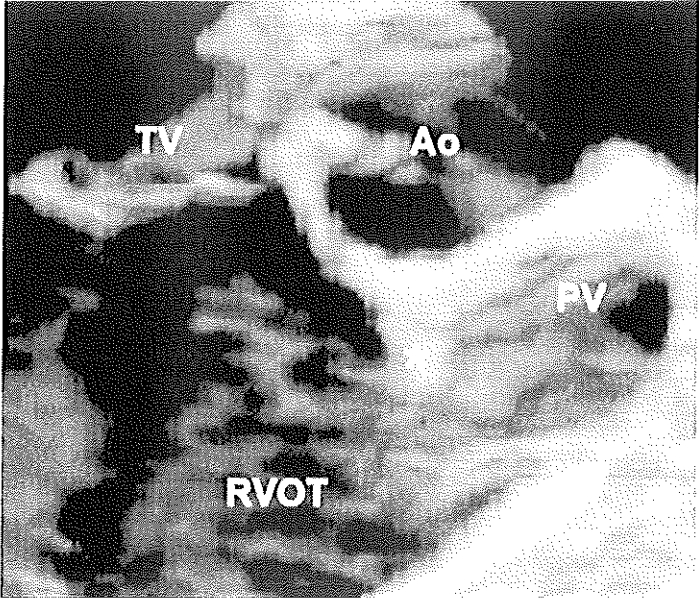
Figure 18

Volume-rendered reconstruction of a sub-pulmonary outflow obstruction in a patient with tetralogy of Fallot. The localisation of the infundibular stenosis (*), the extension and the distance to the pulmonary valve can be well appreciated. PV = pulmonary valve, Ao = aortic valve, TV = tricuspid valve.

In aortic stenosis, volume-rendering reconstruction of the aortic valve displays the opening patterns of the valves, movement of the cusps, visualises their surface and gives a good delineation of the cusp's edges (figure 17). It has been shown that three-dimensional images can adequately diagnose a bicuspid aortic valve, leaflet fenestration and vegetations. However, differentiation between fibrotic and calcified lesions using volume-rendering algorithms is operator dependent and better evaluated with anyplane modality.

Supra-aortic stenosis represents a spectrum of anomalies that may be localised or diffuse both in the pulmonary artery as well as in the aorta. Three-dimensional reconstruction adequately shows the nature of the stenosis, the relationship with the aortic cusps and eventually their abnormality.[27]

Sub-pulmonary stenosis can be reconstructed in any desired cutplane (figure 18). Volume-rendered images add the depth perception allowing display of the underlying muscular anatomy of the right ventricle and the relationship with the tricuspid valve. However, volume-rendered display from above and from below the obstruction is sub-optimal and difficult to interpret. In our experience, it does not add any more anatomical information.[27]

Stenosis of the pulmonary valve is well portrayed from a cutplane above the valve (figure 19). Three-dimensional echocardiography creates dynamic horizontal cross-sections of the pulmonary valves, from which it is possible to evaluate the number of cusps, area or circumference and diameters of the annulus. However, the success rate of these 3D reconstructions is still limited by intrinsic echocardiographic drawbacks (anterior position of the valve and the need for high frequency transducer) and the capability to image the leaflets is directly dependent on their original echodensity. Moreover, the small size of the pulmonary valve and pulmonary artery influences the resolution power of the reconstructions.[27]
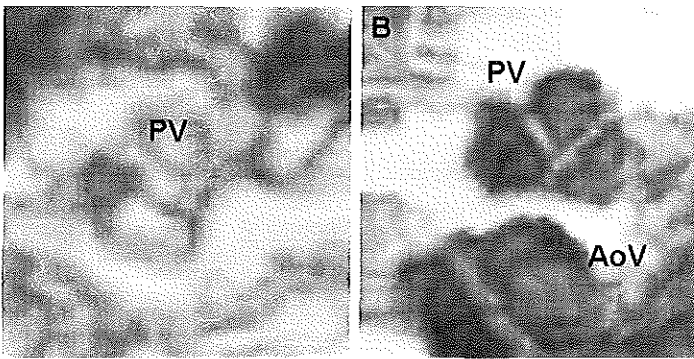
Figure 19

Pulmonary valves as seen from above the pulmonary root. A = stenotic and bicuspid pulmonary valve displayed during diastole. B = tricuspid valve lying anteriorly and to the right of the bicuspid aortic valve.

Anomalies of the ventriculo-arterial connection

A spectrum of cardiac malformations can be diagnosed at the ventriculo-arterial connection. The ventriculo-arterial connection may be concordant, discordant (e.g., transposition

of the great arteries), double outlet or single outlet (e.g., common arterial trunk). Normally, the aorta is in a posterior position to the left of the pulmonary valve, but it can be found in different positions (figure 20). In transposition of the great arteries, the aorta may be located anteriorly and right of the pulmonary valve or can be in a side-by-side position (figures 21 and 22).
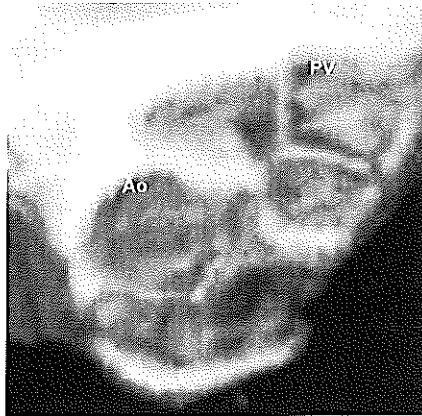
Figure 20

Normal position of the great arteries: the pulmonary valves lie anteriorly and to the right of the aortic valve. Ao = aortic valve, PV = pulmonary valve.
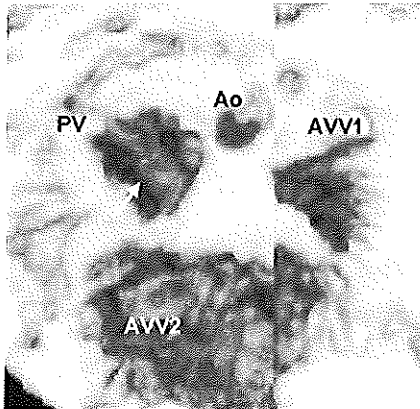
Figure 21

Malposition of the great arteries in a patient with double-outlet right ventricle and transposition of the great arteries. View from above the valves: the aortic valve is smaller than the pulmonary valve, is to the right and side by side with the pulmonary valve. Moreover, from above the pulmonary valve it is possible to appreciate the degree of overriding (> 50%) of the interventricular septum (arrow). PV = pulmonary valve, Ao = aortic valve, AVV1/AVV2 = atrioventricular valves.
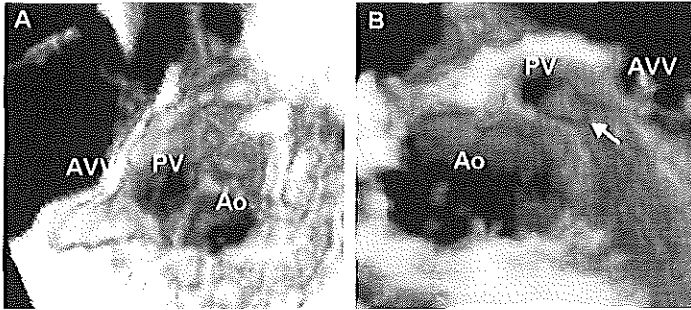
Figure 22

Malposition of the great arteries in two patients with univentricular heart (view from the outflow tract). A = the pulmonary valve is located posteriorly to the aortic valve lying on the same plane, B = the pulmonary valve is located posteriorly to the aortic valve, which is lying in a different plane. In the outflow tract to the pulmonary valve there is a discrete subaortic stenosis (arrow). AV = atrioventricular valve, PV = pulmonary valve, Ao = aorta.

Three-dimensional, volume-rendered imaging from the outflow tract visualises the location and insertion of the outlet septum in relation to the muscular ventricular septum (figure 23). Accurate diagnosis is thus particularly important for the surgical management. Volume-rendered imaging from a cutplane parallel to the aorta, reproducing a surgical aortotomy, provides a view of the interventricular septum beneath and therefore enables evaluation the degree of overriding. It makes it possible to distinguish between the over-riding aorta in the tetralogy of Fallot and that of a double-outlet right ventricle, in which the origin of both the great arteries arises completely or largely from the right ventricle (figure 24).
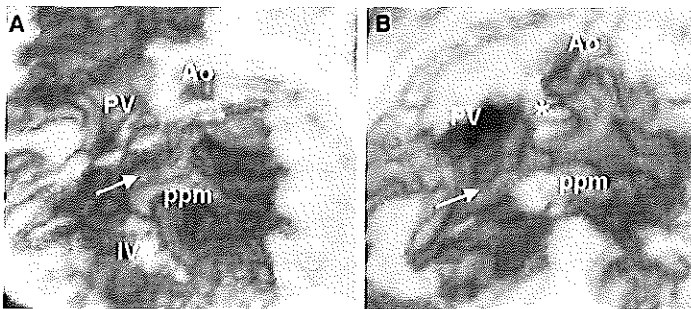
Figure 23

Outflow tract seen from the ventricular viewpoint in a patient with double outlet right ventricle and transposition of the great arteries in diastole (A) and in systole (B): the pulmonary valve, in this patient larger than the aortic valve, overrides the interventricular septum. A muscular ridge (*) separates the semilunar valves. A thick papillary muscle is inserted on the top of the septum, partially obliterating the VSD (arrow). Ao = aorta, PV = pulmonary valve, IVS = interventricular septum, ppm = papillary muscle.
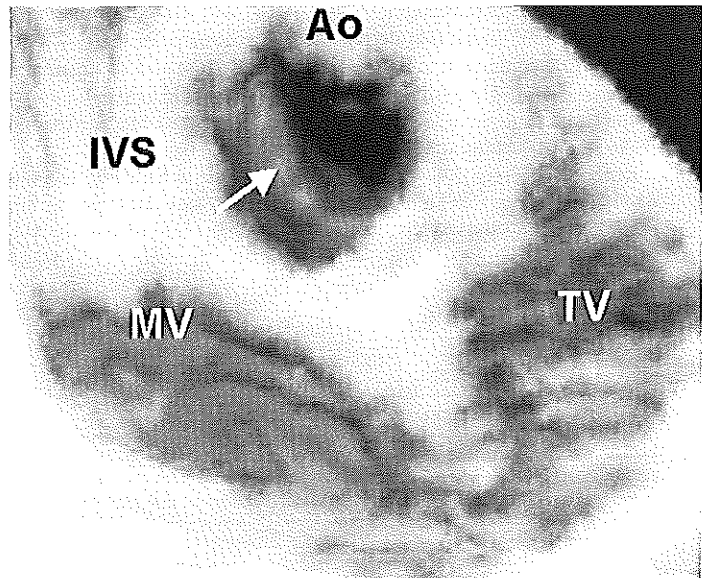
Figure 24

Tetralogy of Fallot: a view from above the aortic valve during systole allows appreciation of the amount of aortic valve overriding the interventricular septum. TV = tricuspid valve, MV = mitral valve, IVS = interventricular septum.

Limitations and perspectives

Despite the accuracy and the advantages in the representation of simple and complex congenital heart diseases,[25-27] the current 3D echocardiographic technique has some limitations at present, which constrain a widespread and routine use in the clinical setting.

The acquisition of the dataset is relatively long. It requires three to five minutes per rotation on top of the time needed for the routine two-dimensional echocardiogram, and the patient has to remain still and quiet during the procedure, in order to avoid artifacts. The latter is difficult, if not impossible, to obtain in children especially when very small. Therefore sedation of the patients becomes essential.

Until recently, three-dimensional transthoracic acquisition in small children was limited by the absence of a specific probe. A relatively large carriage device was usually mounted on the probe, making it cumbersome to position and angulate it properly. Efforts of ultrasound companies have produced a new smaller sized probe with an internal mechanical motor and a high multirange transducer frequency.

Processing and reconstruction are still off-line procedures and time-consuming. In particular, time required for 3D reconstruction depends on the complexity of the pathology. It varies from 30 minutes to hours. Profound knowledge of normal and pathological anatomy and a long learning curve are indispensable for correct orientation, reconstruction and final interpretation of the images. Furthermore, the image quality of the 3D reconstructions strictly depends on the quality of the original 2D data acquired. Drawbacks

present on 2D echocardiography will persist and sometimes be enhanced in the 3D reconstructions. Resolution decreases during transfer of the original ultrasound data from the 2D equipment to the 3D-acquisition system and also is differently distributed in the 3D dataset. The awareness of these aspects should help in the correct interpretation of the final images in order to avoid diagnostic mistakes. Standardisation of views would make reconstructions and interpretation easier for more users

Better display modalities, which make it possible to have multiple reconstructions on one screen, is available on the most recent 3D software. However simulating display for surgical planning and visualisation of colour-Doppler information would be a considerable improvement.

References

1. Feigenbaum H. Congenital heart disease. In: Feigenbaum H. Echocardiography, 5th edition. Lea & Febiger, eds. Malvern, Pennsylvania, 1994:350-446.

2. Stumper O, Sutherland GR. Transesophageal echocardiography in congenital heart disease. Edward Arnold, London; 1994.

3. Roelandt J, Salustri A, Vletter W, Nosir Y, Bruining N. Precordial multiplane echocardiography for dynamic anyplane, paraplane and three-dimensional imaging of the heart. Thoraxcentre J 1994;6/5:3-12.

4. Fulton DR, Marx GR, Pandian NG, Romero BA, Mumm B, Krauss M, et al. Dynamic three-dimensional echocardiographic imaging of congenital heart defects in infants and children by computer-controlled tomographic parallel slicing using a single integrated ultrasound instrument. Echocardiography 1994;11:155-64.

5. Vogel M, Losch S. Dynamic three-dimensional echocardiography with a computed tomography imaging probe: initial clinical experience with transthoracic application in infants and children with congenital heart defects. Br Heart J 1994;71:462-7.

6. Salustri A, Spitaels S, McGhie J, Vletter W, Roelandt JRTC. Transthoracic three-dimensional echocardiography in adult patients with congenital heart disease. J Am Coll Cardiol 1995;26:759-67.

7. Belohlavek M, Foley DA, Gerber TC, Greenleaf JF, Seward JB. Three-dimensional ultrasound imaging of the atrial septum: normal and pathologic anatomy. J Am Coll Cardiol 1993;22:1673-8.

8. Nanda NC, Rahman SMA, Khatri G, Agrawal G, El-Sayed AA, Hassanian HAS, et al. Incremental value of three-dimensional echocardiography over transesophageal multiplane two-dimensional echocardiography in qualitative and quantitative assessment of cardiac masses and defects. Echocardiography 1995;12:619-28.

9. Marx GR, Fulton DR, Pandian NG, Vogel M, Cao QL, Ludomirsky A, et al. Delineation of site, relative size and dynamic geometry of atrial septal defects by real-time three-dimensional echocardiography. J Am Coll Cardiol 1995;25:482-90.

10. Dall'Agata A, McGhie J, Taams MA, Cromme-Dijkhuis AH, Spitaels SE, Breburda CS, et al. Secundum atrial septal defect is a dynamic three-dimensional entity. Am Heart J 1999;137:1075-81.

11. Franke A, Kuhl HP, Rulands D, Jansen C, Erena C, Grabitz RG, et al. Quantitative analysis of the morphology of secundum type atrial septal defects and their dynamic change using transesophageal three-dimensional echocardiography. Circulation 1997;96 [suppl II]:323-7.

12. Magni G, Cao QL, Sugeng L, Delabays A, Marx G, Ludomirsky A, et al. Volume-rendered, three-dimensional echocardiographic determination of the size, shape and position of atrial septal defects: validation in an in vitro model. Am Heart J 1996;132:376-81.

13. Lange A, Walayat M, Turnbull CM, Palka P, Mankad P, Sutherland GR, et al. Assessment of atrial septal defect morphology by transthoracic three-dimensional echocardiography using standard grey-scale and Doppler myocardial imaging techniques: comparison with magnetic resonance imaging and intraoperative findings. Heart 1997;78:382-9.

14. Magni G, Hijazi ZM, Pandian NG, Delabays A, Sugeng L, Laskari C, et al. Two- and three-dimensional transesophageal echocardiography in patient selection and assessment of atrial septal defect closure by the new DAS-Angel Wings device. Circulation 1997;96:1722-8.

15. Vogel M, Ho SH, Anderson RH, Buhlmeyer K, Ludomirsky A, Marx G, et al. 3-dimensional echocardiography provides new information on morphology of AV septal defect. J Am Soc Echocardiogr 1995;8:17D.

16. Vogel M, Marx G, Pandian N, Buhlmeyer K, Fulton D, Cao QL. Delineation of congenital malformations of mitral valve apparatus by dynamic three-dimensional echocardiography and unique image segmentation using a tomographic transthoracic approach. J Am Coll Cardiol 1994;23:169A.

17. Vogel M, Ho SY, Ludomirsky A, Sugeng L, Delabays A, Buhlmeyer K. Transthoracic three-dimensional echocardiography provides new information on straddling or overriding AV valves in complex heart defects. Circulation 1994;90 (Suppl I):531.

18. Ludomirsky A, Vemilion R, Nesser J, Marx G, Vogel M, Deman R, et al. Improved anatomic delineation of Ebstein's anomaly from three-dimensional images obtained by echocardiography and magnetic resonance imaging. Circulation 1994;90(4):I-530.

19. Rivera JM, Siu SC, Handschumacher MD, Lethor JP, Guerrero JL, Vlahakes GJ, et al. Three-dimensional reconstruction of ventricular septal defects: validation studies and in vivo feasibility. J Am Coll Cardiol 1994;23:201-8.

20. Vogel M, Basso C, Ho SY, Anderson RH. In vitro qualitative and quantitative assessment of Taussig-Bing hearts with double outlet right ventricle and subpulmonary VSD by 3-dimensional echocardiography. J Am Soc Echocardiogr 1995;8:2V.

21. Hsieh KS, Lin CC, Chen FL, Wan SL. Anatomical delineation of subarterial doubly committed ventricular septal defect by three-four dimensional echocardiography. Circulation 1995;92 (Suppl I):2118.

22. Kardon RE, Cao QL, Masani N, Sugeng L, Supran S, Waner KG, et al. New insights and observation in three-dimensional echocardiographic visualization of ventricular septal defects: experimental and clinical studies. Circulation 1998;98:1307-14.

23. Dall'Agata A, Cromme-Dijkhuis AH, Meijboom FJ, McGhie JS, Bol-Raap G, Nosir YF, et al. Three-dimensional echocardiography enhances the assessment of ventricular septal defect. Am J Cardiol 1999;83:1576-9.

24. Noto N, Ayusawa M, Karasawa K, Sumitomo N, Okada T, Harada K. Transthoracic three-dimensional echocardiography: therapeutic decision making process of subarterial ventricular septal defect. J Am Coll Cardiol 1997;29 [Suppl A]:509A.

25. Vogel M, Rigby ML, Shore D. 3-dimensional echocardiography of ventricular septal defects before and after transcatheter closure with a modified Rashkind umbrella. Circulation 1995;92 (Suppl I):3105.

26. Fyfe DA, Ludomirsky A, Sandhu S, Dhar PK, Silberbach M, Sahn DJ. Left ventricular outflow tract obstruction defined by active three-dimensional echocardiography using rotational transthoracic acquisition. Echocardiography 1994;11:607-15.

27. Dall'Agata A, Cromme-Dijkhuis AH, Meijboom FJ, Spitaels SE, McGhie JS, Roelandt JRTC, et al. Use of three-dimensional echocardiography for analysis of outflow obstruction in congenital heart disease. Am J Cardiol 1999;83:921-5.

28. Vogel M, Ho SY, Anderson RH. Comparison of three-dimensional echocardiographic findings with anatomical specimens of various congenitally malformed hearts. Br Heart J 1995;73:566-70.

29. Vogel M, Ho SH, Lincoln C, Yacoub MH, Anderson RH. Three-dimensional echocardiography can simulate intra-operative visualization of congenitally malformed hearts. Ann Thorac Surg 1995;60:1282-8.

30. Bartel T, Muller S, Geibel A. Preoperative assessment of cor triatriatum in an adult by dynamic three-dimensional echocardiography was more informative than transesophageal echocardiography or magnetic resonance imaging. Br Heart J 1994;72:498-9.

CHAPTER 3

THE SECUNDUM ATRIAL SEPTAL DEFECT IS A DYNAMIC THREE-DIMENSIONAL ENTITY

Secundum atrial septal defect is a dynamic three-dimensional entity

A. Dall'Agata, MD, J. McGhie, MD, M.A. Taams, MD, A.H. Cromme-Dijkhuis, MD, PhD, S.E.C. Spitaels, MD, PhD, C.S.M. Breburda, MD, PhD, J.R.T.C. Roelandt, MD, PhD, and A.J.J.C. Bogers, MD, PhD *Rotterdam, The Netherlands*

Background The aim of this study was to evaluate the diagnostic relevance of 3-dimensional (3D) echocardiography in the assessment of secundum atrial septum defect (ASD2).

Methods and Results Twenty-three patients (age 2 to 58 years) with an ASD2 were studied by transthoracic (n = 9) or transesophageal (n = 14) echocardiography for the acquisition of a 3D data set before undergoing surgical repair. Qualitative (location, shape, and structure) and quantitative (largest and smallest anteroposterior and superoinferior diameters) characteristics were analyzed and compared with surgical findings. Intraobserver and interobserver variability were assessed. The gross anatomy of the ASD2, shown by the 3D images, was confirmed by the surgeon in 21 of 23 patients, but the presence of membranous or fenestrated remnants of the valvula foramina ovalis in the defect was not optimally visualized in 7 patients. Three-dimensional echocardiography revealed changes in diameter and shape of the ASD2 during the cardiac cycle. The measured largest and smallest anteroposterior diameters and their intraobserver and interobserver agreement were 274 ± 12 mm, r = 0.95 (P < .001), r = 0.92 (P < .001), and 194 ± 9 mm, r = 0.96 (P < .001), r = 0.94 (P < .001), respectively. The measured largest and smallest superoinferior diameter and their intraobserver and interobserver agreement were 304 ± 26 mm, r = 0.90 (P < .001), r = 0.97 (P < .001), and 204 ± 10 mm, r = 0.83 (P < .001), r = 0.84 (P < .001), respectively. The correlation coefficient between 2D and 3D echocardiography for the largest anteroposterior and superoinferior diameter was r = 0.69 (P < .001) and r = 0.68 (P = .05), respectively. The correlation coefficient between the measurements from 3D reconstructions and direct surgical measurements was r = 0.20 (P = not significant) and r = 0.57 (P < .05), whereas between 2D and surgery was r = 0.50 (P < .05) and r = 0.26 (P = not significant).

Conclusions ASD2 has a complex morphology. Three-dimensional echocardiography provides better qualitative and quantitative information on its dynamic geometry, location, and extension as compared with standard 2D echocardiography and might be useful for device selection during catheter-based closure of ASD2. (Am Heart J 1999;137:1075-81.)

Atrial septal defect of the secundum type (ASD2) represents 7% of all congenital cardiac anomalies.[1] Its morphology is variable with regard to its location, size, and number. A recent classification has been proposed by Chan and Godman[2] incorporating these criteria.

In the pediatric population, the clinical diagnosis of an ASD2 is readily confirmed by traditional precordial or transthoracic 2-dimensional echocardiography (2D TTE), and a differentiation between the different types of atrial

septal defects can be made.[3] In adults, the diagnostic accuracy of the 2D TTE method with respect to anatomy is not optimal. This may be explained by the distance between the interatrial septum and the transducer, with the consequence of missing anatomic details.[4] Transesophageal 2-dimensional echocardiography (2D TEE) allows a more detailed visualization of the interatrial septum and represents a more accurate method for the demonstration of both the anatomic and functional aspects of the ASD2.[5-7]

Morphologic classifications and diagnostic methods consider the ASD2 as a static defect with 2 dimensions from which the shunt size may be calculated.[8-10] Until recently, such an approach was adequate with regard to therapy, which was exclusively surgical.[11] However, the introduction of catheter-based techniques for device closure of ASD2 requires selection of patients on the basis of specific criteria such as the absence of remnants of the foramen ovale within the ASD2, a maximal diameter of 20 mm, and at least 5 mm of tissue surrounding the defect.[12] Even with the detailed information derived

Figure 1
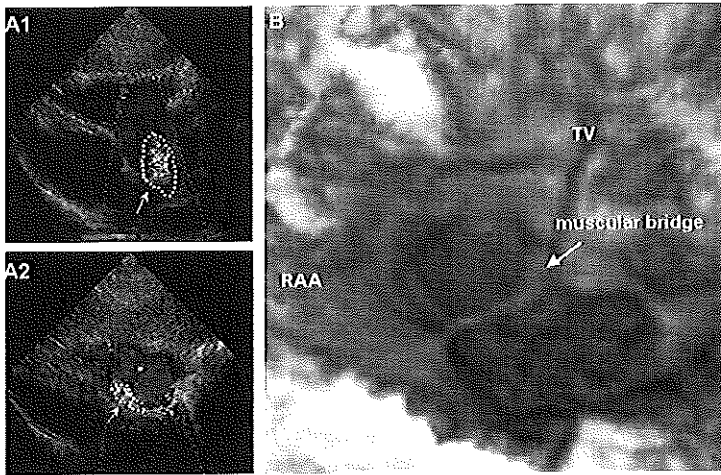
A1, Transthoracic color Doppler image showing flow jet through ASD2; **A2,** with slight tilting of imaging plane, second flow jet is visualized. **B,** 3D image visualizing ASD2 as from right atriotomy: it is clear that defect is constituted by 2 holes separated by muscular bridge. *TV,* Tricuspid valve; *RAA,* right atrial appendage.

from 2D TEE, the therapeutic success with this technique is limited.[12-15] Thus it has become evident that the information derived from both 2D TTE and TEE—when this type of treatment is considered—is limited.

Thus the aim of our study was to evaluate the diagnostic role of 3D echocardiography for morphology, spatial distribution, and geometry of the ASD2. A comparison was made with surgical findings of ASD2.

Methods

Study population

Twenty-three patients (10 female and 13 male patients) with the clinical diagnosis of isolated ASD2 with left-to-right shunt, confirmed by precordial 2D echocardiography and color flow imaging (CFI), were studied before undergoing surgical correction. Fifteen patients were adults (age 22 to 58 years) and 8 were children (age 2 to 17 years). All patients were in sinus rhythm.

On 2D echocardiography, a centrally located single defect was seen in 16 patients. Membranous or fenestrated remnants of the valvula foramina ovalis within the defect were found in 8 patients. In 1 of these, multiple defects were not directly seen but were suggested by 2 color-flow jets coming from different directions after slight tilt of the ultrasound beam (Figure 1, *A1,* and *A2*). There were no abnormal venous connections.

Echocardiography and data acquisition

Two-dimensional echocardiography and CFI were performed with a Toshiba SSH 140-A (Toshiba Corp, Otawara-Shi, Japan) or HP 1500 (Hewlett Packard, Andover, Mass) echo machine.

Nine patients were examined the day before surgical correction in the department of echocardiography and 14 patients just before surgery under general anesthesia in the operating theater.

TTE was performed in subcostal or apical 4-chamber positions in 9 patients with the use of a 3.5-MHz probe. TEE was performed from a mid-esophageal level in the other 14 patients with the use of a 5-MHz multiplane probe (Varioplane, Oldelft, Delft, The Netherlands) in adults and a 5-MHz prototype multiplane probe with 48 elements (Minimulti, Oldelft, Delft, The Netherlands) in children.

After finding the optimal acoustic window, from which the defect could be visualized and encompassed in the conical volume, 3D acquisition was performed, interfacing the 2D equipment to a steering logic system (Echo-scan 3.0, TomTec GmbH, Munich, Germany). The transducer was rotated by a step motor mounted on the ultrasound probe. From a steady position, 90 electrocardiographic and respiratory gated cardiac cross sections were acquired every 2 degrees and immediately stored in the computer memory. The time required to calibrate, to complete 1 rotational acquisition, and to store the data varied from 5 to 8 minutes. Afterward, the data were processed off-line.[16]

Reconstruction of 3D data sets

Reconstruction was done off-line by 2 observers, independently. From the volumetric data sets, computer-generated dynamic 2D images of the ASD2 were obtained with the use of an anyplane mode.[16] The cut planes were taken in a longitudinal plane through the anterior right ventricular free wall, tricuspid valve orifice, and right atrial free wall to face the atrial septum from the right side and a longitudinal plane through

Figure 2
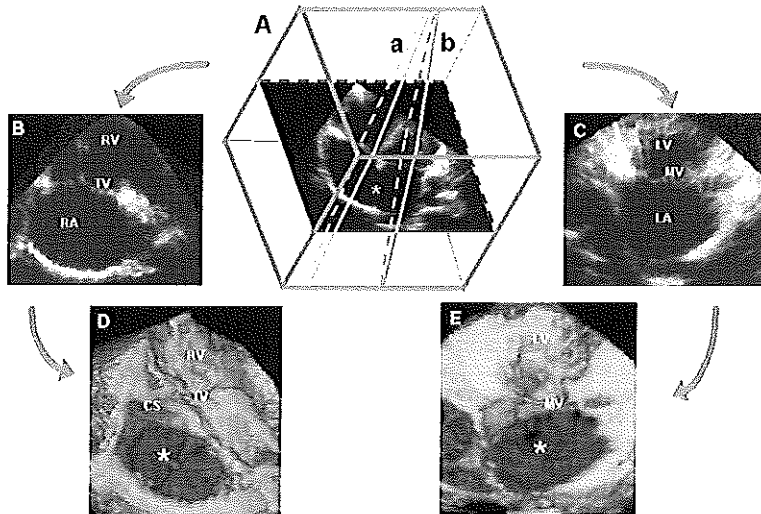
Three-dimensional reconstruction of ASD2 with anyplane mode and volume rendering. **A,** Volumetric data set from which cut planes can be selected: a and b, longitudinal cut planes through right and left heart, facing atrial septum from right and left sides, respectively. **B** and **C,** Computer-generated dynamic 2D images representing en face views of right and left sides of interatrial septum. **D** and **E,** 3D images obtained from previous cut planes after application of volume rendering algorithms showing anatomic structures with depth perception. RV, Right ventricle; TV, tricuspid valve; RA, right atrium; LV, left ventricle; MV, mitral valve; LA, left atrium; CS, coronary sinus. *Atrial septal defect.

the left ventricle and the left atrium to face the septum from the left side. Rendering algorithms, threshold, and opacity were applied on the original gray-scale information within the volumetric data set. The background was separated from the object in order to reconstruct the surface of the cardiac structures.[16] Thus a display with depth perception was created (Figure 2). The time required for reconstruction varied from 20 to 30 minutes.

Data analysis from 3D images

Data analysis was performed separately by the 2 observers. From the rendered display images, the site (central, dorsal, high), shape (round, oval), morphologic characteristics (fenestrated, remnants of foramen ovale), and the relation of the ASD2 with anatomic structures including tricuspid valve, caval veins, coronary sinus, and the aorta were evaluated.

The size of the defect was measured from en face views of the atrial septal defects: the smallest and the largest diameter in the inferosuperior (along the caval veins direction) and in the posteroanterior axes were measured (Figure 3). Measurements were taken from the echo reflection representing the rim of the ASD2, and, because the different surface points of a 3D reconstruction are not in 1 plane and depth is always taken into account, only distances with the lowest error range were considered. Threshold and opacity values used during reconstruction were annotated by both observers.

Surgical assessment

During surgery, the location, shape, and structural characteristics were recorded. With the heart in diastolic arrest, the size of the defect was measured along the anteroposterior and superoinferior directions.

The 3D images were reviewed after surgery by the attending surgeon.

Statistical methods

Echocardiographic measurements were done at least in triplicate and were expressed as mean ± SD. The percentage of reduction between the largest and smallest diameters was calculated. Measurement variability for intraobserver and interobserver and comparison of 3D, 2D, and surgical data were performed with the use of linear regression and analysis of agreement according to Bland-Altman.[17] A value of $P < .05$ was considered significant.

Results

The morphology of the ASD2 was visualized on the 3D images in all 23 patients, and imaging quality was good in 21 of 23 patients. In 2 patients the defect was only partially displayed.

Three-dimensional echocardiography confirmed that

Figure 3
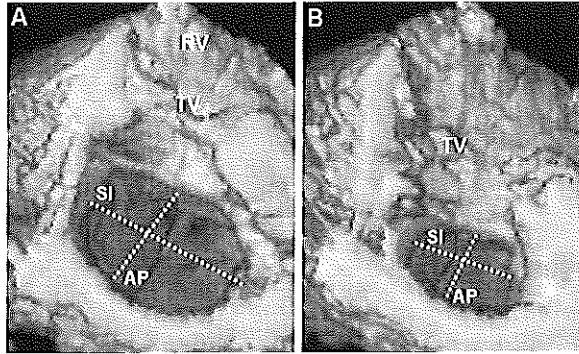
Large ASD2 seen from right side. Three-dimensional image was reconstructed with transthoracic acquisition. Measurements along smallest and largest diameters are taken. During cardiac cycle, it is possible to appreciate variation of its size. RV, Right ventricle; TV, tricuspid valve; AP, anteroposterior; SI, superoinferior.

Table I. Correlations between measurements

	Largest AP mean diff ± SD	r	Smallest AP mean diff ± SD	r	Largest SI mean diff ± SD	r	Smallest SI mean diff ± SD	r
Intraobserver	0.07 ± 0.39	0.95†	0.00 ± 0.26	0.90†	0.04 ± 0.70	0.96†	0.02 ± 0.70	0.83†
Interobserver	0.06 ± 0.47	0.92†	0.04 ± 0.32	0.97†	0.09 ± 0.33	0.94†	0.20 ± 0.49	0.84†
2D vs 3D	−2.23 ± 8.6	0.69*	NA	–	2.46 ± 9.6	0.68*	NA	–
3D vs surgery	5.85 ± 13.5	0.20	NA	–	2.82 ± 13.7	0.57*	NA	–
2D vs surgery	3.70 ± 9.2	0.50*	NA	–	6.92 ± 8.5	0.26	NA	–

AP, anteroposterior diameter; SI, superoinferior diameter; r, correlation coefficient; diff, difference; 2D, 2-dimensional echocardiography; 3D, 3-dimensional echocardiography; NA, not analyzed.
*P < .05, †P < .001.

the anatomy of the atrial defect is more complex on the right side than on the left and that the ASD2 does not lie in a flat plane but in a folded area.

On 3D echocardiography, 16 of the ASD2 were centrally located and 7 were extending dorsally. In 1 patient, a flapping membrane was visualized in the defect. In 4 patients, some fine mobile structures were identified. Two other ASD2 were fenestrated. All patients underwent surgery with primary suture correction.

When the 3D images were compared with the surgical findings in 12 (52%) of 23 patients, the anatomy was confirmed by the attending surgeon. In 7 (30%) of 23 patients, 3D images did not clearly visualize (4 patients) or did not visualize at all (3 patients) the presence of membranous tissue with or without fenestrations. Comparison with surgical findings revealed that the 3D images provided additional morphologic information in comparison with the 2D data about the anatomy of the defect in 2 (9%) of 23 patients. In one of these, it was immediately possible to identify the presence of a muscular bridge

septating the ASD2 (Figure 1), and in the other case the 3D image enabled us to completely define the rim of the defect, which was not clear on the 2D study (Figure 4). There was no agreement about the location of the ASD2 as interpreted with 3D echocardiography compared with the surgical findings in 2 (9%) of 23 patients. On 3D echocardiography, the relation of the ASD2 with the tricuspid valve could be assessed in 21 (91%) of 23 patients with the superior caval vein in 14 (61%) of 23, with the inferior caval vein in 1 (4%) of 23 patients, and with the coronary sinus in 12 (52%) of 23 (Figure 4).

On 3D echocardiography, it was possible to measure both the largest and the smallest diameters in 21 of 23 patients. The measured largest and smallest anteroposterior diameters and their intraobserver and interobserver agreement were 27 ± 12 mm, r = 0.95 (P < .001), r = 0.92 (P < .001), and 19 ± 9 mm, r = 0.96 (P < .001), r = 0.94 (P < .001), respectively. In this regard, no difference was found in adequacy for reconstruction between the data collected with TTE or TEE (TTE

9 of 9 vs TEE 12 of 14, P = not significant [NS]). The measured largest and smallest superoinferior diameters and their intraobserver and interobserver agreement were 30 ± 26 mm, r = 0.90 (P < .001), r = 0.97 (P < .001), and 20 ± 10 mm, r = 0.83 (P < .001), r = 0.84 (P < .001), respectively. Again, no difference was found in adequacy for reconstruction between the data collected with TTE or TEE (TTE 9 of 9 vs TEE 11 of 14, P = NS).

The largest diameter in any direction was ≥20 mm in 18 of the 2D echocardiograms and in 16 of the 3D reconstructions (TTE 9 of 9, TEE 7 of 14). From the 3D reconstructions, 16 cases showed a rim of <5 mm in areas around the defect (TTE 7 of 9, TEE 9 of 16).

The 3D images displayed in motion showed that throughout the cardiac cycle, there was a change in size and in shape of the defect (Figure 3). There was a reduction of 30% in the anteroposterior diameter and 26% in the superoinferior diameter during the cardiac cycle.

The correlation coefficients of the measurements between 2D echocardiography and 3D echocardiography were r = 0.69 (P < .001) and r = 0.68 (P < .05), respectively, in the anteroposterior and superoinferior directions; the correlation coefficients between the 2D measurements and surgical findings were r = 0.20 (P = NS) and r = 0.57 (P < .05); the correlation coefficients between the 2D measurements and surgery were r = 0.50 (P < .05) and r = 0.26 (P = NS) (Table I).

Discussion

Complete assessment of the morphology and size of an ASD2 with the use of conventional echocardiography remains difficult in the perspective of device closure, which requires 3D information.[12,13,15] It has been shown that 3D echocardiography allows evaluation of atrial septal defects and its spatial orientation by providing unique views.[18-20] However, validation by morphologic or surgical inspection is needed. In vitro studies indicate that the technique provides accurate data on the size of the defects.[21]

The current study assesses the morphology and function of ASD2 with 3D echocardiography and validates its results with surgery. A first important result is that on 3D echocardiography, the ASD2 does not appear to be a simple hole between the 2 atria. It is a distinct entity, which varies in shape and extension in the atrial septum. The anatomy of the atrial defect is more complex on the right side than on the left. A striking finding of 3D echocardiography was that an ASD2 does not lie in a flat plane but in a folded area, probably as a result of the embryologic process of fusion of the primitive septa.[22] In addition, an important finding was the dynamic aspect during the cardiac cycle of the ASD2, a characteristic of which the interventional cardiologist should be aware of during device selection and implantation. Three-dimensional echocardiography displayed the
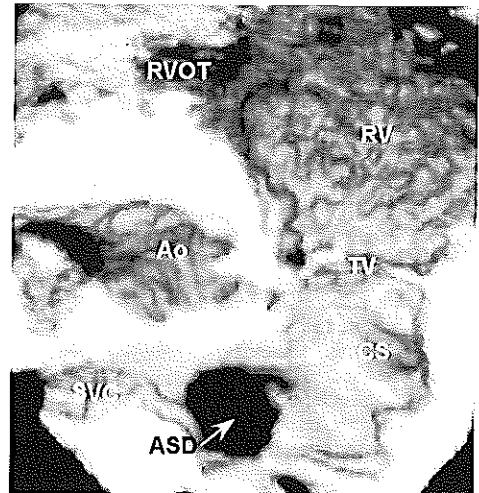
Reconstructed 3D image obtained with TEE of ASD2 seen from right atrium. Shape, size, location, and relation with surrounding anatomic structures are visualized. Ao, Aorta; SVC, superior vena cava; TV, tricuspid valve; CS, coronary sinus; ASD, atrial septal defect.

ASD2 in the view seen during surgical or anatomic inspection, allowing more adequate appreciation in its spatial distribution the relation of the ASD2 with other structures, such as the aorta or the coronary sinus or the superior vena cava. It is important to realize that device closure forces the truly 3D ASD2 into a 2D structure because the rims of the defect must follow the closing mechanism of the device.

Three-dimensional echocardiography allowed measurement of both diameters of the ASD2 on one single image with good intraobserver and interobserver variability correlation. However, what appears from our data is that 3D echo overestimates the 2D echo data. This could be explained as an effect of the application of the rendering algorithms. Measurements are taken from one voxel to the other, giving a distance in space, and therefore a depth factor is introduced in the measurements. Moreover, in our study, there was hardly a correlation between the 3D data and the surgical measurements and there was an overestimation of the superoinferior diameter by surgery in comparison with the anteroposterior diameter. The same observations were found also between the 2D data and the surgical measurements. These results can be explained by the differences in physiologic condition (eg, different cardiac loading con-

ditions and heart rate) in which the two measurements are taken. During operation, the heart is in diastolic arrest, empty, and easy to stretch. This is exaggerated by the surgical selection of the patients, all of them having defects not considered suitable for device closure, mostly because of the large size of the defect. In diastolic arrest, a larger defect may result in larger measurements. This may explain why, in our series, quantitative correlation between surgery and 3D echocardiography, obtained from filled atria, resolves in poor results. A recent study by Franke et al[20] showed a more adequate correlation between maximal diameter at surgery and on 3D echocardiography. However, in their series, in only 12 of 17 patients the atrial septal defects were sized during surgery and only the largest diameters were compared. Remarkably, their absolute figures show definitively smaller sizes of the ASD2, possibly as a result of difference in the technique of measurement.[20] Also, Lange et al[23] found a good correlation between 3D echo data and surgery. However, in this study, measurements were taken in a fibrillating heart, resulting in maintenance of cardiac tone as well as loss of differences between systolic and diastolic dimensions.[23]

Limitations of the study

Three-dimensional data sets derive from a complex assembly of sequentially acquired 2D images.[16] Therefore, optimal 3D images depend on the quality and information included in the 2D TTE or TEE data sets. This is especially true for thin structures such as the Eustachian valve, the Chiari network, or a fenestrated or a flapping remnant of the valvula foramina ovalis. After 3D reconstruction, these structures are sometimes lost either because of inadequate resolution of the 2D and 3D echo or because of their fast motion. It is not always possible to display in the 3D images the relation of the ASD2 with the anatomic structures of the right atrium, such as the caval veins and the coronary sinus. These structures can only be visualized when acquired during 3D rotation and therefore in our study, they were mostly obtained from TEE studies.

Furthermore, a high and dorsal location of the defect technically hampers a complete multiplane rotation around the region of interest, leading to incomplete 3D reconstruction. Moreover, in this study 3D data were compared with data obtained during surgery. Surgical measurements, as mentioned above, are affected by various variables (as different physiologic conditions, accuracy of measurements). Therefore surgery may not be a gold standard method for accurate sizing of the functional ASD2. Currently, imaging and sizing of the ASD2 for routine assessment is done by 2D echocardiography, whereas catheterization is used for therapeutic reasons. These techniques are not devoid of limitations.

Conclusions

Three-dimensional echocardiography truly appreciates the ASD2 as a dynamic 3D entity. It enables us to measure diameters throughout the cardiac cycle and gives a virtually real representation of its cardiac pathology. It gives to the clinicians new insights on this entity, which should help in decision making for alternative therapeutic strategies. At present, 3D echocardiography may have additional clinical value in appropriately selecting patients for catheter-based closure of the defect.

However, for optimal and widespread use of 3D echocardiography, technical improvement, such as higher resolution after acquisition and faster computers allowing on-line reconstructions, are mandatory.

References

1. Beerman LB, Zuberbuhler JR. Atrial septal defect. In: Anderson R, Macartney FJ, Shinebourne EA, Tynan M, editors. Pediatric cardiology. Vol I. London: Churchill Livingstone; 1987. p. 541-62.

2. Chan KC, Godman MJ. Morphological variations of fossa ovalis atrial septal defects (secundum): feasibility for transcutaneous closure with the clam-shell device. Br Heart J 1993;69:52-5.

3. Forfar JC, Godman MJ. Functional and anatomical correlates in atrial septal defects: an echocardiographic analysis. Br Heart J 1985;54:193-200.

4. Mehta RH, Helmcke F, Nanda NC, et al. Uses and limitations of transthoracic echocardiography in the assessment of atrial septal defect in the adult. Am J Cardiol 1991;67:288-94.

5. Hanrath P, Schluter M, Langenstein BA, et al. Detection of ostium secundum atrial septal defects by transesophageal cross-sectional echocardiography. Br Heart J 1983;49:350-8.

6. Sutherland GR. Atrial septal defects. In: Stümper O, Sutherland GR, editors. Transesophageal echocardiography in congenital heart disease. London: Edward Arnold; 1994. p. 59-76.

7. Morimoto K, Matsuzaki M, Tohma Y, et al. Diagnosis and quantitative evaluation of secundum type atrial septal defect by transesophageal Doppler echocardiography. Am J Cardiol 1990,66:85-91.

8. Mehta RH, Helmcke F, Nanda NC, et al. Transesophageal Doppler color flow mapping assessment of atrial septal defect. J Am Coll Cardiol 1990;16:1010-6.

9. Pollick C, Sullivan H, Cujec B, et al. Doppler color-flow imaging assessment of shunt size in atrial septal defect. Circulation 1988;78:522-8.

10. Rao PS, Langhough R. Relationship of echocardiographic, shunt flow, and angiographic size to the stretched diameter of the atrial septal defect. Am Heart J 1991;122:505-8.

11. Brian G. Atrial septal defect and partial anomalous pulmonary venous connection. In: Kirklin JW, Barott-Boyes BG, editors. Cardiac surgery. Vol I. New York: Churchill Livingston Inc; 1993. p. 625-32.

12. Reddy S, Rao PS, Ewenko J, et al. Echocardiographic predictors of success of catheter closure of atrial septal defects with the buttoned device. Am Heart J 1995;129:76 82.

13. Rao PS, Langhogh R, Beekman RH, et al. Echocardiographic estimation of balloon-stretched diameter of secundum atrial septal defect for transcatheter occlusion. Am Heart J 1992;124:172-5.

14. Ishii M, Kato H, Inoue O, et al. Biplane transesophageal echo-Doppler studies of atrial septal defects: quantitative evaluation and monitoring for transcatheter closure. Am Heart J 1993;125:1363-8.

15. Ludomirsky A. Transcatheter occlusion of atrial and ventricular septal defects. In: Stümper O, Sutherland GR, editors. Transesophageal

echocardiography in congenital heart disease. London: Edward Arnold; 1994. p. 200-5.

16. Roelandt J, Salustri A, Vletter W, et al. Precordial multiplane echocardiography for dynamic anyplane, paraplane, and 3-dimensional imaging of the heart. Thoraxcentre J 1994;6/5:4-13.

17. Bland JM, Altman DG. Statistical methods for assessing agreement between 2 methods of clinical measurement. Lancet 1986;1:307-10.

18. Belohlavek M, Foley DA, Gerber IC, et al. Three-dimensional ultrasound imaging of the atrial septum: normal and pathologic anatomy. J Am Coll Cardiol 1993;22:1673-8.

19. Marx GR, Fulton DR, Pandion NG, et al. Delineation of site, relative size and dynamic geometry of atrial septal defects by real time 3-dimensional echocardiography. J Am Coll Cardiol 1995;25:482-90.

20. Franke A, Kuhl HP, Rulands D, et al. Quantitative analysis of the morphology of secundum-type atrial septal defects and their dynamic change using transesophageal 3-dimensional echocardiography. Circulation 1997;96(suppl II).II-323-7.

21. Magni G, Cao QL, Sugeng L, et al. Volume-rendered, 3-dimensional echocardiographic determination of the size, shape, and position of atrial septal defects: validation in an in vitro model. Am Heart J 1996;132:376-81.

22. Sadler TW. Cardiac development. In: Sadler TW, editor. Langman's medical embryology. Baltimore: Williams & Wilkins; 1995. p. 191-7.

23. Lange A, Walayot M, Turnbull CM, et al. Assessment of atrial septal defect morphology by transthoracic three dimensional echocardiography using standard gray scale and Doppler myocardial imaging techniques: comparison with magnetic resonance imaging and intraoperative findings. Heart 1997;78:382-9.

CHAPTER 4

THREE-DIMENSIONAL ECHOCARDIOGRAPHIC ACQUISITION AT 8 DEGREE ROTATIONAL INTERVALS ALLOWS RAPID VOLUME RENDERED RECONSTRUCTION AND ACCURATE QUANTITATIVE ASSESSMENT OF SECUNDUM ATRIAL SEPTAL DEFECTS

Youssef FM Nosir*, Anita Dall'Agata, Ron T van Domburg,

Nicholas M Bom, Ad JJC Bogers, Jos RTC Roelandt

Thoraxcenter, Erasmus University, Rotterdam, The Netherlands

and *Cardiology Department, Al-Hussein University Hospital, Al-Azhar University,

Cairo, Egypt.

Submitted

ABSTRACT

Background. The prolonged acquisition time of the basic images for three-dimensional echocardiographic (3DE) reconstruction currently limits its routine use in clinical practice particularly for perioperative assessment of patients undergoing cardiac surgery.

Objectives. Our aim was to define the largest 3DE rotational acquisition interval that still allows both qualitative and accurate quantitative assessment of patients with a secundum atrial septal defect (ASD2), in order to shorten the acquisition time.

Methods. Twelve patients with ASD2 underwent 3DE and images were acquired with 2° rotational intervals. Images were processed to create data sets containing images at 2°, 4°, 8° and 16° intervals by excluding interjacent images. The volume rendered ASD2 *"en face"* view was reconstructed and its suitability for the morphological assessment (location, shape and structure) was scored by two experienced observers. From the dynamic data set the view with the largest ASD2 size was selected and the defect size [area, superior-inferior (L1) and anterior-posterior (L2) diameters] were measured. Measurements obtained from *"en face"* views reconstructed from data sets with original images at 4°, 8° and 16° were compared with those obtained at 2°.

Results. Volume rendered ASD2 *"en face"* views obtained from 3DE data sets with original images up to 8° interpolation intervals were of adequate quality for morphological assessment. At 16° intervals, 5 data sets were not interpretable. The mean $\pm$ SD of ASD2 area measurement were (4.9±5, 4.9±5, 5.1±5.2 and 6.4±7.2 cm^2), of L1 were (2.2±1, 2.2±1, 2.2±1 and 2.3±1.4 cm) and of L2 were (2.5±1.5, 2.5±1.6, 2.6±1.6 and 2.9±1.2 cm) for data sets obtained at 2°, 4°, 8° and 16° intervals respectively. There were very close limits of agreement between ASD measurements obtained at 2° and the same measurements obtained at 4° [±0.6 (p=0.3), ±0.2 (p=0.7) and ±0.2 (p=0.4)] and with measurements obtained at 8° [±0.4 (p=0.1), ±0.2 (p=0.6) and ±0.4 (p=0.1)] for ASD area, L1 and L2 respectively. There

were wider limits of agreement between ASD2 measurements obtained from 3DE data sets reconstructed at 2° and 16° rotational intervals [($\pm$2.0 (p=0.4), $\pm$0.6 (p=0.7) and $\pm$0.8 (p=0.1)] for area, L1 and L2 respectively.

In addition, measurements obtained from 3DE data sets reconstructed with original images at 2°, 4° and 8° had smaller interobserver variability than those obtained at 16° rotational intervals.

Conclusions. Reconstruction of *"en face"* views of an ASD2 from 3DE data sets with original images at 8° intervals is possible and allows both qualitative and accurate quantitative assessment. Therefore, 3DE acquisition at 8° intervals is sufficient for the reconstruction of adequate volume rendered views of cardiac defects, considerably reducing the acquisition time and making 3DE more practical as a routine method.

INTRODUCTION

In patients with secundum atrial septal defects (ASD2), understanding of the spatial relationships of atrial septum is becoming increasingly important with the development of percutaneous transcatheter closure of ASD2.[1-3] Complete visualization of the limbus surrounding the defect and of adjacent structures is mandatory for closure of the defect with a device.[4] In addition, ASD2 varies in shape and extension with the inter-atrial septum with more anatomical complexity in the right side than the left side.[8]

Conventional two-dimensional echocardiography (2DE) provides adequate information for diagnosis, however its ability to depict the anatomic relationships is difficult or even impossible to determine.

Three-dimensional echocardiography (3DE) allows to create an unlimited number of cutting planes through the heart, independently from the window of acquisition, and unique *"en face"* views. It is therefore helpful in better assessment of congenital heart disease and in planning surgical procedures. In patients with ASD2 undergoing transcatheter closure, 3DE provides important dynamic information to the operator for device selection and planning for implantation procedure.[5-8] In addition, 3DE allows to reconstruct the anatomical and surgical *"en face"* view that provides adequate spatial and anatomical information with the surrounding structures like the aorta, coronary sinus and superior vena cava.[8]

3DE has been validated in vitro[9] and in vivo[8] studies to provide optimal qualitative and accurate quantitative data for the size of ASD2. However, prolonged 3DE acquisition and reconstruction time currently restricts its routine use in clinical cardiology, particularly in special scenarios as for perioperative assessments of cardiac patients.

Therefore, this study was designed to define a faster method for 3DE acquisition and to evaluate its accuracy for reconstructing volume rendered ASD2 *"en face"* view. In

addition, the suitability of the reconstructed views for morphological and quantitative assessment of the defects was studied.

Subjects and Methods

3DE was performed in 12 consecutive patients with the clinical diagnosis of isolated ASD2 without abnormal venous connection. All patients had left to right shunt as confirmed by 2DE and color flow imaging. Patients included 5 males and 7 females (age 27 ± 16 years, ranging from 22 to 41 years). Informed verbal consent was obtained from each patient after a detailed explanation of the procedure. All patients were in sinus rhythm with a mean heart rate of 78 ± 9 bpm.

3DE examination

3DE requires 3 steps: image acquisition, image processing and image analysis.

(A) Image acquisition

3DE was acquired with the transthoracic approach (TTE) in 6 patients from apical 4-chamber or subcostal position and with transesophageal approach (TEE) in the other 6 patients from a mid-esophageal level. 3DE acquisition was performed with a commercially available ultrasound unit (Toshiba Sonolayer SSH-140A, Otawara-Shi, Japan) for both TTE (3.75 MHz transducer frequency) and for TEE (5 MHz transducer frequency). The transducer was rotated by a step motor mounted on the ultrasound probe and coupled with a 3DE processing computer (Echo-scan 3.0, TomTec GmbH, Munich, Germany) for data acquisition. [10,11] After finding the optimal acoustic window, from which the ASD2 could be visualized and encompassed in the conical volume, the echocardiographic images were collected in a rotational format at 2° intervals from 0° to 178°, gated to proper R-R intervals

of ECG and thoracic impedance of expiration. The time required to calibrate, to complete one rotational acquisition and to store the data varied from 5 to 8 minutes.

(B) Image Processing

The acquired data were processed and analyzed off line on a 3DE work station (TomTec 4.1, GmbH, Munich, Germany). Images selected at intervals of 2°, 4°, 8° and 16° from the original data set were readjusted in their correct spatial and temporal sequence, digitally reformatted and processed to obtain 4 different data sets (Fig.1). Gaps between the images were interpolated using a "trilinear cylindric interpolation" algorithm. [12]
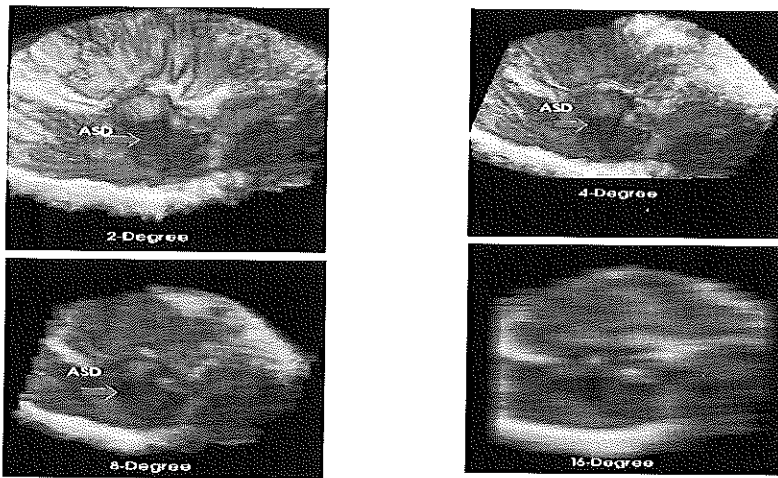
Figure 1.This figure shows the ASD2 volume rendered "*en face*" view reconstructed from 3DE data sets obtained at 2°, 4°, 8° and 16° rotational intervals (A to D, respectively). Volume rendered ASD2 "*en face*" views obtained from 3DE data sets up to 8° (A, B and C) rotational intervals were of adequate quality for diagnosis, morphological and quantitative assessment. While, image obtained at 16° intervals (D) was not interpretable.

(C) Image Analysis

Two independent observers performed data analysis of data sets obtained at 2°, 4°, 8° and

16° of rotational intervals. From each data set, dynamic *"en face"* views of the atrial septum

were computed with the use of anyplane method.[8] Rendering algorithms, threshold and

opacity were applied on the original gray scale information within the 3D data set in order to

obtain images with a depth perception (Fig.2).

Each *"en face"* 3D image was scored by subjective estimation for its suitability for qualitative

assessment of ASD2 (location, shape and relation to the surrounding structures).

In addition, after choosing the frame with the largest ASD2 size, the largest diameter in the

infero-superior (along the caval veins direction) (L1) and in the antero-posterior (from the

posterior atrial wall along the tricuspid valve) (L2) directions and the ASD2 area were

measured by each observer for each data set (Fig.2). Measurements were taken from the echo

reflection representing the rim of the ASD2.
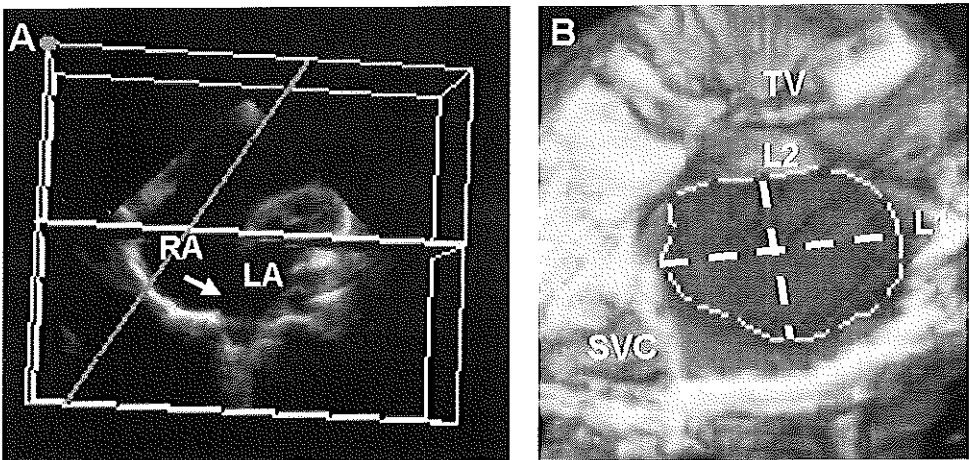
Figure 2. Panel A shows the reference image obtained from the 3DE data set from which ASD2 *"en face"* view
is obtained for volume rendered reconstruction. Panel **B** shows the principle of ASD2 quantitative
measurements of area, infero-superior (L1) and postero-anterior (L2) diameters performed on the 3DE volume
rendered *"en face"* view.

Statistical analysis

All values of the ASD2 area, L1 and L2 measurements were expressed as mean ± SD. Interobserver variability was calculated as the standard error of the estimate (SEE). Limits of agreement were computed using Altman and Bland method[13] in order to compare measurements of ASD2 area, L1 and L2 obtained from 3DE data sets at 4°, 8° and 16° rotational intervals with values obtained from 3DE data sets at 2° rotational intervals. A paired t-test was performed and significance was stated at the 0.05 probability level. Pearson's correlation coefficients were used.

RESULTS

3DE data acquisition was possible in all patients recruited in this study.

Visual scoring of volume rendering *"en face"* views

Visual estimation of volume rendered ASD2 *"en face"* views obtained from 3DE data sets up to 8° rotational intervals were of adequate quality for diagnosis, morphological and quantitative assessment. Images obtained at 16° rotational intervals included 5 data sets with inadequate quality for interpretation.

Comparison between ASD2 measurements by 3DE at 4°, 8 °and 16° rotational intervals and values obtained from 3DE data set at 2° rotational intervals

Mean ± SD of ASD2 area, L1 and L2 obtained from 3DE data sets at 2°, 4°, 8°and 16° rotational intervals are presented in Table 1. There was excellent correlation, close limits of agreements and non-significant differences between measurements of ASD2 area, L1 and L2

obtained from 3DE at 4°and 8° rotational intervals and that measured from images obtained at 2° of interpolation intervals (Table 2). While ASD2 measurements obtained from images reconstructed at 16° rotational intervals had very wide limits of agreement with values obtained from images reconstructed at 2° rotational intervals (Table 2).

Mean ± SD	2°	4°	8°	16°
Area (cm²)	4.9 ± 5.0	4.9 ± 5.0	5.1 ± 5.2	6.4 ± 7.2
L1 (cm)	2.2 ± 1.0	2.2 ± 1.0	2.2 ± 1.0	2.3 ± 1.4
L2 (cm)	2.5 ± 1.5	2.5 ± 1.6	2.6 ± 1.6	2.9 ± 2.1

Table 1. Mean ± SD of ASD2 area, infero-superior (L1) and antero-posterior (L2) diameters measured from 3DE volume rendered *"en face"* view reconstructed from data sets obtained at 2°, 4°, 8° and 16° rotational intervals.

Observer variability of ASD2 measurements at different rotational intervals

Interobserver variability for calculating ASD2 area, L1 and L2 from 3DE *"en face"* volume rendered view at 2°, 4°, 8° and 16° rotational intervals were calculated and presented as the standard error of the estimate (SEE) between the two observers (Table 2, Fig.3). Interobserver measurements of ASD2 area, L1 and L2 obtained from images reconstructed at 16° of rotational intervals had very large SEE (Fig.3).

	2°			4°			8°			16°		
	Area	L1	L2	Area	L1	L2	Area	L1	L2	Area	L1	L2
p	-	-	-	0.3	0.7	0.4	0.1	0.6	0.1	0.4	0.7	0.1
agr.	-	-	-	±0.6	±0.2	±0.2	±0.4	±0.2	±0.4	±2	±0.6	±0.8
r	-	-	-	0.99	0.98	0.99	0.99	0.99	0.99	0.98	0.98	0.98
SEE	0.04	0.02	0.02	0.05	0.04	0.04	0.05	0.04	0.03	0.3	0.03	0.05

Table 2. Comparison between ASD2 area, infero-superior (L1) and antero-posterior (L2) diameters obtained from 3DE data sets reconstructed from images selected at 2°, 4°, 8° and 16° rotational intervals (agr=limits of agreement, *p*=significance, r=correlation coefficient, SEE=standard error of estimate)
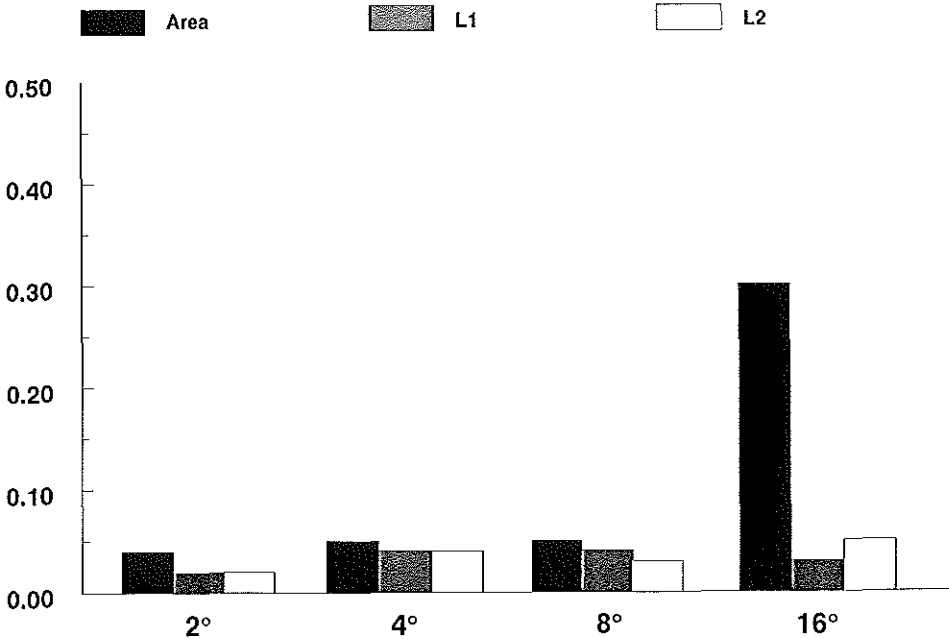

Figure 3. Interobserver variability (SEE) measurements of ASD2 area, infero-superior (L1) and antero-posterior (L2) diameters obtained from volume-rendered "*en face*" views reconstructed from 3DE data sets at 2°, 4°, 8° and 16° of rotational intervals

DISCUSSION

Complete assessment including morphology, size and shape of an ASD2 using 2DE remains difficult in the perspective of device closure, which requires spatial structure information. [14, 15] 3DE allows evaluation of ASD2 and its spatial orientation by providing the surgical "*en face*" views [5-8] and more particularly for ensuring an adequate limbus around the defect before placement of the device. [16]

The results of this study demonstrated that volume rendered "*en face*" views with images acquired at 8° rotational intervals are still adequate for the diagnosis as well as for assessments of the size, shape and encircling limbic tissue rims of an ASD2. This implies that the data acquisition time may be reduced in average from 5 minutes to 1 minute, as only 23 instead of 90 basic 2D images are required and further reducing both the image processing and analysis time.

Measurements of area, infero-superior and antero-posterior diameters of ASD2 from "*en face*" views using data sets with basic 2D imaging at 8° rotational intervals has close limits of agreement, non-significant difference and excellent correlation with values obtained from "*en face*" views reconstructed from data sets acquired at 2° rotational intervals.

Study limitation and Clinical Implications

Volume rendered 3DE, using sequentially collected images, produces reproducible data sets of the heart and is therefore an ideal technique for follow-up studies of cardiac patients. Rotational 3DE data acquisition at 2° requires 90 cutting planes of the heart with each containing images of a whole cardiac cycle. With ECG and respiratory gating, the acquisition usually requires approximately 5 minutes. This is not only a limitation for the

routine use of this technique, but also increases the possibility of patient or operator induced artifacts that may lead to inaccurate or unreadable data.

Since the introduction of 3DE, efforts has been directed to find a simple, rapid and accurate protocol that would facilitate its routine use in clinical practice. The results of this study demonstrate that 3DE rotational acquisition at 8° can considerably shorten the acquisition time with adequate image quality for morphological and quantitative assessment. The reconstructed 3DE volume rendering view is derived from the sequentially acquired 2DE images. 3DE images depend on the original quality and information obtained from 2DE images. [8] In this study none of the patients had multiple or complicated ASD2 (fenestrated or flapping remnant of the foramina ovalis), which is one of the most important exclusion criteria for transcatheter device closure. Moreover, it is known that, despite a preliminary screening with 2DE to individuate patients suitable for transcatheter closure, pre-operative TEE is highly recommended in order to avoid misdiagnosis of the ASD2 structure. In our study only a small group (12 patients) were studied during routine TTE or TEE examination. Therefore, there is still a need to study the suitability of 3DE, both TTE and TEE, using 8° rotational intervals in patients with multiple or complicated ASD2.

Conclusions

3DE data sets reconstructed with images selected at 8° intervals from data sets obtained at 2° rotational acquisition interval allowed the reconstruction of ASD2 volume rendered "*en face*" view with adequate quality for both morphological and quantitative assessment. This would reduce the acquisition time with enough accuracy for clinical decision making and therefore make 3DE more practical as a routine method.

REFERENCES

1. Hausdorf G., Schneider M, Franzbach B, et al: Transcatheter closure of secundum atrial septal defects with the atrial septal defect occlusion system (ASDOS): Initial experience in children. Heart 1996;75:83-88

2. Sideris EB, Sideris SE, Fowlkes JP, et al: Transvenous atrial septal defect occlusion in piglets with a buttoned double-disk device. Circulation 1990;81:312-318

3. Rao PS, Sideris EB, Hausdorf G, et al: International experience with secundum atrial septal defect occlusion by the buttoned device. Am Heart J 1994;128:1022-35

4. Ferreira S, Ho SY, Anderson RH. Morphologic study of defects of the atrial septum within the fossa ovalis: Implications for transcatheter closure of left-to-right shunt. Br Heart J 12992;67:316-20

5. Belohlavek M, Foley DA, Geerber TC, Greenleaf JF, Seward JB. Three-dimensional ultrasound imaging of the atrial septum: normal and pathologic anatomy. J Am Coll Cardiol 1993;22:1673-8

6. Marx GR, Fulton DR, Pandian NG, et al. Delineation of site, relative size and dynamic geometry of atrial septal defects by real time three-dimensional echocardiography. J Am Coll Cardiol 1995;25:482-90

7. Franke A, Kuhl HP, Rulands D, Jansen C, Erena C, Grabitz R, et al. Quantitative analysis of the morphology of secundum type atrial septal defects and their dynamic change using transesophageal three-dimensional echocardiography. Circulation 1997;96(suppl II):II-323-7

8. Dall' Agata A, McGhie J, Taams MA, Cromme-Dijkhuis AH, Spitaels SEC, Breburda CSM, Roelandt JRTC, Bogers AJJC. The secundum atrial septal defect is a dynamic three-dimensional entity. Am Heart J. 1999;137:1075-81

9. Magni G, Cao QL, Sugeng L, et al. Volume rendered three-dimensional echocardiographic determination of the size, shape, and position of atrial septal defects: validation in an in vitro model. Am Heart J 1996;132:376-81

10. Roelandt J, Salustri A, Vletter W, Nosir Y, Bruining N. Precordial multiplane echocardiography for dynamic anyplane, paraplane and three-dimensional imaging of the heart. Thoraxcentre J 1994;6:4-13

11. Salustri A, Roelandt J. Ultrasonic three-dimensional reconstruction of the heart. Ultrasound in Med & Biol 1995; 21:281-93.

12. Nosir YFM, Salustri A, Vletter WB, et al. Accurate measurements of left ventricular ejection fraction by three-dimensional echocardiography: a comparison with radionuclide angiography. Circulation 1996;94,:460-6.

13. Altman DG, Bland JM. Measurement in medicine: the analysis of method comparison studies. Statistician 1983;32:307-17

14. Reddy S, Rao PS, Ewenko J, Koscik R, Wison AD. Echocardiographic predictors of success of catheter closure of atrial septal defects with the buttoned device. Am Heart J 1995;129:76-82

15. Rao PS, Langhogh R, Beekman RH, Lioyed TR, Sideris EB. Echocardiographic estimation of balloon-stretched diameter of secundum atrial septal defect for transcatheter occlusion. Am Heart J 1992;124:172-5

16. Lu JH, Hsu TL, Hwang B, Weng ZC. Visualization of secundum atrial septal defect using transthoracic three-dimensional echocardiography in children: implication for transcatheter closure. Echocardiography 1999;15:651-9

CHAPTER 5

THREE-DIMENSIONAL ECHOCARDIOGRAPHY
ENHANCES THE ASSESSMENT OF
VENTRICULAR SEPTAL DEFECT

.

Three-Dimensional Echocardiography Enhances the Assessment of Ventricular Septal Defect

Anita Dall'Agata, MD, Adrie H. Cromme-Dijkhuis, MD, PhD,
Folkert J. Meijboom, MD, PhD, Jackie S. McGhie, BSc, G. Bol-Raap, MD,
Youssef F.M. Nosir, MD, Jos R.T.C. Roelandt, MD, PhD, and Ad J.J.C. Bogers, MD, PhD

Functional and morphologic assessment of ventricular septal defect (VSD) is routinely done with 2-dimensional (2-D) and color Doppler echocardiography.[1-5] Usually, this provides adequate information to decide on surgical repair.[6,7] Nevertheless, the anatomy of the VSD is complex[8,9] and cannot be presented by actual imaging techniques in a single plane.[10] Furthermore, advances in cardiac surgical procedures increasingly demand support of highly accurate imaging techniques. Three-dimensional (3-D) echocardiography has been proposed as a new technique able to simulate the intraoperative visualization of cardiac structures and to improve the understanding of the anatomy of congenital heart disease.[11] An experimental study conducted on animals has shown that 3-D echocardiography is feasible for VSD analysis.[12] However, until now, studies on patients for the assessment of VSD with 3-D echocardiography are scanty and not validated by intraoperative findings.[13,14] To define the clinical use of 3-D echocardiography, we evaluated whether 3-D echocardiography can accurately identify and characterize the morphology of the VSD and assess its geometry and size in patients undergoing surgery.

• • •

Thirty patients (16 males and 14 females) with diagnosis on routine 2-D echocardiography of VSD were studied. The mean age was 6 ± 13 years (range 20 days to 61 years). Three patients were adults (age 18 to 61 years) and 27 were children (age 20 days to 6 years). Body surface area was 0.72 ± 0.6 m^2 (range 0.22 to 2.1). In 12 patients, the VSD was isolated. In 11 patients the VSD was associated with tetralogy of

Fallot and in 3 with pulmonary atresia. In 1 patient the VSD was associated with double-outlet right ventricle and transposition of the great arteries, and in another patient with simple transposition of the great arteries. In the remaining 2 patients the VSD was a residual defect after correction of a complete atrioventricular VSD.

Complete diagnostic transthoracic examination (2-D echocardiography, pulsed Doppler wave, and color flow mapping) for clinical assessment was performed using HP 1500 (Hewlett-Packard, Andover, Massachusetts) echocardiographic equipment. Multiple cross sections imaging the VSD were taken from all windows, following a standard procedure.[6] The 3-D echocardiographic acquisition was performed with a Toshiba SSH 140-A (Toshiba, Otawara-Shi, Japan) or HP 1500, of which the video output was interfaced to the Echo scan 3.0 (TomTec, Munich, Germany) 3-D reconstruction system. Twenty patients were studied by the transthoracic and 10 by the transesophageal approach. Transesophageal echocardiography was performed only in children using the Mini-multi probe (Oldelft, Delft, The Netherlands), which contains 48 transmitting elements and operates at a frequency of 5 MHz. Transthoracic echocardiography was performed with a 3.5-MHz probe. All children were studied under general anesthesia just before surgery or cardiac catheterization. The 3 adult patients were studied in the Department of Echocardiography. Acquisition was performed with rotational scanning at 2° intervals for 90 steps, applying electrocardiography and respiratory gating.[15] During rotation, the VSD was kept in the center of the scan sector and care was taken that other cardiac structures like the tricuspid valve and the aortic valve were also encompassed for further spatial orientation and morphologic definition of the VSD.

The data were processed off-line and presented as a conical volumetric data set.[15] The 3-D data sets were reconstructed and analyzed independently by 2 ob-
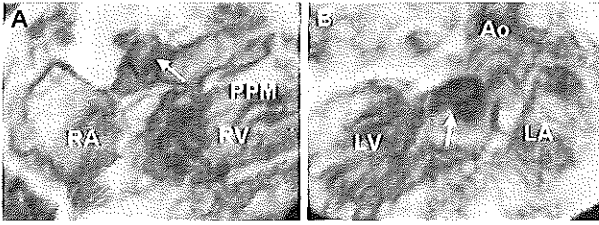
FIGURE 1. Perimembranous ventricular septal defect (outlet) (arrow). A, view of the defect from the right aspect. The location of the defect in relation to the tricuspid valve and the outflow tract is shown. B, view of the defect from the left aspect. The location of the defect in relation to the aorta and the mitral valve is shown. Ao = aortic valve; LA = left atrium; LV = left ventricle; PPM = posterior papillary muscle; RA = right atrium; RV = right ventricle.
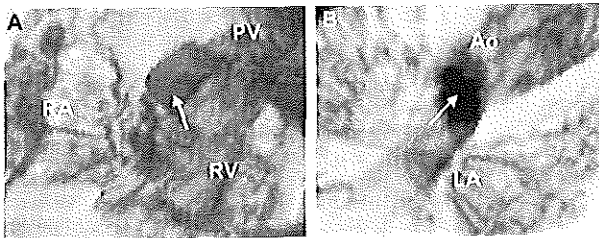

FIGURE 2. Morphologic aspects of the ventricular septal defect (arrow) associated with pulmonary atresia, seen from the right (A) and from the left (B) surface. PV = pulmonary valve; other abbreviations as in Figure 1.

servers (AD, JMcG). From the volumetric data set, cut planes were selected using anyplane mode to visualize the ventricular septum on its left and right surface and in a longitudinal cross section. A gray level threshold was applied on the computer-generated 2-D cut planes to separate the object from the background. Thus, 3-D dynamic images with depth perception were created. A third observer (AC-D) analyzed the VSD on 2-D echocardiography.

The location of the VSD (perimembranous, muscular, inlet, outlet), the relation to the tricuspid valve (tethering of the tricuspid valve leaflet, presence of abnormal chordae), and to the aortic valve (degree of overriding) and its size were analyzed on both 2-D and 3-D echocardiographic images. On the 3-D reconstruction, the anteroposterior and superoinferior diameters were measured, whereas on 2-D echocardiography only the diameter derived from a 4-chamber view (corresponding to the anteroposterior direction) was measured. The largest anteroposterior diameter of the VSD measured on 3-D images was compared with the largest anteroposterior diameter derived from 2-D echocardiography. Morphologic accuracy was assessed postoperatively by presenting the dynamic 3-D reconstructions of the VSD to the attending surgeon and correlating the data to the annotated intraoperative description.

Measurements are expressed as mean $\pm$ SD. Intra- and interobserver variability and comparison between 3-D and 2-D data were analyzed by linear regression

and Bland-Altman analysis of agreement.[16] A p value <0.05 was considered significant.

• • •

The 3-D data sets were adequate for reconstruction in 28 of 30 patients. In the other 2 patients, a wrong gain setting and the presence of a large rotational artifact in the dataset hampered the quality of the final reconstruction. Seventy-nine 3-D reconstructions, displaying the VSD from the right and the left aspect, from above the aortic valve and along its longitudinal cross section, were used for analysis. Twenty-four of 28 patients had a single perimembranous VSD with extension to the outlet septum, situated just below the aortic valve (Figures 1 and 2). In 1 of these patients there was an associated aneurysm of the sinus of Valsalva. Two patients had an inlet VSD, 1 a doubly committed VSD. In 1 patient multiple VSDs were visualized: 2 were muscular defects and 1 a perimembranous outlet defect. In 2 patients the tricuspid valve leaflet was tethering the defect and in 6 patients abnormal chordae from the tricuspid valve were attached to the ventricular septum and crossing the defect area (Figure 3). From 28 adequate horizontal 3-D cross sections above the aortic valve, overriding of approximately 50% was seen in 12 patients and of $>50\%$ in 1 patient (Figure 4).

There was complete agreement on morphology of the VSD between 3-D and 2-D echocardiography. However, 3-D reconstructions were of additional value compared with 2-D echocardiography in 6 of 28 patients (21%). Views of the right side of the VSD displayed the presence of abnormal chordae crossing the defect in 3 patients (Figure 3), the amount of tricuspid valve surrounding the defect in 2 other patients, and the number of VSDs in another patient better than 2-D echocardiography. Three-D echocardiography did not give better visualization of the doubly committed VSD and of the VSD in relation to the Valsalva aneurysm. This was most probably due to the small size of the defects and the difficulty in obtaining an optimal 3-D acquisition. Twenty-seven of 28 patients underwent surgical correction. The VSD was visualized through the right atrium and the tricuspid valve and closed in all cases with a Gore-Tex patch (Flagstaff, Arizona). The agreement on anatomy between 3-D reconstructions and intraoperative findings was complete in all patients.

Twenty-two facing views of the VSD were reconstructed and used for diameter measurement. The anteroposterior diameter was 13 $\pm$ 8 mm (intraobserver agreement r = 0.9, p <0.001; interobserver agreement r = 0.9, p <0.001), the superoinferior diameter was 18 $\pm$ 6 mm (intraobserver agreement r = 0.7, p
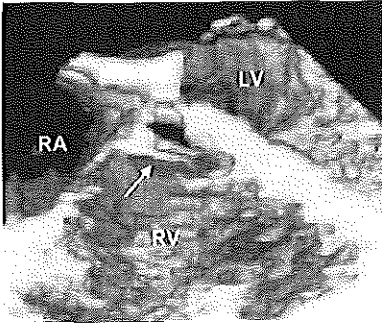
FIGURE 3. Volume rendered image of the right ventricle (RV) displaying the right aspect of the ventricular septal defect (arrow) and abnormal chordae from the tricuspid valve crossing the defect. Abbreviations as in Figure 1.
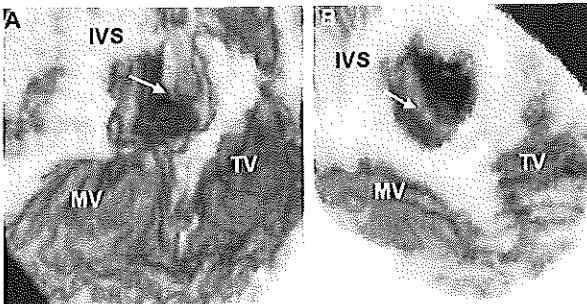

FIGURE 4. Horizontal cross section through the aortic valve from which it is possible to estimate the degree of overriding aorta (arrow). A, aortic valve overrides the ventricular septum (IVS) by <50%; B, in a patient with tetralogy of Fallot the overriding aorta is about 50%. MV = mitral valve; TV = tricuspid valve.

ened, immobile, and tethering the VSD, thereby limiting visualization of the VSD. Three-D echocardiography offers the possibility of overcoming this limitation, exposing the defect completely by electronically deleting the leaflet or by creating a new cut plane in which the tricuspid leaflet is not present.

Shunt size is a critical factor in management decisions. We are aware that shunt size does not necessarily correlate with the anatomic size of the defect. Nevertheless the dimensions of a defect play a role in the hemodynamic status of a patient with VSD. The most reliable way to size the defect is usually to measure its diameter either by 2-D color flow imaging or at cineangiography.[17-19] However, sizing can be difficult when the VSD is associated with another lesion, such as coarctation or pulmonary stenosis. In this study, we demonstrate that 3-D echocardiography can be considered a technique for accurate and reliable sizing. On 3-D reconstructed images, it was possible to evaluate the exact shape and orientation of the VSD in 1 single plane and consequently to measure its 2 largest diameters in both directions. Sizing the VSD on 3-D echocardiography has been shown to have good intra- and interobserver reproducibility.

In summary, this study shows that 3-D echocardiography can be considered a valuable diagnostic tool, which may accurately identify the location, size, and spatial relation of a VSD.

<0.001; interobserver agreement r = 0.9, p <0.001). The largest 3-D anteroposterior diameter was compared with the corresponding 2-D anteroposterior diameter (11.8 ± 4 mm). The correlation coefficient between the measurements was r = 0.6 (p <0.05).

• • •

In this study we evaluated the accuracy and the potential of 3-D echocardiography in the preoperative assessment of VSD. We showed that 3-D echocardiography presents an accurate view of the anatomy of the VSD. The creation of cut planes, which display the VSD from its right aspect, reproduce the surgical viewpoint of a right ventriculotomy. From these images it is possible to define the morphologic nature of the margins of the defect, its shape, and the direction in which the defect extends into the ventricular septum. Other anatomic structures such as the tricuspid valve leaflet, the right ventricular outflow tract, and the aortic valve can be displayed in their realistic spatial distribution. More than 2-D echocardiography, 3-D views facilitate more complete visualization of chordae supporting the tricuspid valve leaflet crossing the defect. The tricuspid valve is sometimes thick-

1. Cheatham JP, Latson LA, Gutgesell HP. Ventricular septal defect in infancy: detection with two-dimensional echocardiography. Am J Cardiol 1981;47:85–89.
2. Bierman FZ, Fellows K, Williams RG. Prospective identification of ventricular septal defects in infancy using subxiphoid two-dimensional echocardiography. Circulation 1980;62:807–817.
3. Murphy DJ, Ludomirsky A, Huhta JC. Continuous-wave Doppler in children with ventricular septal defect: noninvasive estimation of interventricular pressure gradient. Am J Cardiol 1986;57:428–432.
4. Ludomirsky A, Huhta J, Vick W III, Murphy DJ, Danford DA, Morrow WR. Color Doppler detection of multiple ventricular septal defects. Circulation 1986; 74:1317–1322.
5. Sutherland GR, Smyllie JH, Cogilvie B, Keeton BR. Color flow imaging in the diagnosis of multiple ventricular septal defects. Br Heart J 1989;62:43–49.
6. Sutherland G, Godman MJ, Smallhorn JF, Guiterras P, Anderson RH, Hunter S. Ventricular septal defect. Two-dimensional echocardiographic and morphological correlations. Br Heart J 1982;47:316–328.
7. Johnson TB, Derek AF, Thompson RP, Kline CH, Swindle MM, Anderson RH. Echocardiographic and anatomic correlation of ventricular septal defect morphology in newborn Yucatan pigs. Am Heart J 1993;125:1067–1072.
8. Anderson RH, Wilcox BR. The surgical anatomy of ventricular septal defects associated with overriding valvar orifices. J Card Surg 1993;8:130–142.
9. Anderson RH, Wilcox BR. The surgical anatomy of ventricular septal defect. J Card Surg 1992;7:17–35.
10. Hagler DJ, Edwards WD, Seward JB, Tajik AI. Standardized nomenclature of the ventricular septum and ventricular septal defects, with applications for two-dimensional echocardiography. Mayo Clin Proc 1985;60:741–752.
11. Schwartz SL, Cao Q, Azevedo J, Pandian NG. Simulation of intraoperative visualization of cardiac structures and study of dynamic surgical anatomy with real time three-dimensional echocardiography. Am J Cardiol 1994;73:501–507.
12. Rivera JM, Siu SC, Handschumacher MD, Lethor JP, Guerrero JL, Vlahakes GJ, Mitchell JD, Weyman AE, King MEE, Levine RA. Three-dimensional reconstruction of ventricular septal defects: validation studies and in vivo feasibility. J Am Coll Cardiol 1994;23:201–208.
13. Salustri A, Spitaels S, McGhie J, Vletter W, Roelandt JRTC. Transthoracic three-dimensional echocardiography in adult patients with congenital heart disease. J Am Coll Cardiol 1995;26:759–767.

14. Vogel M, Ho SY, Buhlmeyer K, Anderson RH. Assessment of congenital heart defects by dynamic three-dimensional echocardiography: methods of data acquisition and clinical potential. *Acta Paediatr* 1995;410(suppl):34–39.

15. Roelandt JRTC, Salustri A, Vletter WB, Nosir Y, Bruining N. Precordial multiplane echocardiography for dynamic anyplane, paraplane and three-dimensional imaging of the heart. *Thoraxcentre J* 1994;6/5:6–15.

16. Bland JM, Altman DG. Statistical methods for assessing agreement between two methods of clinical measurement. *Lancet* 1986;1:307–310.

17. Sharif DS, Huhta JC, Marantz p, Hawkins HK, Yoon GY. Two-dimensional echocardiographic determination of ventricular septal defect size: correlation with autopsy. *Am Heart J* 1989;117:1333–1336.

18. Rupprecht T, Hofbeck M, Singer H, Harms D, Deeg KH, Benson L. Determination of the anatomical size of ventricular septal defects on the basis of hemodynamic data and non invasive assessment of pulmonary to systemic vascular resistance ratio Rp/Rs by Doppler-echocardiography. *Cathet Cardiovasc Diagn* 1991;22:93–99.

19. Fukazawa M, Honda S, Fukushige J, Sunagawa H, Yacui H, Ueda K. To what extent does the size of a ventricular septal defect correlate with hemodynamic data derived from cardiac catheterization? *Br Heart J* 1987;58:19–23.

CHAPTER 6

BIPLANE, OMNIPLANE AND PARAPLANE ECHOCARDIOGRAPHIC ANALYSIS FOR ACCURATE RIGHT VENTRICULAR VOLUME MEASUREMENT: A COMPARISON WITH MAGNETIC RESONANCE IMAGING

Youssef FM Nosir, Maarten H Lequin, Anita Dall'Agata,

Jaroslaw D Kasprzak, Jos RTC Roelandt

With technical assistance of Ron T vanDomburg, Wim B Vletter and René Frowijn

From the Thoraxcenter, Division of Cardiology, Erasmus University Medical Center,

Rotterdam, The Netherlands

Submitted

ABSTRACT

Objectives. We studied both the feasibility and accuracy of right ventricular volume (RVV) measurements by three-dimensional echocardiography (3DE) using magnetic resonance imaging (MRI) as the reference method.

Background. RVV measurement, which has important diagnostic and prognostic value in most cardiac conditions, remains a challenge in clinical practice because of the RV complex shape. By obviating geometric assumptions, 3DE would offer an accurate method.

Methods. 12 patients were examined {2 patients with an atrial septal defect (type II), 8 with ischaemic heart disease and 2 normals}. Precordial acquisition of RV cross-sections to obtain datasets containing the RV was performed at 2-degree rotational intervals with ECG and respiratory gating algorithm. MRI measurements of end-diastolic (ED) and end-systolic (ES) RVV and ejection fraction (EF) were computed by Simpson's rule at 9-mm slice intervals. RVV and EF were calculated from 3DE data sets by (a) biplane modified Simpson's method (BMS), (b) omniplane method (OMN) with long axis views obtained at 22.5° of rotational intervals and by (c) Simpson's method (3DS) with 8 parallel equidistant RV short axis views. The endocardial border was traced manually in all methods.

Results. The mean±SD of ED- and ES-RVV (ml) and EF (%) from MRI were (143±70 and 85±40 and 40±11), from BMS were (140±74, 84±45 and 41±12), from OMN were (141±74 and 87±46 and 38±11) and those from 3DS were (141±72 and 86±44 and 40±12) respectively. There were no significant differences between measurements of RVV and EF obtained from MRI and the 3DE methods. However, there were closer limits of agreement between MRI measurements and both OMN and 3DS methods (±18, ±18 and ±6.6) and (±16, ±16 and ±6.6) than with BMS (±24, ±21 and ±11.8) for ED- and ES RVV and EF respectively. Inter-observer variability measurements of RVV and EF obtained from the 3DE

methods were not significantly different. The interobserver standard error of the estimate (SEE) for ED-RVV, ES-RVV and EF were (7.3, 6.2 and 3.4), (5.1, 3.5 and 2.3) and (4.9, 3.6 and 2.2) for BMS, OMN and 3DS respectively.

Conclusions. Precordial rotational acquisition for 3DE RV reconstruction is feasible. Simpson's method and omniplane analysis provides more accurate and reproducible measurements of RVV and EF than the modified Simpson's method.

INTRODUCTION

Measurement of right ventricular volume (RVV) is challenging because of its complex shape and irregular trabecularised walls. In patients with RV pressure or volume overload conditions, significant shape changes occur.

With quantitative angiography RVV is measured from two perpendicular projections using area length method or Simpson's rule.[1-5] The recording of two perpendicular views by cross-sectional echocardiography is difficult and often impossible. To date only limited data are available with echocardiographic techniques.[6-11]

Three-dimensional echocardiography (3DE) is a recent method that allows the calculation of volumes without the need of geometric assumptions and is therefore an ideal method for RVV calculation. In vitro and in vivo studies have shown that RVV could be accurately calculated by 3DE.[12-14] However, these studies are limited and there is still a need for further validation of 3DE RVV measurements.

Therefore, we studied the feasibility and accuracy of 3DE for calculating RVV with comparison to magnetic resonance imaging.

SUBJECTS and METHODS

Study population.

3DE was performed after magnetic resonance imaging in 12 patients, including 8 with ischaemic heart disease, 2 with an atrial septal defect (type II) and 2 normals. Patients included 10 men; ranging in age from 22 to 45 years with a mean of 31 ± 7.5 years.

Informed verbal consent was obtained from each subject after the procedure was fully explained.

Magnetic resonance imaging

Magnetic resonance imaging (MRI) was performed at 0.5 T (Gyroscan T5-11 Philips Medical Systems, The Netherlands). Axial coronal and sagittal spin-echo views were performed for localization followed by multislice multiphase ECG-triggered T1 weighted fast field echo {repetition time = 800-1200 ms, echo time = 22ms, flip angle = 70°, field of view 240 x 300 mm, slice thickness 9 mm, inter slice gap 0.9 mm, imaging matrix (90 x 128)}. Heart phase interval was 32-39 ms and the number of heart phases 14-32 (median 21).

In every subject the window level and width were selected for the optimal contrast between the relatively hypointense ventricular wall and the relatively hyperintense blood in the ventricular cavity. A short axis view was performed with a coronal and a sagittal survey. On the best images the short axis slices were positioned perpendicular to the interventricular septum.[15] (Fig.1)

RVV measurements were performed off-line on a workstation (Gyroview HR). End-diastole was defined as the time frame with maximal RVV and end-systole was defined as the time frame with minimal RVV. End-diastolic and end-systolic RVV, stroke volume and ejection fraction (EF) were calculated by manual endocardial tracing of the short axis series spanning the RV from the apex to the base.

Three-dimensional Echocardiography

Echocardiographic studies were performed in the 45-degree left recumbent position. A commercially available 3.75 MHz sector scanning transducer (Toshiba Sonolayer SSH-140A system) was used. The basic images for 3DE reconstruction of the RV were acquired by precordial rotational scanning at 2° intervals with ECG and respiratory gating (Echo-scan, TomTec GmbH, Munich, Germany).[16,17]

The operator has to find the central axis around which the imaging plane is rotated to encompass the whole RV cavity. Therefore, in order to locate the transducer position where the RV is maximally visualized, an apical 4-chamber view was first obtained. With this view the central scan axis was aligned with the line connecting the left ventricular apex and the mitral valve. From this position the scan axis is shifted medially in a parallel way until it passes through the tricuspid valve. Then the transducer is slightly rotated to maximally open the RV cavity and to include the RV apex. 90 sequential cut planes are acquired from 0 to 178°, each during a complete cardiac cycle (Fig.2) and images are formatted in their correct rotational sequence according to their ECG phase in conical data sets. To fill the gaps between the images a "trilinear cylindric interpolation" algorithm is used.[18] The end-diastolic (the first frame before tricuspid valve closure) and the end-systolic (the first frame before tricuspid valve opening) phases are selected before starting the processing procedure for subsequent analysis.
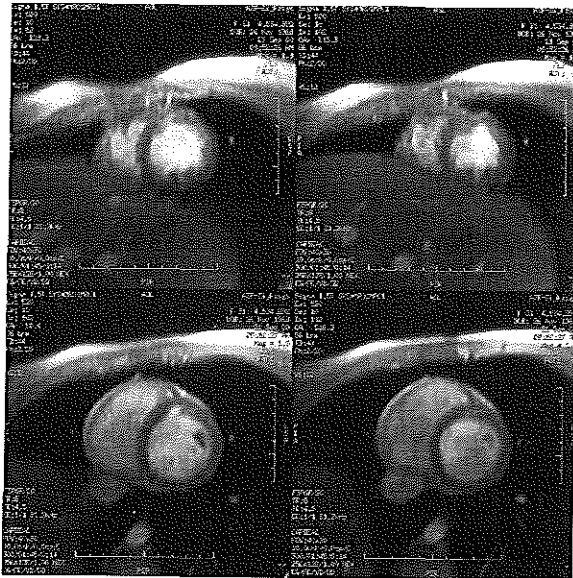
Figure1. Example of equidistant short-axis slices of the right ventricle with magnetic resonance analysis
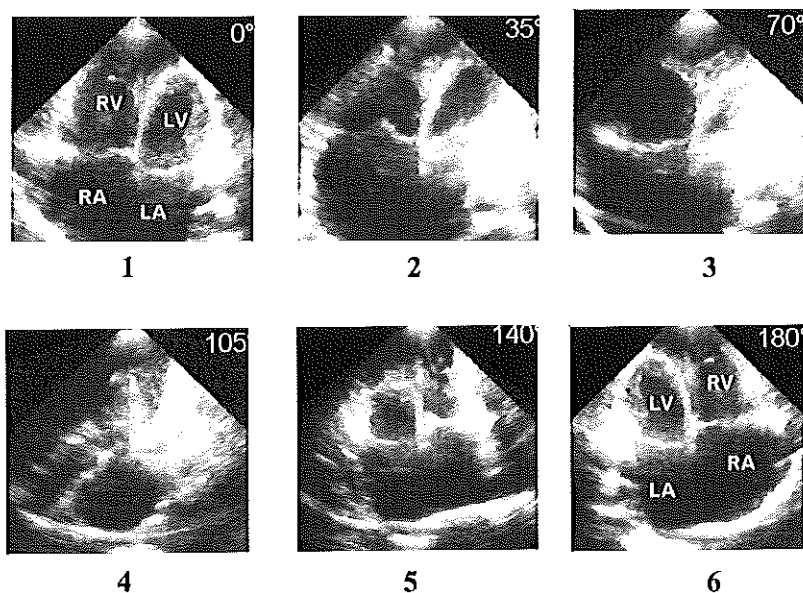
Figure 2. This figure shows the principle of precordial three-dimensional echocardiographic acquisition of the right ventricle at 2° rotational intervals with ECG and respiratory gating technique. From the data set images from 1 to 6 shows the sequence of right ventricular images obtained at 35° of rotational intervals. Figure 6 is a mirror image of figure 1. LA = left atrium, LV = left ventricle, RA = right atrium and RV =right ventricle.

Image analysis

On every conical data set, the best RV long axis view was selected and RVV and EF were calculated by the three following methods:

(A) Biplane modified Simpson's method (BMS)

The best RV 4-chamber view was selected in end-diastolic and end-systolic data sets and the algorithm gives its orthogonal view. RVV and EF were calculated by manual endocardial tracing of the two orthogonal long axis views at end-diastole and end-systole. (Fig.3)

Two experienced observers (YFMN and ADA) blinded to each other's results performed 3DE measurements of RVV and EF. In addition, for each method the two

observers scored for the suitability of the 3DE data for endocardial border identification and

manual tracing.

(A)   (B)
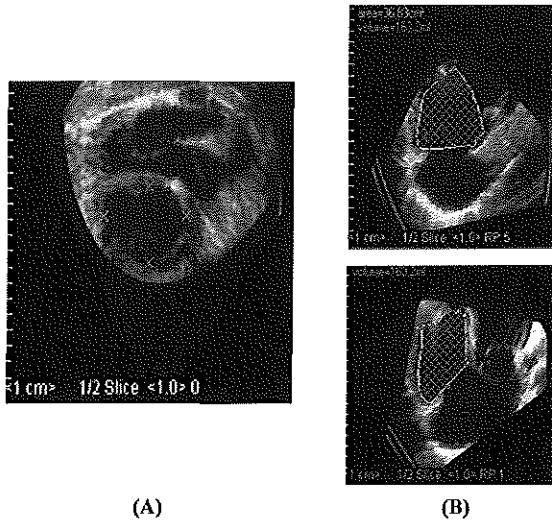
Figure 3. The principle of right ventricular volume measurement by biplane modified Simpson's method. Right ventricular volume is calculated through manual endocardial tracing of the right ventricular cavity at 4-chamber view (lower right) and its computer derived orthogonal view (upper right).

(B) Omniplane method (OMN)

The reference RV long axis view was selected from the end-diastolic and end-systolic

data set (as in the paraplane analysis). With the omniplane analysis, the system gives 8 long axis

views at 22.5° of rotation around the defined best RV long axis. RVV and EF were calculated

by manual endocardial tracing of the reflected 8 long axis views at end-diastole and end-systole.

(Fig.4)

(A)   (B)
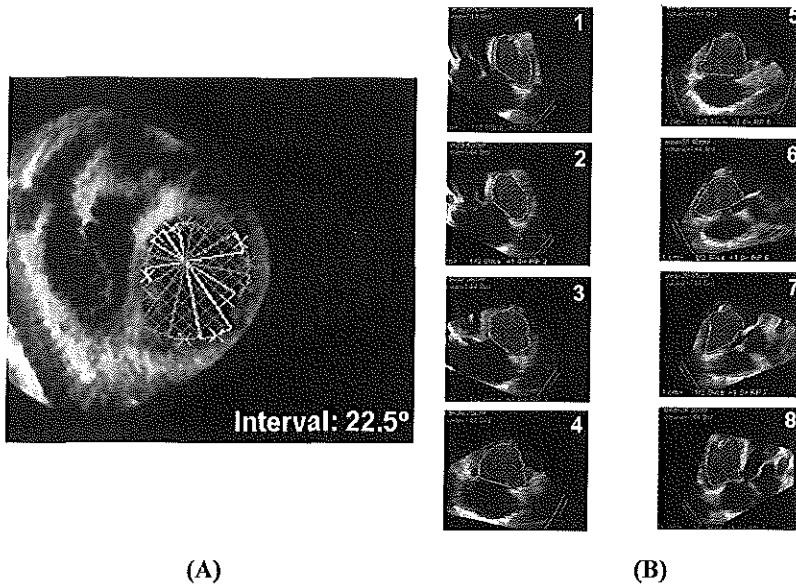
Figure 4. This figure shows the principle of right ventricular volume measurements using the omniplane method. From the three-dimensional echocardiographic data set the reference image is selected with the best right ventricular long axis at 4-chamber view. Around the vertical right ventricular central axis of the reference image, the system gives 8 long axis view at 22.5° of rotational intervals. Panel A shows the segmentation of right ventricular reference cross section around its central axis, to give rise to the 8 long axis views (panel B). Right ventricular volume is calculated by manual endocardial tracing of the 8 right ventricular long axis views at end-diastole and end-systole (panel B).

(C) Paraplane (Simpson's) method (3DS)

From the data set the image with the longest RV long axis was selected. With the paraplane analysis we generate a series of 8 parallel equidistant short axis slices from the apex to tricuspid annulus. The endocardial borders of these short axis slices at end-diastole and end-systole were manually traced and RVV and EF were calculated by Simpson's rule. [19] (Fig.5)

(A) (B)
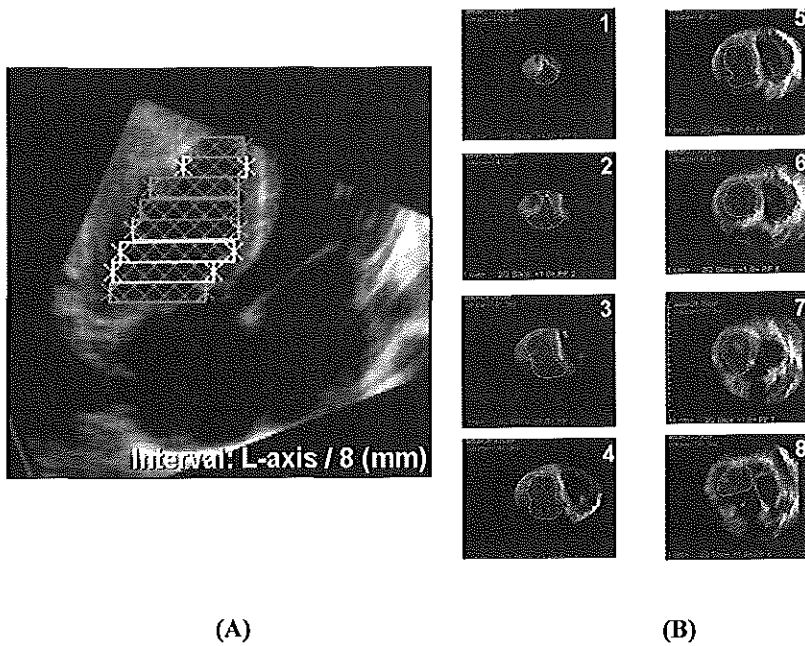
Figure 5. The principle of right ventricular volume measurements using Simpson's rule. The right ventricle is sliced by the paraplane analysis into 8 equidistant parallel short axis slices that spanning the right ventricular cavity from the apex to tricuspid annulus (panel A). The surface area of each cross-section is measured by planimetry and the volume of each slice is calculated by adding the voxels included in the traced area. Adding up the volume of all slices (1 to 6) provide the volume measurement of right ventricle at end-diastole and end-systole.

Statistical analysis.

RVV and EF measurements from magnetic resonance imaging and the 3DE methods were performed independently and expressed as mean±SD. Interobserver variability of the 3DE methods was calculated and expressed as the standard error of the estimate (SEE).

Paired student t-test was performed to compare RV measurements obtained from each 3DE method and measurements obtained from magnetic resonance imaging (the reference standard). Significance was stated at 0.05 probability level. The limits of agreement were

calculated by the method described by Bland and Altman.[20] Pearson correlation coefficient was also presented.

RESULTS

3DE acquisition could be performed in all patients recruited in this study. All patients were in sinus rhythm with a mean heart rate of 78 ± 12 b/m. With the paraplane method the mean $\pm$ SD (mm) of slice thickness was 8.2 ± 0.8 and 6.9 ± 0.6, for end-diastole and end-systole respectively. The echocardiographic observers scored the adequacy of RV views obtained from both paraplane and omniplane analysis of the 3DE data sets, for endocardial border identification and manual tracing (Table I).

TABLE1

	Scoring				Preferred	Equally good
	a	b	c	d		
Paraplane	3	4	5	-	4	3
Omniplane	3	4	5	-	5	3

a = very good, b = good, c = moderate and d = poor quality

Table I. Observer scoring for the suitability of right ventricular (RV) paraplane (3DS) and omniplane (OMN) views obtained from 3DE data sets for manual endocardial tracing.

Right ventricular volume calculation

The mean $\pm$ SD of RVV and EF calculation for magnetic resonance imaging and the 3DE methods are presented in Table II. Interobserver measurements of RVV and EF obtained from 3DE biplane, omniplane and paraplane methods were not significantly different. Interobserver variability measurements for paraplane and omniplane methods were comparable and smaller than that for biplane modified Simpson's method. The interobserver

standard error of the estimate (SEE) for end-diastolic, end-systolic RVV and EF were (7.3, 6.2 and 3.4), (5.1, 3.5 and 2.3) and (4.9, 3.6 and 2.2) for biplane, omniplane and paraplane methods respectively.

	EDV				ESV				EF			
	Mean±SD	p	r	Agreem.	Mean±SD	p	r	Agreem.	Mean±SD	p	r	Agreem.
MRI	143.3±70.2				84.8±39.8				40.3±10.8			
BMS (Y)	140.4±73.9	0.4	0.99	2.9±23.8	84.0±45.2	0.8	0.98	0.8±20.6	40.6±11.8	0.98	0.87	-0.3±11.8
(A)	130.8±84.3	0.1	0.98		76.2±44.4	0.1	0.93		40.6±12.6	0.9	0.86	
OMN (Y)	140.7±74.4	0.3	0.99	2.7±18.4	87.2±45.6	0.4	0.99	-2.4±17.8	38.4±11.3	0.1	0.96	1.9±6.6
(A)	144.8±87.5	0.9	0.96		87.2±52.2	0.7	0.90		39.8±12.4	0.8	0.90	
3DS (Y)	141.4±71.8	0.4	0.99	2.8±16.2	85.7±43.5	0.7	0.99	-0.1±15.8	39.5±11.6	0.3	0.98	1.2±6.6
(A)	139.8±84.8	0.5	0.98		85.6±52.0	0.9	0.96		39.8±12.5	0.8	0.92	

Agreem. = limits of agreement, BMS = biplane modified Simpson's method, OMN=omniplane method. 3DS=Simpson's method. ED- = end-diastole, EF = ejection fraction, ES- = end-systole, p = p value. r = correlation coefficient. MRI=magnetic resonance imaging, RVV=right ventricular volume.

Table II. Comparison of RVV and EF measurements obtained from MRI (reference standard) and 3DE methods (3DS, OMN and BMS).

Comparison between three-dimensional echocardiography and magnetic resonance imaging for right ventricular volume calculation

3DE methods had good correlation, nonsignificant differences and close limits of agreement with magnetic resonance imaging for calculating RVV and EF (Table II, Fig.6).

Comparison between three-dimensional echocardiographic methods for right ventricular volume calculation

The comparison between measurements of RVV and EF obtained from each two 3DE methods was presented in Table III.

	EDV			ESV			EF		
	P	*r*	Agreem.	*p*	*r*	Agreem.	*p*	*r*	Agreem.
3DS-OMN	0.1	0.99	-2.1±6.8	0.2	0.99	-2.3±4.2	0.3	0.99	0.3±2.2
3DS-BMS	0.4	0.99	-1.8±14.6	0.6	0.99	0.8±13.2	0.1	0.95	-1.8±7.6
OMN-BMS	0.9	0.99	0.3±12.0	0.1	0.99	3.2±12.4	0.1	0.94	-2.2±8.2

All abbreviations as in tables II.

Table III. Comparison between measurements of RVV and EF obtained from each two three-dimensional echocardiographic method.
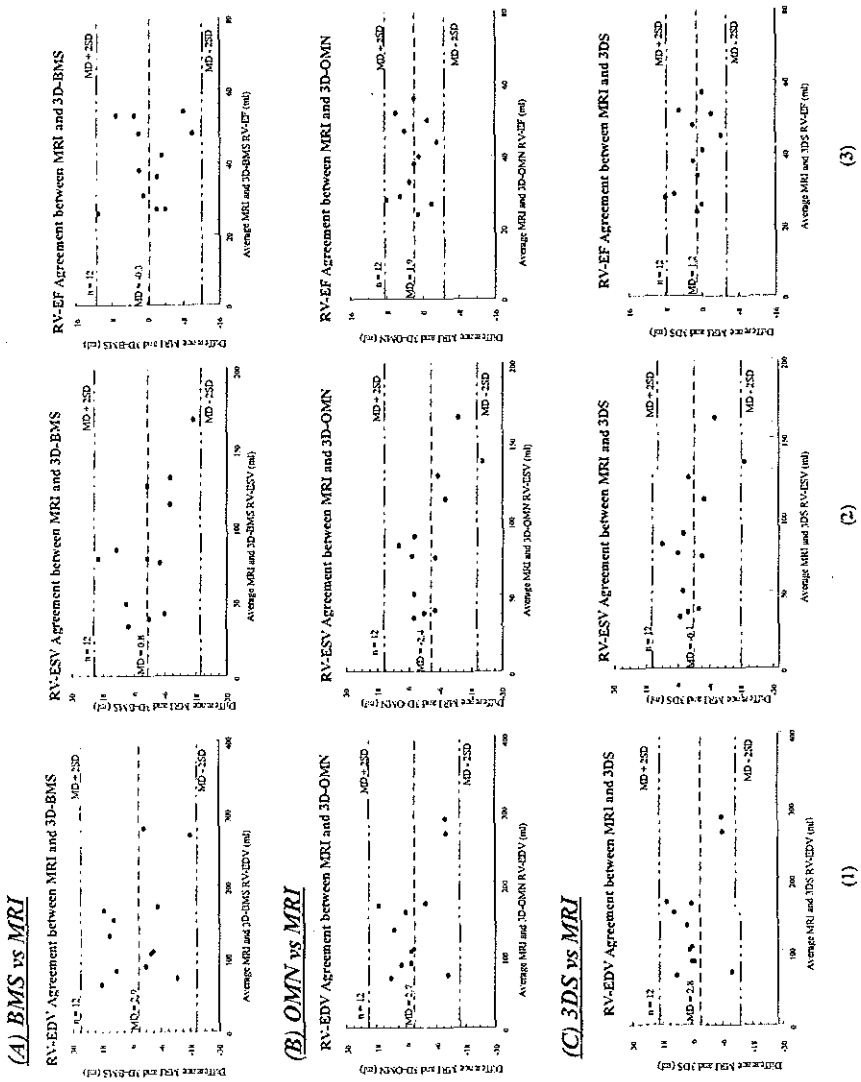
Figure 6. The limits of agreement between three-dimensional echocardiographic methods (Simpson's method=panel A, Omniplane method=panel B and Biplane modified Simpson's method=panel C) and magnetic resonance imaging (reference method) for calculating right ventricular end-diastolic volume (1), end-systolic volume (2) and ejection fraction (3)

DISCUSSION

RVV and function determination is important for patient management in most cardiac conditions when corrective surgery is considered. In chronic obstructive lung disease and RV infarction, serial determination of RV function is helpful in evaluating severity of the disease and the therapeutic response.

However, RV is difficult to study because of its asymmetric shape and trabeculated structure and therefore defies description in terms of a simple geometric model. In addition, any such simple model would have to allow for the changes RV shape in response to volume and pressure load conditions.[21] Consequently, many different approaches has been proposed and RVV is not routinely calculated.[1-5]

Our results demonstrate that 3DE allows accurate and reproducible measurements of RVV and function. Among the three analytic methods, paraplane and omniplane methods have comparable measurement accuracy, when compared with magnetic resonance imaging. They are more reproducible, as they have smaller interobserver variability than the biplane approach. When RV measurements obtained from the 3DE methods were compared together, paraplane and omniplane methods had closer limits of agreement than when they were compared with the biplane method (Table III).

Assessment of RVV and function by the biplane method is based on geometric assumptions. This explains why the accuracy and reproducibility for the assessment of RV function is not as good as the paraplane and omniplane methods which corrects better for shape abnormalities. Therefore, omniplane and paraplane analysis provides more accurate results. The mean ±SD of slice thickness with the paraplane analysis, using 8 short axis slices, were within the recommended limits previously reported.[18,19]

Our results are in agreement with those obtained by Vogel et al.[12] He compared RVV obtained by 3DE with values obtained from magnetic resonance imaging in 16 patients and found a good correlation (r = 0.95 and 0.87), and close limits of agreement (-3.5 to 12.5 ml, and –4.0 to 16.4 ml) for calculating end-diastolic and end-systolic RVV respectively. In addition, 3DE had small interobserver variability (4.3% and 4.5%) for calculating end-diastolic volume and end-systolic volume respectively.

Technical difficulties and study limitations

Paraplane and omniplane methods show comparable scoring of technical difficulties from the two observers, concerning the endocardial border identification and manual tracing. Manual endocardial border tracing was better in the paraplane derived short axis slices in 4 patients, while the long axis views obtained through the omniplane analysis scored better in 5 patients. Both methods allowed equally good tracing in 3 patients. Areas of echocardiographic dropout, particularly from surfaces that are nearly parallel to the imaging beam, generate error. Endocardial border tracing of the RV short axis views (particularly at RV free wall) or long axis views (particularly at the RV apex) is more difficult in patients with a dilated RV.

Finding the proper scanning window for rotational acquisition that encompassing the whole RV is difficult. Most successful was the procedure where the transducer is placed over the apex to obtain the apical 4-chamber view and shift the rotational scan axis medially until it passes through the tricuspid valve. Then the transducer is slightly rotated to maximally open the RV cavity and to include the RV apex.

This study includes small number of patients mostly with no right-sided heart disease (only 2 patients with ASD type II). RV endocardial borders were traced manually: this is

laborious and time consuming. In future, applying an automated border detection algorithm for area and volume analysis will reduce the analysis time.

CONCLUSIONS

Precordial 3DE reconstruction of RV is feasible. Paraplane and omniplane analysis produces more accurate and reproducible measurements of RVV and EF than that of biplane modified Simpson's method when compared to magnetic resonance imaging. Therefore, they are recommended for serial noninvasive assessment of RV function.

REFERENCES

1. Ferlinz J, Gorlin R, Cohn PF, Herman MV. Right ventricular performance in patients with coronary artery disease. Circulation 1975;52:608-15.
2. Felinz J. Measurements of right ventricular volumes in man for single plane cineangiograms. Am Heart J 1977;94:87-90.
3. Fischer EA, DuBraw IW, Hastreiter AR, Right ventricular volume in congenital heart disease. Am J Cardiol 1975;36:67-75.
4. Gentzler RD, Briselli MF, Gault JH. Angiographic estimation of right ventricular volume in man. Circulation 1974;50:324-30.
5. Graham TP, Jamakani JM, Arwood GF, Canent RV,. Right ventricular volume determination in children. Circulation 1973;47:144-53.
6. Chaundery KR, Ogawa A, Pauletto FJ, Hubbard FE, Dreifus LS. Biplane measurement of left and right ventrular volumes using wide angle cross-sectional echocardiography (abstract). Am J Cardiol 1978;41:391.
7. Levine RA, Gipson TC, Aretz T, Gillam LD, Guyer DE, King ME, Weyman AE. Echocardiograhic measurement of right ventricular volume. Circulation 1984;69:497-505.
8. Starling MR, Crawford MH, Sorensen SG, O,Rourke A. Anew two-dimensional echocardiographic technique for evaluating right ventricular size and performance in patients with obstructive lung disease. Circulation 1982;66:612-20.

9. Wann SL, Stickels KR, Bamrah VS, Gross CM. Digital processing of contrast echocardiograms: a new technique for measuring right ventricular ejection fraction. Am J Cardiol 1984;53:1164-8.

10. Ninomiya K, Duncan WJ, Cook DH, Olley PM, Rowe RD. Right ventricular ejection fraction and volumes after Mustard repair: correlation of two-dimensional echocardiograms and cineangiograms. Am J Cardiol 1981;48:317-24.

11. Watanabe T, Katsume H, Matsukubo H, Furukawa K, Ijichi H. Estimation of right ventricular volume with two-dimensional echocardiography. Am J Cardiol 1982;49:1946-53.

12. Vogel M, Gutberlet M, Dittrich S, Hosten N, Lange PE. Comparison of transthoracic three-dimensional echocardiography with magnetic resonance imaging in the assessment of right ventricular volume and mass. Heart 1997;78:127-30.

13. Pini R, Giannazzo G, Di Bari M, Innocenti F, Rega L, Casolo G, Devereux RB. Transthoracic three-dimensional echocardiographic reconstruction of left and right ventricles; in vitro validation and comparison with magnetic resonance imaging. Am Heart J 1997;133:221-9.

14. Jiang L, Siu S, Handschumacher MD, Guererro JL, de Prada JAV, King ME, Picard MH, Weyman AE, Levine RA. Three-dimensional echocardiography in vivo validation for right ventricular volume and function. Circulation 1994;89:2342-50.

15. Nosir YFM, Lequin MH, Kasprzak JD, vanDomburg RT, Vletter WB, Yao J, Stoker J, Ten Cate FJ, Roelandt JRTC. Measurements and day to day variabilities of left ventricular volumes and ejection fraction by three-dimensional echocardiography and comparison with magnetic resonance imaging. Am J Cardiol 1998;82:209-214.

16. Roelandt J, Salustri A, Vletter W, Nosir Y, Bruining N. Precordial multiplane echocardiography for dynamic anyplane, paraplane and three-dimensional imaging of the heart. Thoraxcentre J 1994;6:4-13.

17. Salustri A, Roelandt J. Ultrasonic three-dimensional reconstruction of the heart. Ultrasound in Med & Biol 1995; 21:281-93.

18. Nosir YFM, Salustri A, Vletter WB, Boersma E, Salustri A, Tjoa Postma J, Reijs AEM, Ten Cate FJ, Roelandt JRTC. Accurate measurements of left ventricular ejection fraction by three-dimensional echocardiography: a comparison with radionuclide angiography. Circulation 1996;94:460-6.

19. Nosir YFM, Stoker J, Kasprzak JD, Lequin MH, Dall'Agata A, Ten Cate FJ, Roelandt JRTC. Paraplane analysis from precordial three-dimensional echocardiographic data sets for rapid

and accurate quantification of left ventricular volume and function: a comparison with magnetic resonance imaging. Am Heart J 1999;137(1):134-43.

20. Altman DG, Bland JM. Measurement in medicine: the analysis of method comparison studies. Statistician 1983;32:307-17.

21. Aebischer NM, Czegledy F. Determination of right ventricular volume by two-dimensional echocardiography with a crescentic model. J Am Soc Echo 1989;2:110-8.

CHAPTER 7

USE OF THREE-DIMENSIONAL ECHOCARDIOGRAPHY FOR ANALYSIS OF OUTFLOW OBSTRUCTION IN CONGENITAL HEART DISEASE

Use of Three-Dimensional Echocardiography for Analysis of Outflow Obstruction in Congenital Heart Disease

Anita Dall'Agata, MD, Adri H. Cromme-Dijkhuis, MD, PhD, Folkert J. Meijboom, MD, PhD, Silja E.C. Spitaels, MD, PhD, Jackie S. McGhie, BSc, Jos R.T.C. Roelandt, MD, PhD, and Ad J.J.C. Bogers, MD, PhD

To evaluate the feasibility and accuracy of 3-dimensional (3D) echocardiography in analysis of left and right ventricular outflow tract (LVOT and RVOT) obstruction, 3D echocardiography was performed in 28 patients (age 4 months to 36 years) with outflow tract pathology. Type of lesion and relation to valves were assessed. Length and degree of obstruction were measured. Three-D data sets were adequate for reconstruction in 25 of 28 patients; 47 reconstructions were made. In 13 patients with LVOT obstruction, 3D echocardiography was used to study subvalvular details in 8, valvular in 13, and supravalvular in 1. Four of these 13 patients had complex subaortic obstruction. In 12 patients with RVOT lesions, 3D echocardiography was used to study subvalvular details in 11, valvular in 12, and supravalvular in 2. Three-dimensional reconstructions were suitable for analysis in 100% of subvalvular LVOT, 77% valvular LVOT, 100% supravalvular LVOT, 100% subvalvular RVOT, 50% valvular RVOT, and 50% supravalvular RVOT. Twenty patients underwent operation, and surgical findings served as morphologic control for thirty-four 3D reconstructions (LVOT 17, RVOT 17). Operative findings revealed an accuracy at subvalvular LVOT of 100%, valvular LVOT 90%, supravalvular LVOT 100%, subvalvular RVOT 100%, valvular RVOT 100%, and supravalvular RVOT 100%. Quantitative measurements could adequately be performed. Three-D echocardiography is feasible and accurate for analyzing both outflow tracts of the heart. Particularly, generation of nonconventional horizontal cross sections allows a good definition of extension and severity of lesions. ©1999 by Excerpta Medica, Inc.

(Am J Cardiol 1999;83:921–925)

Congenital obstruction of both the left and right ventricular outflow tract (LVOT and RVOT) may be located at the subvalvular, valvular, or supravalvular level and may occur at multiple levels.[1,2] These obstructions are usually well displayed by 2-dimensional (2D) echocardiography, and often no additional investigation is required before surgical intervention.[3-10] However, the information obtained by cross-sectional echocardiography does not give a perception of the depth. Consequently, the true nature of the obstruction may be difficult to perceive. Three-dimensional (3D) echocardiography generates nonconventional cross sections and a display in a realistic perspective, thereby providing additional information.[11] However, data on the in vivo assessment of outflow tract obstructions with 3D echocardiography are limited and scanty and are not validated by anatomic findings.[12-14]

Our study evaluates whether 3D echocardiography is able to define outflow pathology in detail and to provide information that could be helpful in directing

the surgical approach. Morphologic accuracy is obtained by comparison with surgical findings.

METHODS

Patients: Twenty-eight patients (23 male and 5 female, age range 4 months to 36 years), with a previous diagnosis of pathology of the outflow tract by 2D echocardiography, were studied. The 2D studies were independently performed and analyzed by the attending pediatric cardiologist, blindly with regard to 3D data. Fifteen patients had anomalies of the LVOT all at 1 level. Ten patients had subvalvular obstruction, 4 valvular, and 1 supravalvular. Thirteen patients had anomalies of the RVOT at only 1 level in 4 and at multiple levels in 9. Ten patients had subvalvular obstruction, 7 valvular, and 2 supravalvular.

Three-dimensional echocardiography: Three-D echocardiographic acquisition was done with a Toshiba SSH 140-A (Toshiba, Otawara-Shi, Japan) or an HP 1500 (Hewlett-Packard, Andover, Massachusetts). The video output was interfaced to the Echo-scan 3.0 3D reconstruction system (TomTec, Munich, Germany).[15] Eighteen patients were studied by transesophageal approach under general anesthesia before surgery, and 10 patients by transthoracic approach. Transesophageal acquisition was performed with a 5-MHz multiplane probe. The Minimulti miniaturized 5-MHz multiplane probe with 48 elements (Oldelft, Delft, The Netherlands) was used in children. The
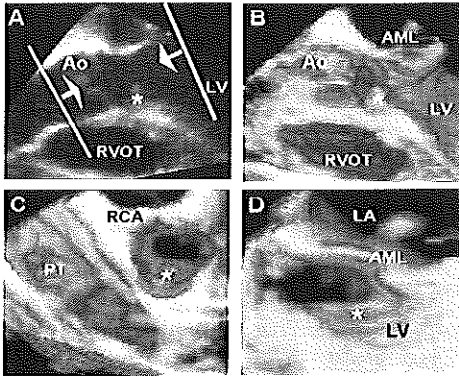
FIGURE 1. Any-plane and volume-rendered reconstructions of a discrete subaortic obstruction of the LVOT. A, cut-planes taken through a 3D data set; B, volume-rendered representation of the obstruction along a computer-generated long-axis view; C, seen as looking from the aortic valve (Ao); D, seen as looking from the left ventricle and looking toward the outflow tract. AML = anterior mitral leaflet; LA = left atrium; LV = left ventricle; PT = pulmonary trunk; RCA = right coronary artery; RVOT = right ventricular outflow tract.

probe was placed in the midesophageal level. LVOT and portions of the aortic valve were visualized in the longitudinal axis centering the image at 120° to 135°. From a slightly more cranial position, centering the image at 70° to 100°, the whole length of the RVOT with the pulmonary valve and the anterolateral free wall of the right ventricle was displayed, usually together with the septal leaflet of the tricuspid valve. Transthoracic acquisition was performed with a 3.5-MHz probe. Images were derived from either the parasternal or apical window for evaluation of the LVOT and from the subcostal position for evaluation of the RVOT. When the region of interest was adequately in view, a rotation sequence was performed to confirm that the conical volume was well directed and to optimize the gain setting of the echo machine. The images for 3D reconstruction were acquired with rotational scanning at 2° intervals for 90 steps using echocardiographic and end-expiration gating. The acquired images were stored and processed off-line.[15]

Morphologic and quantitative analysis: Reconstructions from the 3D data sets were independently analyzed with any plane mode[12] by 2 observers (A.D., J. McG.). The outflow tract was displayed along its longitudinal axis and in horizontal cross sections at different angles and distance, from above the annulus of the semilunar valve and from below the obstruction, by scanning the data set. Volume-rendering algorithms, threshold, and opacity were applied on the 2D computer-generated cut-planes (Figure 1).[15] From the volume-rendered reconstructions, the morphology of the subvalvular obstruction, its extension, and relation to valves were assessed. Aortic and pulmonary valves were imaged from a computer-generated short-axis view, which allowed for identification of the

number of cusps, the fusion of the commissures, and the presence of calcification.

The obstruction was reconstructed, and the length of obstruction, the distance from the aortic or pulmonary valve (if appropriate), and the degree of obstruction in relation to body surface area (BSA) were calculated. Length and distance from the semilunar valves were measured from a selected 2D computer-generated long-axis image, in which the maximal extension of the lesion was displayed. To estimate the degree of obstruction, electronic parallel slicing (paraplane echocardiography) of the outflow tract perpendicular to its vertical axis was performed. For the LVOT the first cut-plane was positioned at the hinge point of the anterior mitral valve leaflet and the last one at the point of coaptation of the mitral leaflets and for the RVOT at the pulmonary annulus level and at the trabecula septomarginalis, respectively. The corresponding 2D images were displayed, and the smallest luminal diameter and cross-sectional area of the obstruction were measured (Figure 2) at the onset of ventricular systole, defined as the first frame during the cardiac cycle in which the atrioventricular valve appears closed.

All results are expressed as mean ± SD.

RESULTS

Three-dimensional echocardiography: Three-dimensional data sets were adequate for analysis in 25 of 28 patients (89%). In the other 3, analysis was not possible due to inadequate gain settings in 2 patients with subvalvular LVOT obstruction and to large image artifacts in 1 patient with subvalvular RVOT obstruction. From these twenty-five 3D data sets, 47 reconstructions were made. Agreement between the 2 observers on morphologic assessment of the 3D reconstructions was complete.

Subvalvular left ventricular outflow tract obstruction: In 8 patients a reconstruction of this area was made, and all were suitable for analysis (feasibility 100%) (Table I). In 5 patients the obstruction was a discrete subaortic stenosis (Figure 1). In 4 of these the membrane extended to the mitral valve and onto the septum. This was demonstrated in a horizontal cross section, looking from the left ventricle toward the LVOT and from computer-generated long-axis views. In these 5 data sets the smallest LVOT area was 0.6 ± 0.3 cm² (range 0.3 to 1.0) and area/BSA 0.9 ± 0.5 cm²/m² (range 0.3 to 1.5). The smallest LVOT diameter was 0.6 ± 0.1 cm (range 0.5 to 0.7). The obstruction length was 1.6 ± 1.1 cm (range 0.6 to 1.8). The distance from the obstruction to the aortic valve was 0.7 ± 0.6 cm (range 0 to 1.6). In 1 patient with transposition of the great arteries, the protrusion of an aneurysmatic interventricular septum into the LVOT was visualized. In 2 patients the obstruction was caused by hypertrophic cardiomyopathy. Views from above through the aortic valve appreciated the amount of septum obstructing the outflow tract. The 2 patients with hypertrophic cardiomyopathy did not have surgery. In the other 6, morphologic findings from the 3D data sets were confirmed at surgery (accuracy 100%,
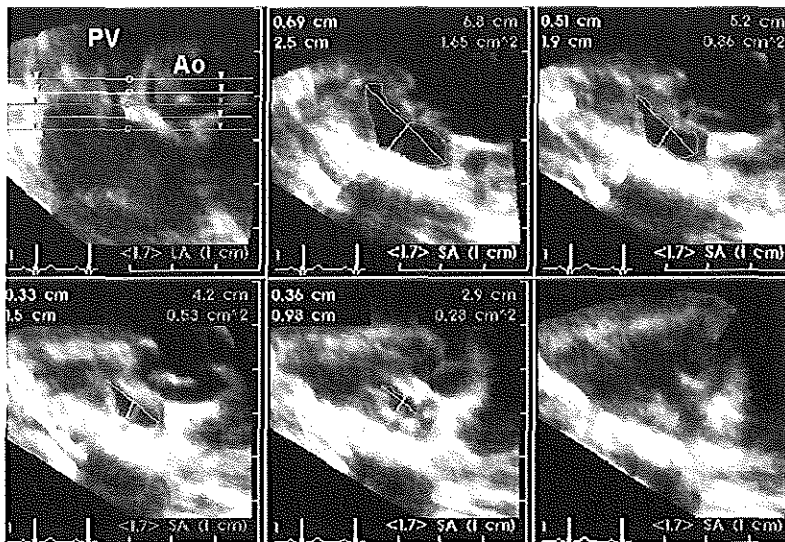
FIGURE 2. Five parallel and equidistant cut-planes (top left level panel) are taken through the right ventricular outflow tract to obtain horizontal cross sections. The luminal area, the outflow area, and the diameters are automatically calculated after free-hand tracing. The horizontal cross sections show the true shape of the lumen of outflow tract and, therefore, the smallest area can be detected and calculated without mathematical assumptions. Ao = aortic valve, PV = pulmonary valve.

Outflow Tract Level	Feasibility	Accuracy
TABLE I Feasibility and Morphologic Accuracy of 3-Dimensional Reconstruction of Both Left and Right Ventricular Outflow Tract		
LVOT		
Subvalvular	(8/8) 100%	(6/6) 100%
Valvular	(10/13) 77%	(9/10) 90%
Supravalvular	(1/1) 100%	(1/1) 100%
RVOT		
Subvalvular	(11/11) 100%	(11/11) 100%
Valvular	(6/12) 50%	(6/6) 100%
Supravalvular	(1/2) 50%	(2/2) 100%

Table I), providing time needed for intraoperative exploration.

Valvular aortic level: In 10 of 13 3D reconstructions, the information was adequate for analysis (feasibility 77%, Table I). Three valves were analyzed as bicuspid. The 7 remaining valves were tricuspid, and in 4 of them thickened and dysplastic cusps were found. Calcified deposits were visualized in 2 valves. Diameter measurements could be done in 12 data sets. Aortic annular area was 5.5 ± 3.0 cm^2 (range 2.0 to 8.2), the area/BSA 3.5 ± 1.1 cm^2/m^2 (range 2.2 to 5.0). The smallest aortic valve diameter was 2.3 ± 0.8 cm (range 1.0 to 3.8). All 10 patients with adequate 3D data sets underwent operation. All tricuspid valves with the described details were confirmed, but only 2 bicuspid valves were confirmed (accuracy 90%, Table I). The false-positive diagnosis of a bicuspid valve was due to a foreshortened rotation.

Supravalvular aortic stenosis: In the only patient with a supravalvular stenosis, the 3D data set was suitable for analysis (Table I). The stenosis was displayed from above, simulating an aortotomy. A fibrous ring was shown, closely related to the commissural top, at 16 mm from the hinge points of the aortic cusps. These findings were confirmed at surgery (Table I).

Subvalvular right ventricular outflow tract obstruction: Three-dimensional subvalvular RVOT reconstructions were made in 11 patients. All were suitable for analysis (feasibility 100%, Table I). In 6 the obstruction was located in the infundibulum and was of the fibromuscular type. The smallest RVOT area was 0.6 ± 0.6 cm^2 (range 0.2 to 1.8), the area/BSA 1.6 ± 1.6 cm^2/m^2 (range 0.4 to 4.0). The smallest RVOT diameter was 0.5 ± 0.1 cm (range 0.3 to 0.6). The obstruction length was 1.8 ± 0.3 cm (1.3 to 2.6). The distance of the obstruction from the pulmonary valve was 0.4 ± 0.3 cm (0.1 to 0.8). In 3 patients the infundibulum was hypoplastic. In 1 patient a midventricular dynamic stenosis was found. In 1 patient a large trabecula septomarginalis was well visualized and led to the diagnosis of double-chambered right ventricle. This was not diagnosed on 2D echocardiography (Figure 3). All 11 patients underwent surgical correction, and in all, the 3D reconstructed findings were confirmed (accuracy 100%, Table I), thus allowing for a reduction in the time needed for intraoperative exploration.

Pulmonary valvular level: The pulmonary valve was reconstructed in 12 patients. In 8 three-dimensional data sets, leaflets showed adequate echo density to be
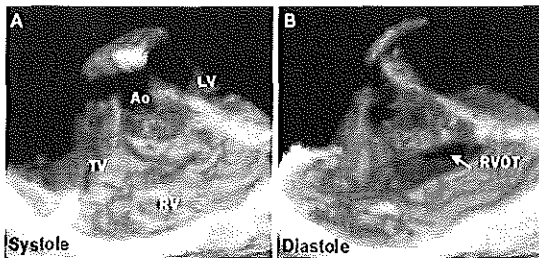
FIGURE 3. View from below right ventricular outflow. In this patient a hypertrophic trabecula septomarginalis is transsepting the ventricle, creating a double-chambered right ventricle. RV = right ventricle; TV = tricuspid valve; other abbreviations as in Figure 1.
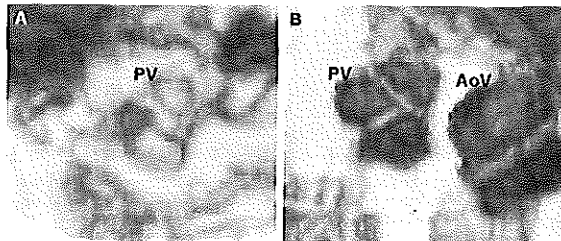

FIGURE 4. Horizontal cross sections of pulmonary valves (PV) displayed with volume-rendering algorithms. A, example of a bicuspid and stenotic pulmonary valve; B, example of a tricuspid pulmonary valve and its relation to the aortic valve, which is bicuspid. Abbreviations as in Figures 1 and 2.

identified, but this was sufficient for analysis only in 6 (feasibility 50%, Table I). Three tricuspid and 2 bicuspid valves were identified as such (Figure 4). In 1 case a small mobile vegetation was identified. Measured in 10 data sets, the pulmonary annular area was 1.3 ± 0.9 cm^2 (range 0.3 to 2.8), area/BSA 3.9 ± 4.3 cm^2/m^2 (0.6 to 15). The smallest valve diameter was 1.1 ± 0.3 cm (range 0.6 to 1.7). All 6 patients with analyzed pulmonary valves underwent operation. The anatomic findings from the 3D data sets were all confirmed during surgery (accuracy 100%, Table I).

Supravalvular pulmonary stenosis: In the 2 patients with a supravalvular pulmonary stenosis, a 3D data set was constructed, but in 1 the obstruction was not optimally visualized due to inadequate lateral resolution (feasibility 50%, Table I). Both patients underwent operation, and the 3D findings were confirmed during surgery (accuracy 100%, Table I).

DISCUSSION

Indications for surgical therapy are based on clinical and hemodynamic parameters, and data in this regard are now obtained by 2D and Doppler echocardiography rather than cardiac catheterization.[4-9] The success rate of the outcome after surgery depends on the nature of the morphology and the adequacy of surgical correction.[1,2,16,17] The surgical approach needs excellent exposure and should avoid inadvertent damage. The approaches to the LVOT through the

aorta and to the RVOT through the pulmonary root or the right atrium do not always offer an ideal presentation of the site and extension of obstruction. This may lead to inadequate correction or more extensive surgery. Therefore, it is important to obtain complete data on the morphology before surgical repair.

We demonstrated that 3D reconstruction of both LVOT and RVOT is feasible, either by transthoracic or the transesophageal approach, and may offer advantages by providing more realistic information with depth perception. Horizontal cross sections above the aortic valve, simulating a surgical aortotomy, provide information on the shape of the lesion and on its distance from the semilunar valve. Views looking to the LVOT from below the obstruction allow for evaluation of its extension into the ventricle and its relation to the septum and to the ventricular surface of the anterior mitral valve leaflet, providing, in particular, a more accurate and realistic depiction of the complex lesions.[12] Volume-rendered reconstructions display the opening patterns of the aortic valve, the movement of the cusps, visualize their surface, give a better delineation of the cusp edges, and have an advantage for the diagnosis of bicuspid aorta and of vegetations.[18,19] However, differentiation between fibrotic and calcified lesions using volume-rendering algorithms is operator dependent, and the any-plane modality should be used.[18] Moreover, considering the time needed for 3D reconstruction of the aortic valve, its practical use and clinical relevance are not clear.

It appears from our study that reconstruction RVOT is feasible and accurate. Any cross-section of the RVOT can be obtained from the data set. The depth perception has the advantage to comprehend better the underlying anatomy of the right ventricle and the relation to the tricuspid valve, being an advantage over 2D echocardiographic examination. However, contrary to LVOT obstructive lesions, volume-rendered imaging of the pathology from above or from below the obstruction was difficult to interpret and did not add anatomic information. Our study demonstrates the possibility of creating dynamic horizontal cross sections of the pulmonary valve and of evaluating the number of cusps, the area or circumference, and the diameters of the annulus. Although the short axis of the annulus could be reconstructed in all but 1 patient, the capability of imaging the leaflets is highly dependent on their original echo density. Moreover, because all patients with RVOT lesions had a Fallot-type anomaly, the small size of the pulmonary valve and the pulmonary artery also influenced the reconstruction, since the resolution was insufficient.

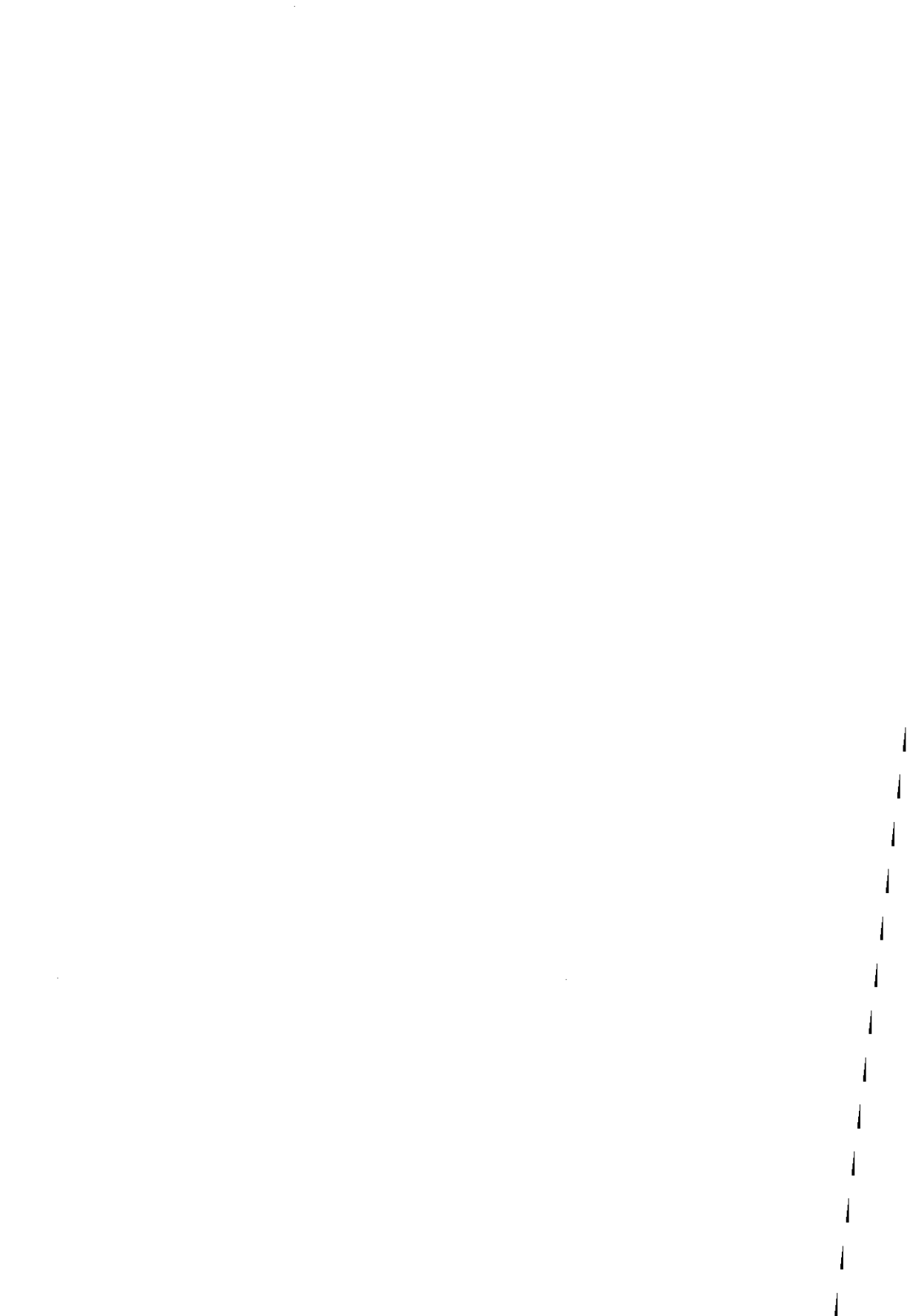Three-dimensional echocardiography makes it pos-

sible to obtain a data set that can be scanned to determine the smallest luminal area and the degree of obstruction, as well as its length. Extension and severity of the outflow tract lesion are adequately characterized and may provide data that allow a more specified surgical approach. With regard to assessment of the outflow tract after operation, further studies should be undertaken.

In conclusion, 3D echocardiography allows adequate assessment of both LVOT and RVOT, providing a more realistic visualization. It provides additional information for a more complete diagnosis, as well as for surgical planning.

1. Choi JY, Sullivan ID. Fixed subaortic stenosis: anatomical spectrum and nature of progression. *Br Heart J* 1991;65:280–286.
2. Kirklin JW, Barratt-Boyes BG. Cardiac Surgery. 2nd ed. New York: Churchill Livingstone, 1993.
3. Berry TE, Aziz KU, Paul MH. Echocardiographic assessment of discrete subaortic stenosis in childhood. *Am J Cardiol* 1979;43:957–961.
4. Motro M, Schneeweiss A, Shem Tov A, Vered Z, Hegesh J, Neufeld HN, Rath S. Two-dimensional echocardiography in discrete subaortic stenosis. *Am J Cardiol* 1984;53:896–898.
5. Ten Cate FJ, Van Dorp WG, Hugenholtz PG, Roelandt J. Fixed subaortic stenosis: value of echocardiography for diagnosis and differentiation between various types. *Br Heart J* 1979;41:159–166.
6. Silove ED, De Giovanni JV, Shiu MF, Yi MM. Diagnosis of right ventricular outflow obstruction in infants by cross-sectional echocardiography. *Br Heart J* 1983;50:416–420.
7. Isaaz K, Cloez JL, Danchin N, Marcon F, Worms AM, Pernot C. Assessment of right ventricular outflow tract in children by two-dimensional echocardiography using a new subcostal view. Angiographic and morphological correlative study. *Am J Cardiol* 1985;56:539–545.
8. Caldwell RL, Weyman AE, Hurwitz RA, Girod DA, Feigenbaum H. Right ventricular outflow tract assessment by cross-sectional echocardiography in Tetralogy of Fallot. *Circulation* 1979;59:395–402.
9. de Vries AG, Hess J, Witsenburg M, Frohn-Mulder IME, Bogers AJJC, Bos E. Management of fixed subaortic stenosis: a retrospective study of 57 cases. *J Am Coll Cardiol* 1992;19:1013–1017.
10. Gnanapragasam JP, Houston AB, Doig WB, Jamieson MPG, Pollock JCS. Transesophageal echocardiographic assessment of fixed subaortic obstruction in children. *Br Heart J* 1991;66:281–284.
11. Wang XF, Li ZA, Cheng TO, Deng YB, Zheng LH, Hu G, Lu P. Clinical application of three-dimensional transesophageal echocardiography. *Am Heart J* 1994;128:380–388.
12. Fyfe DA, Ludomirsky A, Sandhu S, Dhar PK, Silberbach M, Sahn DJ. Left ventricular outflow tract obstruction defined by active three-dimensional echocardiography using rotational transthoracic acquisition. *Echocardiography* 1994; 11:607–615.
13. Vogel M, Losch S. Dynamic three-dimensional echocardiography with a computed tomography imaging probe: initial clinical experience with transthoracic application in infants and children with congenital heart defects. *Br Heart J* 1994;71:462–467.
14. Salustri A, Spitaels S, McGhie J, Vletter W, Roelandt JRTC. Transthoracic three-dimensional echocardiography in adult patients with congenital heart disease. *J Am Coll Cardiol* 1995;26:759–767.
15. Roelandt JRTC, ten Cate FJ, Vletter WB, Taams MA. Ultrasonic dynamic three-dimensional visualization of the heart with a multiplane transesophageal imaging transducer. *J Am Soc Echocardiogr* 1994;7:217–229.
16. de Leval M. Surgery of the left ventricular outflow tract. In: Stark J, de Leval M, eds. Surgery for Congenital Heart Defects. 2nd ed. Philadelphia: WB Saunders, 1994:511–538.
17. de Leval M. Pulmonary stenosis and pulmonary atresia with intact ventricular septum. In: Stark J, de Leval M, eds. Surgery for Congenital Heart Defects. 2nd ed. Philadelphia: WB Saunders, 1994:389–405.
18. Kasprzak JD, Salustri A, Roelandt JRTC, Ten Cate FJ. Three-dimensional echocardiography of the aortic valve: feasibility, clinical potential and limitations. *Echocardiography* 1998;15:127–138.
19. Abraham TP, Warner JG, Kon ND, Lantz PE, Fowle KM, Brooker RF, Ge S, Nomeir AM, Kitzman DW. Feasibility, accuracy and incremental value of intraoperative three-dimensional transesophageal echocardiography in valve surgery. *Am J Cardiology* 1997;80:1577–1582.

CHAPTER 8

3D ECHOCARDIOGRAPHY AS A DIAGNOSTIC AID FOR SURGERY IN TETRALOGY OF FALLOT

3D-Echocardiography as a Diagnostic Aid for Surgery in Tetralogy of Fallot

A. Dall'Agata[1,2], J. S. McGhie[2], F. J. Meijboom[3], J. R. T. C. Roelandt[2], A. J. J. C. Bogers[1]

Background: Current 2-dimensional echocardiography does not always completely disclose the surgical anatomy of tetralogy of Fallot (TF).

Methods: Fifteen patients (range 4 months-61 years), undergoing surgical repair for TF, were examined by 3-dimensional (3D) echocardiography. Location and size of the ventricular septal defect (VSD), location and degree of right ventricular outflow tract (RVOT) obstruction, degree of overriding aorta and imaging of coronary arteries were randomly analyzed. Morphological accuracy was assessed postoperatively by comparison with surgical findings.

Results: In 14/14 data sets the VSD was accurately reconstructed. In the 11 datasets of the RVOT, 3D-echocardiography showed 10 sub-pulmonary obstructions, 3 bicuspid pulmonary valves and in 3 others a hypoplastic pulmonary trunk.

There was aortic overriding of about 50% in 13 patients, less than 50% in 2 patients and more than 50% in 1 patient. Origin and path of coronary arteries could be assessed in only 2 patients. The accuracy of the morphological findings was confirmed by the surgical findings in all the reconstructions.

Conclusion: 3D-echocardiography accurately assesses the features of surgical interest in TF. The anatomical insight is improved by depth perception. 3D-echocardiography might be used as an additional tool in determining surgical strategy in TF.

(CVE. 2000; 5 (1): 21-25)

Key words: tetralogy of Fallot, surgical anatomy, 3-dimensional echocardiography

Introduction

Three-dimensional (3D) echocardiography has been proposed as a new technique enabling to improve the understanding of the anatomy of congenital heart disease by simulating the surgical views (1). Although at present the clinical applications are still limited, 3D-echocardiography allows virtually realistic imaging and analysis of particular structures of the heart, for instance atrial and ventricular septal defect (VSD) and different types of outflow obstruction (2-6). In this regard tetralogy of Fallot (TF) is a specific morphologic entity, which encompasses a wide spectrum of morphological subsets (7). In TF there is still a number of patients in whom intraoperative assessment is required on the VSD and the right ventricular outflow tract (RVOT) (7). Accurate assessment of these anatomic variations is essential for the surgical intervention. The present two-dimensional (2D) diagnostic methods do not always provide all the details necessary for diagnosis as well as intraoperative decision making, because 2D-echocardiography is limited to selected cross-sectional views, underestimating the complex 3D-anatomy of congenital heart disease.

The aim of this study is to assess the accuracy of 3D-echocardiography in morphological diagnosis of TF and to evaluate its potential role in the preoperative assessment of TF.

Methods

Study Population

Fifteen patients (10 male and 5 female) undergoing surgical repair for TF, were studied. The mean age was 10 years (range 4 months-61 years). Three patients were adults (age 18-61 years) and 12 were children (age 4 months-6 years). The mean body surface area (BSA) was 0.7 ± 0.6 m^2 (range 0.3-2.1).

3D-Echocardiography

Image acquisition was performed with a Toshiba SSH 140-A (Toshiba, Otawara-Shi, Japan) or HP 1500 (Hewlett-Packard, Andover, MA, USA) echo-system. The video output was interfaced to the 3D-reconstruction system Echo-scan 3.0 (TomTec, Munich, Germany) (8). Seven patients were studied by transthoracic approach and 8 by transesophageal approach. Transesophageal echocardiography in children was performed using the Minimulti probe (Oldelft, Delft, The

Netherlands), which operates at a frequency of 5MHz, while transthoracic echocardiography was performed with a 3.5 MHz probe. All children were studied under general anesthesia, just before surgery. The adult patients were studied in the laboratory of echocardiography. Twenty-four volumetric data sets were totally acquired by rotational scanning at 2 degree intervals for 90 steps, applying EKG gating and respiratory gating (8). The transducer was placed in different positions on the chest or at different levels in the esophagus in order to obtain the view which best displayed the particular region of interest. Volumetric data sets of VSD were acquired in 14 patients, of the RVOT in 11 patients. In the optimal echocardiographic window, care was taken to keep the region of interest in the center of the scanning-sector and to include the surrounding structures like the tricuspid valve and the aortic valve for further spatial orientation. Acquisition time was 3 to 5 minutes for a rotation, depending on the heart rate of the patient. The stored data were processed off-line and presented as a conical volumetric data set (8). The data processing time was 20 to 30 minutes per data set, depending on the size of the data set.

Three-D-reconstructions were independently done by two observers (AD, JMcG). From the obtained volumetric data set, cut-planes were selected using the anyplane mode in order to visualize the interventricular septum on its left and right surface and in its longitudinal cross-section (3,4). The outflow tract was displayed along its longitudinal axis and in horizontal cross-sections at different angles and distance, from above the annulus of the semilunar valve and from below the obstruction, by scanning the data set (5). A grey level threshold was applied on the dynamic computer-generated 2D-cutplanes in order to separate the object from the background. Thus, 3D-dynamic images with depth perception were created (8). The time for a reconstruction was 10 to 15 minutes, depending on the complexity of the acquired data set.

Surgery

All patients were operated through median sternotomy using cardiopulmonary by-pass with aorta and bicaval cannulation, moderate hypothermia and aortic cross-clamping with cardioplegic arrest.

In all patients the VSD was closed with a Goretex® patch. In 5 patients the RVOT was reconstructed by transatrial-transpulmonary approach with pulmonary valvotomy and resection of infundibular obstruction. In 7 patients a transannular patch was inserted of autologous gluteraldehyde pretreated pericardium. In 3 adult patients the RVOT was primarily repaired with the use of a pulmonary allograft.

There was no hospital mortality. There were no complications related to the 3D-echocardiography.

Data Analysis

The location, margins and size (largest antero-posterior and supero-inferior diameter) of the VSD as well as the spatial relationship with the tricuspid valve and with the aortic valve (degree of overriding) were analyzed on 3D-echocardiographic images. The location, the nature and the degree of the RVOT obstruction were assessed. The degree of aortic overriding was visually assessed from the rendered horizontal cross-section of the aortic valve, reproducing the surgical viewpoint and described as less than, equal to or more than

50%. The number, origin and path of the coronary arteries were assessed from the data sets containing the aortic root.

All measurements were expressed as mean ± standard deviation (SD).

After reconstruction the 3D-images were submitted to the attending cardiac surgeon, for assessing the morphological accuracy of the 3D-reconstruction.

Results

VSD

In all 14 data sets of the VSD could be reconstructed from the right ventricular perspective (feasibility 100%). The VSD was in all sets perimembranous with extension to the outlet septum and was in sub-aortic position. The complete margins of the VSD as well as the spatial relation with the tricuspid valve and the RVOT were visualized (Fig. 1). All 3D-reconstructions were morphologically confirmed by the surgical findings (accuracy 100%).

The largest diameter of the VSD in the antero-posterior direction was 14 ± 7 mm and the largest diameter in the supero-inferior direction was 16 ± 8 mm.

Overriding Aorta

In 15 out of 24 data sets an adequate short-axis of the aortic valve could be reconstructed (feasibility 63%). The degree of overriding of the aorta was assessed as 50% in 13 patients, less than 50% in 2 patients and more than 50% in one patient (Fig 2) (accuracy 100%). Computer-generated horizontal cross-sections of the aortic root allowed visualizing the origin of the left coronary artery in 2 patients (feasibility 13%). The right
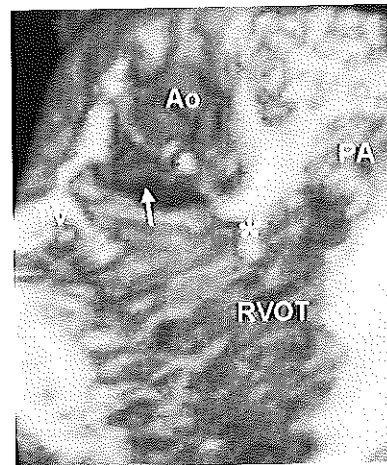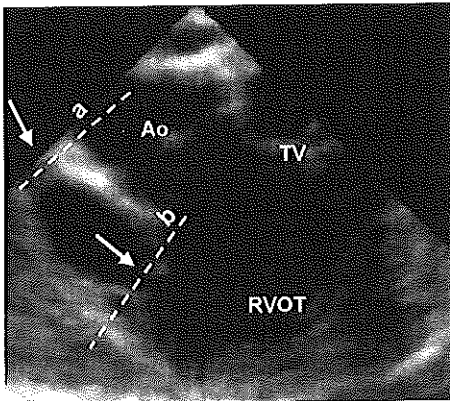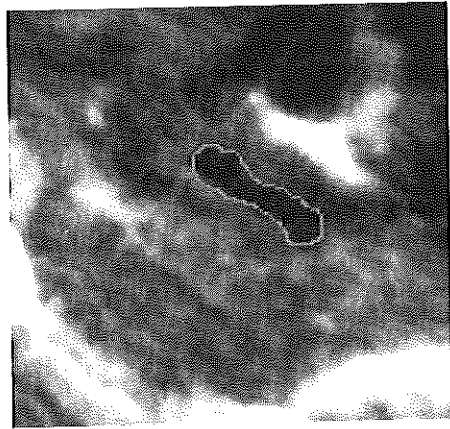

Fig. 1: 3D-reconstructed image of the right ventricular surface of the ventricular septum. The position and geometry of the VSD and its spatial distribution with respect to the tricuspid and aortic valve and the RVOT are displayed (arrow) Ao: aortic valve, PA: pulmonary artery, RVOT: right ventricular outflow tract, TV: tricuspid valve.

(A)

(B)

(C)

Fig. 2: 3D-reconstruction and analysis of the RVOT. A) 2D computer-generated long-axis of the RVOT. Horizontal cutplanes through the pulmonary valve plane (a level at dotted line a) and through the subpulmonary obstruction (a level at dotted line b). B) the volume-rendered image derived from level a shows a thickened and bicuspid pulmonary valve. C) the 2D computer-generated cross-section derived from level b shows the smallest luminal area of the RVOT. Ao: aortic valve, TV: tricuspid valve, RVOT: right ventricular outflow tract.

coronary artery was not visualized. The course of the coronary arteries could be followed for 1-2 cm. Accuracy could not be determined because in none of the patients the aorta was opened.

RVOT Obstruction

Ten out of 11 3D data sets containing information about the RVOT were adequate for analysis (feasibility 90%). Obstructions below the pulmonary valve level were visualized in all patients. In 5 patients the infundibulum was hypoplastic. In the remaining 5 patients there was a fibromuscular stenosis of the infundibulum, with a mean length of 0.6 ± 0.3 cm (range 0.3-0.8 cm) and a mean distance from the pulmonary valve of 1.6 ± 0.4 cm (range 1.3-2.2 cm) (Fig 3). The mean smallest RVOT diameters were 0.7 ± 0.2 cm (range 0.5-0.9 cm) and 0.5 ± 0.1 cm (range 0.5-0.6 cm). The mean smallest RVOT area was 0.7 ± 0.7 cm^2 (range 0.2-1.8 cm^2, area/BSA

1.8 ± 1.6 cm^2/m^2). The anatomy displayed on the 3D reconstructions was confirmed by the surgical findings (accuracy 100%).

The pulmonary valve was reconstructed and analyzed from a computergenerated short-axis cross-section in 9 data sets. The number of leaflets could be determined in 8 out of 9 reconstructions (feasibility 89%). Three bicuspid and 2 tricuspid valves were identified and confirmed by surgery (accuracy 100%). The mean pulmonary valve diameters were antero-posteriorly 1.1 ± 0.5 cm (range 0.5-1.8 cm) and latero-laterally 1.0 ± 0.4 cm (range 0.6-1.5 cm). The mean annular area of the pulmonary valve was 1.2 ± 1.0 cm^2 (range 0.3-2.8 cm^2, area/BSA 3.0 ± 2.4 cm^2/m^2).

The pulmonary trunk could be imaged for 2-3 cm of length in 9 out of the 10 data sets (feasibility 91%). In 3 patients the pulmonary trunk was hypoplastic, which was confirmed by surgery. In all the remaining patients the pulmonary artery was normal.
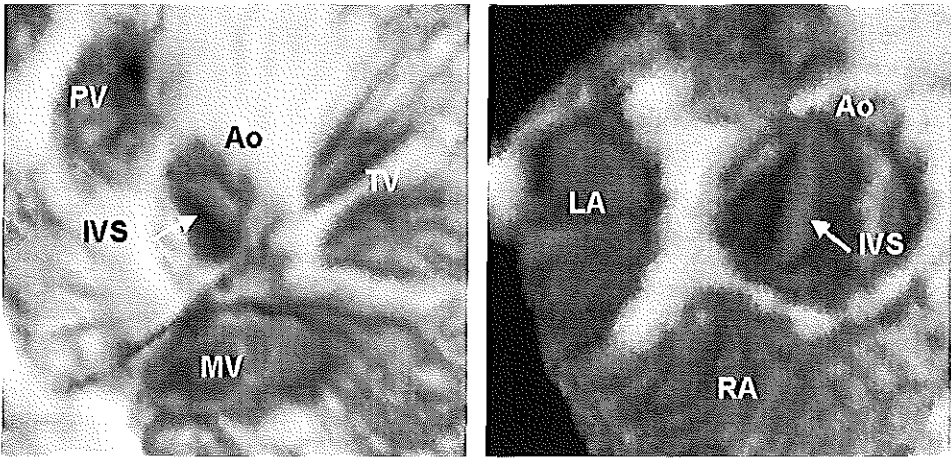
Fig. 3: Aorta overriding as seen from a surgical point of view. The interventricular septum is displayed beneath the aortic valve (arrow). From this view it is possible to estimate the percentage of aorta above the right ventricle. In A) there is a minimal overriding of the aortic valve, while in B) it is about 70-80%. Ao: aortic valve, IVS: interventricular septum, MV: mitral valve, TV: tricuspid valve, PV: pulmonary valve.

Conclusions

Primary surgical repair of tetralogy of Fallot essentially consists in closing the VSD preserving an unobstructed outflow of the left ventricle to the aortic valve and in creating an adequate outflow from the right ventricle to the pulmonary artery, preferably with a competent pulmonary valve. The approach to repair requires good exposure of the infundibular obstruction, the dimensions of the RVOT and the pulmonary arteries in order to allow an optimal repair and minimize the operative risks and management (9). Therefore, a clear mental image of the morphology is needed prior to surgery.

Diagnostic assessment was until recently mainly done by angiography, but it has been gradually substituted by 2D-echocardiography (10,11). It has been shown that the latter gives accurate information in selected patients (10). However, information offered by 2D-echocardiography, concerning the spatial distribution of the structures and their geometry, is limited. Imaging of the lesion from several windows and their sequential mental integration is required in order to build up a 3D-picture. Moreover, evaluation of shape and size of the lesion is based on geometrical assumptions.

In our study we reconstructed in a 3D-fashion the most important features of TF, using views which resemble the surgical perspective. We demonstrated that 3D-echocardiography adequately displays the VSD, the morphology of the RVOT obstruction and the degree of overriding of the aorta. The VSD in TF is not a simple hole lying in one single plane. Anatomically, there is a cone of space beneath the aortic valve leaflets extending down to the crest of the ventricular septum in which any plane can be considered as part of the defect (7). 3D-reconstruction of the VSD from the right ventricular surface easily represents its location in the ventricular septum and its geometry. All the margins are identified in one single view. It provides the visualization of the right margin of the defect, just like in the surgical view at closure of the defect. This

margin allows to categorize the defect and, consequently, to assess the anatomy of the conduction system (7).

3D echocardiography enables to assess the RVOT obstruction at any level. Horizontal cross-sections through the outflow tract allow to evaluate the nature and extension of the infundibular lesion, and to measure its degree of obstruction. The anatomy of the pulmonary valve is fairly well displayed, although the accuracy of the reconstruction is affected by echocardiographic drawbacks, such as echogenicity of the structure or suitable echocardiographic window. Additional information might be derived by the possibility to measure the area of the pulmonary annulus, which could be used for better sizing of and, eventually, selection of a pulmonary homograft.

Adequate preoperative information on the degree of overriding of the aorta in TF is helpful in deciding the repair technique (9,12). Estimation of aortic overriding is usually done from longitudinal 2D cross-section of the left ventricle. However, this method depends on the angulation of the ultrasound probe. In our study we evaluated the degree of overriding of the aortic from 3D-reconstruction of the surgical view. Results were the same as surgical findings, pointing at the accuracy of this method in this regard.

On the other hand, from our study it is not possible to derive a conclusion regarding the feasibility and the accuracy of evaluation of the coronary arteries, which is another important aspect for correction of TF. Although 3D-imaging of the coronary arteries has been successfully investigated in adult patients (13,14), we did not achieve the same results in our study population. A likely explanation is that the coronary arteries of these patients are of small size and the resolution power of our echoequipment was not sufficient for their imaging.

Despite the advances in computer technology, 3D-echocardiography is currently not available as a routine technique. A variable time for optimal acquisition, processing of the data sets and 3D-reconstruction is still necessary and makes it an

off-line technique. Furthermore, profound knowledge of normal and pathologic anatomy and long learning curve are indispensable for correct orientation, reconstruction and final interpretation of the images. Imaging resolution and drawbacks of 2D-echocardiography may affect the 3D-echocardiography results (14).

In conclusion, 3D-echocardiography provides accurate information on the most important anatomical features of TF. Three-D-echocardiography might help in reducing the time of intraoperative inspection and therefore anticipating on more adequate surgical reconstruction of TF.

Acknowledgment

References

[1] Schwartz SL, Cao Q, Azevedo J, Pandian NG (1994) Simulation of intraoperative visualization of cardiac structures and study of dynamic surgical anatomy with real time three-dimensional echocardiography. Am J Cardiol 73: 501-507

[2] Dall'Agata A, McGhie J, Taams MA et al. (1999) Secundum atrial septal defect is a dynamic three-dimensional entity. Am Heart J 137: 1075-1081

[3] Rivera JM, Siu SC, Handschumacher MD et al. (1994) Three-dimensional reconstruction of ventricular septal defects: validation studies and in vivo feasibility. J Am Coll Cardiol 23: 201-208

[4] Kardon RE, Cao QL, Masani N et al. (1998) New insights and observation in threedimensional echocardiographic visualization of ventricular septal defects. Experimental and clinical studies. Circulation 98: 1307-1314

[5] Fyfe DA, Ludomirsky A, Sandhu S, Dhar PK, Silberbach M, Sahn DJ (1994) Left ventricular outflow tract obstruction defined by active three-dimensional echocardiography using rotational transthoracic acquisition. Echocardiography 11: 607-15

[6] Dall'Agata A, Cromme-Dijkhuis AH, Meijboom FJ et al. (1999) Use of threedimensional echocardiography for analysis of outflow obstruction in congenital heart disease. Am J Cardiol 83: 921-925

[7] Anderson HR, Path MRC, Allwork SP et al. (1981) Surgical anatomy of tetralogy of Fallot. J Thorac Cardiovasc Surg 81: 887-896

[8] Roelandt JRTC, Salustri A, Vletter WB, Nosir Y, Bruining N (1994) Precordial multiplane echocardiography for dynamic anyplane, paraplane and threedimensional imaging of the heart. Thoraxcentre J 6: 6-15

[9] Kirklin JW, Barratt-Boyes BG (1993) Ventricular septal defect with pulmonary stenosis or atresia. In: Kirklin JW, Barratt-Boyes BG (Eds.) Cardiac surgery, 2nd edition. New York: Churchill Livingstone, pp. 863-1012

[10] Santoro G, Marino B, Di Carlo D et al. (1994) Echocardiographically guided repair of tetralogy of Fallot. Am J Cardiol 73: 808-811

[11] Saraclar M, Ozkutlu S, Ozme S et al. (1992) Surgical treatment in tetralogy of Fallot diagnosed by echocardiography. Int J Cardiol 37: 329-335

[12] Becker AE, Connor M, Anderson RH (1975) Tetralogy of Fallot: a morphometric and geometric study. Am J Cardiol 35: 402-412

[13] El-Rahman SMA, Khatri G, Nanda N et al. (1996) Transesophageal threedimensional echocardiographic assessment of normal and stenosed coronary arteries. Echocardiography 13: 503-510

[14] Lancee CT, Djoa KK, de Jong N et al. (1998) Resolution in three-dimensional echocardiography. Thoraxcenter J 10: 6-11

CHAPTER 9

QUANTIFICATION OF THE AORTIC VALVE AREA IN THREE-DIMENSIONAL ECHOCARDIOGRAPHIC DATA SETS: ANALYSIS OF THE ORIFICE OVERESTIMATION RESULTING FROM SUBOPTIMAL CUT-PLANE SELECTION

Jaroslaw D. Kasprzak* MD,PhD, Youssef F.M. Nosir MD,
Anita Dall'Agata MD, Abdou Elhendy MD, Meindert Taams MD,PhD,
Folkert J. Ten Cate MD,PhD Jos R.T.C. Roelandt MD,PhD

Thoraxcenter, Division of Cardiology, Erasmus University and University Hospital
Rotterdam - Dijkzigt, Rotterdam, The Netherlands
*Cardiology Department, Medical University of Lodz, Poland

ABSTRACT

Background Our study was designed to determine the feasibility of three-dimensional echocardiographic (3DE) aortic valve area planimetry and to evaluate potential errors resulting from suboptimal imaging plane position.

Methods and Results Transesophageal echocardiography with acquisition of images for 3DE was performed in 27 patients. Aortic valve orifice was planimetered in two-dimensional echocardiogram (2DE) and in two-dimensional views reconstructed from 3DE datasets optimized for level of the the cusp tips. To evaluate the errors caused by suboptimal cutplane selection, orifice was also measured in cutplanes angulated by 10°, 20° and 30° or shifted by 1.5 to 7.5 mm.

Planimetered orifice areas was similar in 2DE and 3DE studies: 2.09 ± 0.97 cm^2 vs 2.07 ± 0.92 cm^2. Significant overestimation was observed with cutplane angulation (0.09, 0.19 and 0.34 cm^2 at 10° increments) or parallel shift (0.11, 0.22, 0.33, 0.43 and 0.63 cm^2 at 1.5mm increments). 3DE measurement reproducibility was very low and superior to that of 2DE.

Conclusions 3DE allows accurate aortic valve area quantification with excellent reproducibility. Relatively small inaccuracy in cutplane adjustment is a major source of errors in aortic valve area planimetry.

(Am Heart J 1998;135:995-1003)

Introduction

Two-dimensional (2DE) and Doppler echocardiography are principal noninvasive tools used to obtain quantitative information concerning the aortic valve. In transthoracic echocardiography, the most common approach includes Doppler evaluation of aortic valve flow, enabling quantification of transvalvular gradient and valve resistance. Valve area calculation is usually indirect, based upon the continuity equation.[1] Transesophageal echocardiography provides a better acoustic window and superior image resolution, enabling direct aortic valve area planimetry in the majority of patients.[2-6] This approach has been well validated and the best results are achieved by multiplane transesophageal probes. However, in some patients an optimal two-dimensional imaging plane for true aortic orifice cannot be obtained, which leads to area overestimation. Recently introduced, three-dimensional echocardiography (3DE) allows the objective visualization and quantification of cardiac structures. [7-10] The method can be used for the imaging of the aortic valve, [11,12] but its value for area planimetry has not been assessed. Our study was conducted to analyze the feasibility, accuracy and reproducibility of the measurements of aortic valve area in two-dimensional views reconstructed from a 3DE dataset. In addition, the unique opportunity of unrestricted cutplane manipulation in registered dataset allowed us to quantify the errors resulting from planimetry in suboptimally selected cross-sectional images.

Methods

The study group consisted of 7 patients with normal aortic valves and 20 consecutive patients with aortic valve abnormalities diagnosed by transesophageal echocardiography and subsequently undergoing transesophageal study. All patients were in sinus rhythm. The group included 13 women and 14 men of mean age 53.2 ± 17.7 years (range 22-82). Aortic

pathology included 3 patients with bicuspid valve and 15 patients with acquired valve lesions; 2 patients had undergone aortic valve replacement with Ross procedure. Calcification of the aortic valve was identified in 5 patients. There was no preselection of the patients for 3DE examination based on two-dimensional image quality.

Two-dimensional echocardiography was performed using a Toshiba SSH-140A system with a 5 MHz, 64-element multiplane transesophageal transducer and a transthoracic 3.75 MHz probe. In the transesophageal study, standard precautions, patients preparation and probe insertion procedure were followed as described elsewhere. [13] For the aortic valve area planimetry, a short-axis view of the aortic valve, optimized for the smallest orifice area was used. The gain was set at the lowest value providing complete delineation of cusps.

Transthoracic imaging was used to collect the data used in continuity equation. Left ventricular outflow tract (LVOT) diameter was measured immediately below the aortic anulus in a long axis parasternal view and its area was calculated assuming a circular geometry. The LVOT flow velocity was registered at the same level using pulsed wave Doppler in apical five-chamber view. The peak transaortic flow velocity was measured with continuous wave Doppler from the apical, right parasternal or suprasternal window.

Three-dimensional echocardiographic data acquisition and processing

Informed consent for three-dimensional echocardiographic examination was obtained from all patients. After the diagnostic multiplane transesophageal study had been finished, the probe was located at mid-esophageal level. A test sequence with 180° rotation of the transducer array was performed to ensure whether the aortic valve is encompassed within the conical acquisition volume. The basic images were acquired at 2° intervals and sampled at

25 Hz using a 3DE system (Echo-Scan 3.0, TomTec GmbH, Munich, Germany). The system has been described in detail elsewhere. [8]

Data processing was performed off-line by the analysis program of 3DE system. Rewritable optical disks were used for the permanent storage of data.

Aortic valve area measurements

Two-dimensional echocardiography. After the identification of the video frame with the maximal opening of the aortic valve in early systole, the area was measured by tracing of the inner cusps contours using a digitizing tablet. The mean value of five consecutive measurements was calculated. Measurements were made independently by two experienced observers, blinded to each other's results. Additional measurements were performed after 7 days for the evaluation of the intraobserver variability.

Aortic valve area measurement by continuity equation. Planimetry of a stenotic aortic valve may be less reliable due to orifice non-planarity and calcifications. Therefore, in the subgroup of patients with planimetered aortic valve area below 2 cm^2, additional calculation of aortic valve orifice area was performed using the continuity equation. [1] The mean value of five consecutive measurements was calculated.

Anyplane 3DE. The dataset was used to generate two-dimensional cross-sectional views of the aortic valve at its maximal opening during a heart cycle. A series of long-axis views was displayed as a reference for localization of the level at which the separation of aortic cusps tips was smallest (Fig 1). A cut-line was placed at this level and a corresponding orthogonal (short-axis) view was reconstructed. Subsequently, a fine angulation of this cross-sectional image was performed to ensure a continuous orifice outline. This optimized view was used to trace the inner contour of aortic cusps using the 3DE system software. The mean

value of five consecutive measurements was calculated. Measurements were made independently by two experienced observers, blinded to each other's results and to those from two-dimensional planimetry. These measurements were repeated after 7 days for the evaluation of intraobserver variability.

Evaluation of suboptimal cutplanes. To evaluate possible errors in aortic valve area calculation, a series of suboptimal valve cross-sections images was analyzed. Aortic valve area was measured in five parallel planes shifted toward the aortic anulus in 1.5 mm intervals and in three planes, angulated by 10, 20 and 30 degrees from the initially selected, optimal plane through the valve (Fig 1). The mean value of three consecutive measurements was used for each plane.
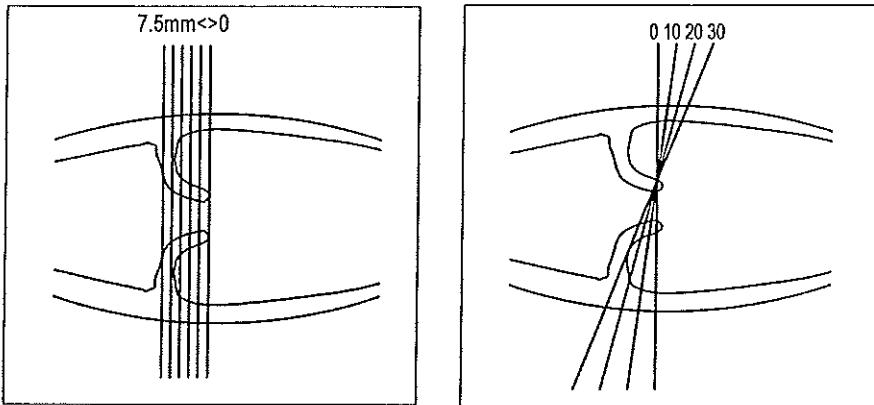

Figure 1. The principle of two-dimensional echocardiographic planimetry error evaluation. Left panel - cutplane adjustment with parallel shifts towards the anulus at 1.5mm interval from the optimal plane. Right panel - cutplane angulation at 10° interval from the optimal cutplane.

Statistical analysis

All data are expressed as mean ± standard deviation. Linear regression was used to evaluate relations between measurements obtained with two methods and Bland-Altman [14] analysis was performed for agreement assessment. Limits of agreement were defined as mean ±1.96 times SD of differences. Repeated-measures analysis of variance (ANOVA) was used to assess the influence of imaging plane shift and angulation on measurement of the aortic valve area. Pairwise comparisons against the optimal plane were performed with the Dunnett test. A value of $p < 0.05$ was considered statistically significant. Equality of variances was tested with F test. Observer variability was expressed in coefficients of variation (calculated as SD of differences between measurements divided by the mean area value).

Results

Feasibility of 2D and 3DE aortic valve area measurements

Transesophageal echocardiography with image acquisition for 3D reconstruction was successfully performed in all patients. Additional examination time required for the calibration procedures and the 3DE data acquisition never exceeded 10 minutes. The time required for data postprocessing ranged from 5 to 15 minutes and for image analysis - between 5 and 15 minutes.

In 2DE, aortic valve planimetry was feasible in 26 of 27 studies (96%): in one patient an adequate short-axis image of the aortic valve could be obtained. Planimetric measurements of aortic orifice in reconstructed anyplane views, optimally positioned at the level of cusp tips could be performed in 26 of 27 patients (Fig 2). In one 3D dataset the

measurements were precluded by a motion artifact; minor artifacts, not interfering with aortic valve planimetry were found in six other studies.
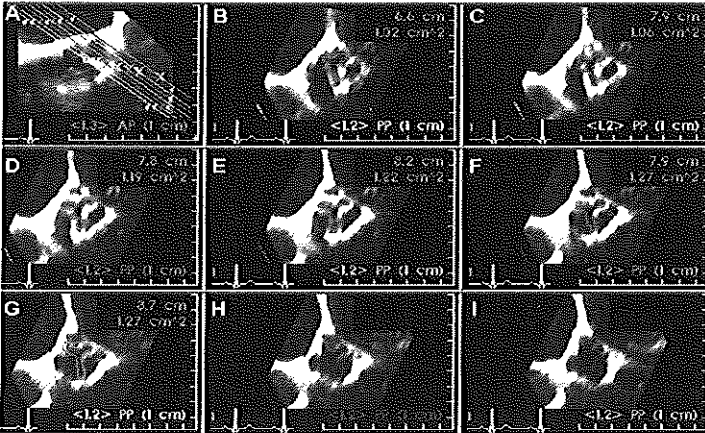

Figure 2. Paraplane echocardiography using the three-dimensional dataset of a patient with a stenotic aortic valve. All the two-dimensional views are computer-reconstructed A, reference long-axis image enabling placement of short-axis cutplanes at different levels through the valve (distance between cutplanes 1.5mm) (B through G). Optimized short-axis cross-section through the orifice at the level of cusp tips is shown in B. Images in H and I (shift of 9mm and 10.5mm) did not contain the area information and were not used for analysis.

Aortic valve area measurements

Head-to-head analysis was feasible in 25 patients (one exclusion because of low quality 2DE planimetry and one due to a large artifact in 3DE dataset). Aortic valve area measured in 2DE ranged from 0.6 to 4.31 cm^2 (mean 2.09 ± 0.97 cm^2). The values obtained in three-dimensional planimetry were similar, ranging 0.64 to 3.92cm^2 (mean 2.07 ± 0.92 cm^2). Excellent correlation between the area estimates in both methods was found: r=0.982, p<0.0001, y = 1.033x -0.04, SEE=0.19 cm^2 (Fig 3). Mean difference between methods was not statistically significant with close limits of agreement (0.02 ± 0.19 cm^2) as shown in Fig. 3.
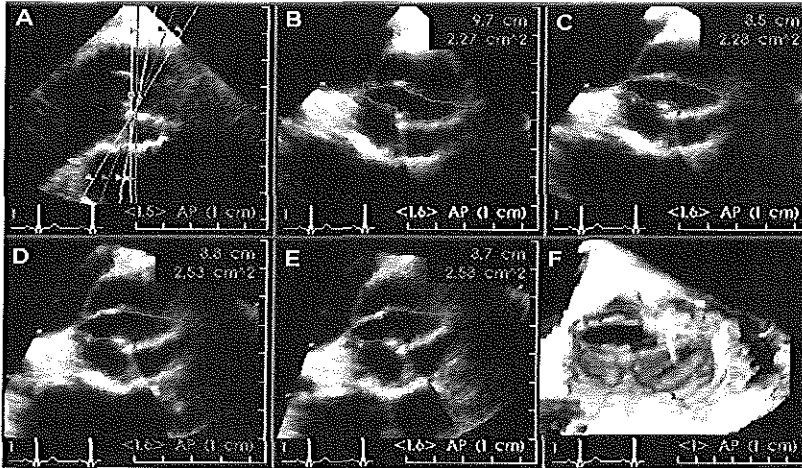
Figure 3. Anyplane echocardiography with three-dimensional dataset of a patient with a bicuspid aortic valve. All two-dimensional views are computer-reconstructed Optimized short-axis cross-section through the orifice at the level of cusp tips is shown in **B**. **A** displays reference long-axis image enabling placement of tangulated cutplanes (**C**, 10 degrees; **D**, 20 degrees; **E**, 30 degrees). **F** is a corresponding volume-rendered view, not used for direct planimetry with current software.

Additionally, three-dimensional planimetry results were compared with aortic valve area calculated using the continuity equation in the subgroup of 11 patients with planimetered aortic valve area <2 cm^2. There was no significant difference (bias=-0.06±0.11cm^2, p=NS) and a close correlation (r=0.954, p<0.0001, SEE=0.09cm^2) between the area estimates obtained by 3DE and continuity equation (Fig.4).
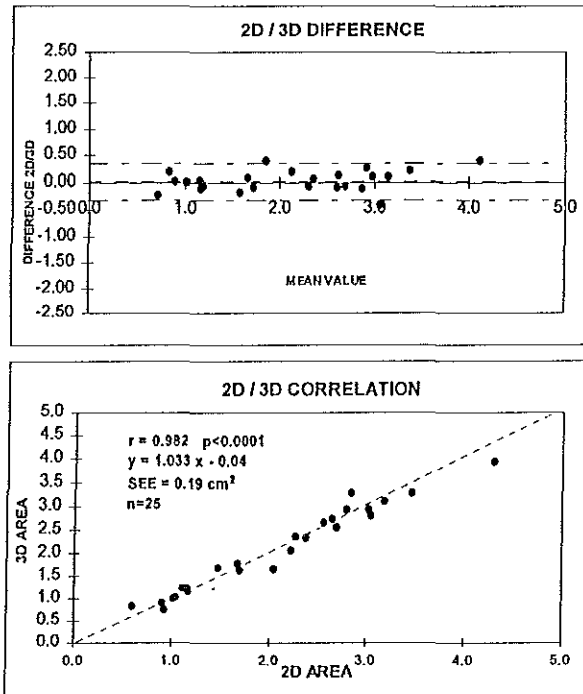
Figure 4. *Upper panel,* Plot of agreement between 2DE and 3DE estimates of the aortic valve area. Difference in area (y axis) is plotted against mean value of two measurements (x axis). There are close limits of agreement between the values obtained by the two methods (-0.34, +0.40). *Lower panel,* Linear regression plot of area values obtained in 2DE (x axis) and 3DE (y axis).

Importance of optimal cutplane position.

A significant area overestimation (O) was observed at each cutplane angulation (O = 0.09 cm^2 at 10 degrees, 0.19 cm^2 at 20 degrees and 0.34 cm^2 at 30 degrees) and confirmed by repeated-measures ANOVA ($p<0.001$) with Dunnett test. Overestimation was linearly correlated to the angle ($r=0.992$, $p<0.008$). Similarly, every parallel shift of viewing plane caused a significant overestimation of the area (O = 0.11cm^2/1.5 mm, 0.22cm^2/3 mm, 0.33cm^2/4.5 mm, 0.43cm^2/6 mm and 0.63cm^2/7.5 mm; ANOVA $p<0.001$. Linear correlation

of overestimation and plane shift was found (r=0.993, p<0.001). The degree of error was not correlated with the optimal planimetered area of the valve. The influence of cutplane optimalization on mean measured valve area is summarized in Fig. 5.
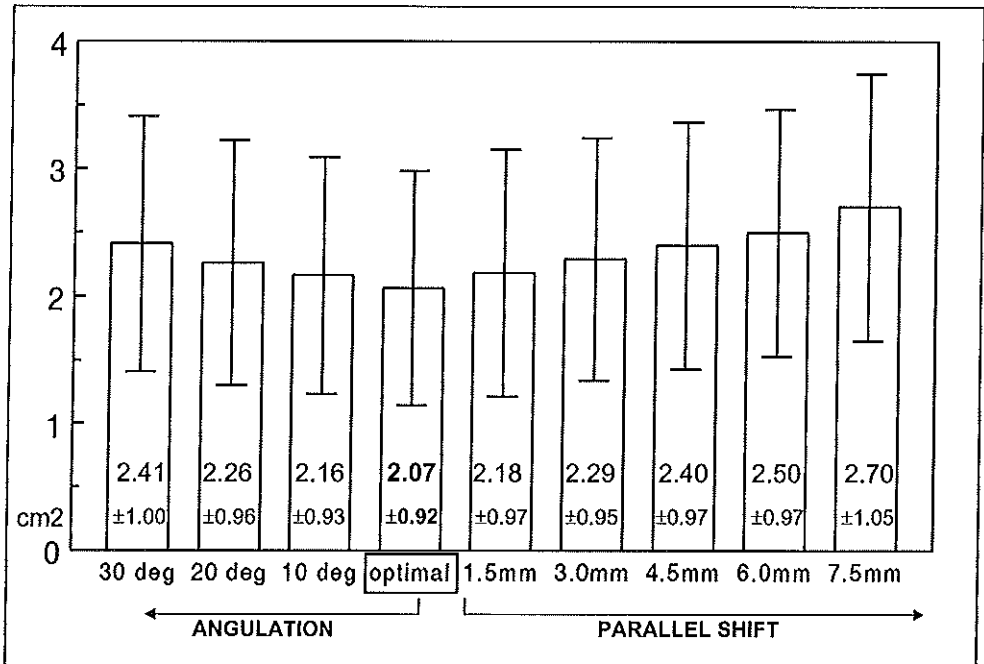
Figure 5. Bar plot demonstrating an increase in measured aortic valve area in angulated (30,20 and 10 degrees) cut-planes and parallel shifted (1.5, 3, 4.5, 6 and 7.5 mm) compared with optimal cutting plane.

Variability

Intraobserver and interobserver variability of aortic valve area planimetry in 3DE was very low (mean difference 0.03 ± 0.08cm^2, 0.01 ± 0.11cm^2 respectively; coefficients of variation: intraobserver 3.9%, interobserver 5.3%). The variability of 3DE measurements compared favorably against 2DE: mean intraobserver difference 0.04 ± 0.10 cm^2, coefficient

of variation 4.8%, *F* test against 3D: *p*=NS and mean interobserver difference 0.10 ± 0.21

cm^2 , coefficient of variation 10.0%, *F* test against 3D: *p*= 0.002.

Discussion
Invasive aortic valve area quantification

The formula of Gorlin and Gorlin, [15] introduced in 1951, is still used as a reference

method for aortic valve area calculation but its significant limitations are known. [16] The area

estimates are clearly flow-dependent and related to the functional rather than anatomical

orifice. In practice, it is sometimes difficult to obtain accurate values for cardiac output and a

mean transvalvular pressure difference. The method requires tedious standardization and due

to the invasive character is expensive and not suited for everyday routine use and repetitive

studies. Recently described, accurate measurement of aortic valve area with intracardiac

ultrasound probes shares the same limitation. [17,18] Nowadays, the use of pre-operative cardiac

catheterization for the assessment of aortic stenosis severity is decreased and reserved for

patients with inconsistency between clinical symptoms and non-invasive imaging data.

Therefore, a need exists for a cheaper, noninvasive technique for the calculation of the aortic

valve area.

Two-dimensional echocardiographic assessment of the aortic valve

Transthoracic 2D and Doppler echocardiography are the main techniques used for the

noninvasive assessment of aortic valve stenosis. Aortic valve area can be calculated with the

continuity equation but small inaccuracy in data collection may result in major error. Direct

planimetry of the aortic valve area is limited by valve calcifications and not widely used in

clinical practice. This may improve with better images of new generation echocardiographs.[19]

Most limitations encountered in precordial studies are overcome by transesophageal approach. The use of the continuity equation for aortic valve area calculation with this modality has been reported recently. [20] A more common and simple approach, however, is to measure aortic valve area using direct planimetry. Higher frequency ultrasound transducers providing better image resolution with no chest wall interference enable such evaluation and yield reliable values of aortic valve area. The method has been well validated and provides values close to those calculated with the Gorlin formula. [2-5] A recent study by Kim et al. [6] demonstrates that the aortic valve area estimates from both methods are practically equivalent. Optimal feasibility and accuracy was found with multiplane transesophageal echocardiography, due to easier image plane manipulation than single plane or biplane probes. [5,21] The variability of transesophageal echocardiographic planimetry of the aortic valve area in our study is similar to the values reported previously. [2-6,21]

Although the results obtained with transesophageal 2DE are encouraging, the alignment of viewing plane with real short axis of the aortic valve is subjective and remains a major problem. During the data collection there are no obvious anatomical landmarks confirming that imaging plane is positioned at the smallest anatomical area, which is at the tips of aortic cusps exactly in the plane of the valve orifice. To the best of our knowledge, the quantitative aspects of improper cutplane location on aortic valve area quantification have not been investigated.

Three-dimensional echocardiography

The reconstruction of cardiac morphology from 3DE datasets represents a major advance in noninvasive imaging techniques. The structures of the heart can be displayed in "anatomical" or "surgical" perspectives, [22] with direct perception of correct spatial relations.

Recognition of complex anatomy and pathology is thus facilitated. [23] Three-dimensional reconstruction of the aortic valve with transesophageal approach is feasible and provides reliable information in various types of pathology. [11,24,25] Three-dimensional echocardiographic datasets allow unrestricted off-line manipulation, unlike the images stored on videotapes. Off-line reconstruction of any desired view, even not present in originally acquired images can now be performed (anyplane mode). However, only preliminary data are available about the quantification of aortic valve area with this approach. Good feasibility and agreement versus Gorlin or continuity equation method [26,27] as well as direct intraoperative measurements were reported. [28]

An important part of our study was dedicated to the evaluation of potential errors, resulting from the measurements in inappropriate short-axis cutplanes. Significant overestimation of the area was caused by as little displacement as 1.5mm parallel shift or 10 degree angulation. Overestimation was linearly related to angle or distance in the analyzed range of values. Majority of images obtained at 10 and 20 degree angles or 1.5mm and 3 mm were clear and could be mistaken for the optimal short axis view. This identifies a potential source of errors in two-dimensional studies taken by less experienced operators. Such overestimation may be of clinical importance in borderline cases, considering that the absolute magnitude of error was similar in valves with stenotic and with normal orifice. It is noteworthy that this kind of error analysis could be performed exclusively with use of three-dimensional datasets, because no other technique allows the controlled modification of cutplane parameters in the same analyzed heart cycle.

In our study, the feasibility of aortic valve planimetry in optimal cross-sections obtained from three-dimensional datasets was good and similar to that obtained in 2DE. The measurements of aortic valve area, obtained for a wide range of values, were in close

agreement with those provided by two-dimensional planimetry and, in a subgroup of patients with the most diseased valves, by continuity equation. Excellent reproducibility of three-dimensional measurements compared favorably with two-dimensional data, the difference reaching statistical significance for interobserver variability. This can be explained by the unique possibility of unrestricted off-line cutplane selection from the 3DE dataset, which allows precise alignment of a viewing plane with the true orifice of the valve. In our study, a long axis view of the ascending aorta was used to optimize the selection of orthogonal short-axis view. Such visual feedback can explain better reproducibility due to easier selection of an optimal cutplane used for planimetry in three-dimensional dataset.

Clinical potential

The quantification of aortic valve area from three-dimensional datasets acquired using a rotational method can be performed in the vast majority of patients. The time necessary for both reconstruction and selection of optimized two-dimensional imaging planes with modern hardware is acceptable. However, the method is more time-consuming, however, than 2DE and requires some experience for efficient data manipulation. The possibility to reconstruct a short-axis image of aortic orifice from original imaging planes, aligned parallel to the long axis of the valve, provides a potential to minimize the artifacts caused by calcifications as the artifacts are cast off the plane of aortic orifice.

Three-dimensional planimetry of the aortic valve can be an additional tool in equivocal cases and, due to its low variability, might be useful to monitor the progression of borderline aortic valve stenosis.

Limitations

Invasive aortic valve area assessment with Gorlin formula, still considered as a reference method, was not available in our patients. However, recent studies suggest that the Gorlin formula and multiplane transesophageal planimetry provide very similar values of aortic valve area.[6] Transesophageal data collection can be considered semi-invasive but transthoracic images of a thin, rapidly moving object such as aortic valve do not provide sufficient quality of data for reliable three-dimensional reconstruction and area quantification in majority of adult patients.

The flow-dependence of aortic valve area is another potential source of variability in studies comparing different quantitative techniques, particularly when measurements are taken at different time points and under variable medication regimens. In our study, however, all measurements were taken within one hour (including transthoracic imaging) in hemodynamically stable patients so that significant changes in cardiac output were unlikely. As regards the error evaluation, the measurements were taken from the same dataset as the optimized 3DE planimetry and this source of variability was completely eliminated.

Despite technological progress, three-dimensional technique is still subject to limitations. The acquisition of images may be complicated in patients with very irregular arrhythmia. Inadvertent patient or transducer movements during data acquisition often produce significant artifacts in three-dimensional datasets. In our experience, a rotational transesophageal approach provides a sufficient stability and appropriate instructions given to a patient before the procedure help to acquire acceptable quality data. Spatial and temporal resolution of computer-reconstructed two-dimensional views are worse than original two-dimensional data, possibly leading to area underestimation. However, the agreement of both methods was good in our study, suggesting sufficient three-dimensional data quality. Finally,

current software does not allow area measurements in volume-rendered three-dimensional views, which provide most direct visual information about the valve orifice (Fig. 3, *F*). This implementation may simplify the planimetry procedure in future software updates.

Conclusions

Our study demonstrates that 3DE can be used for aortic valve area planimetry with excellent reproducibility. The results are in close agreement with transesophageal two-dimensional planimetry and continuity equation estimates. Our observations confirm the risk of significant, clinically relevant aortic valve area overestimation resulting from relatively small inaccuracy in two-dimensional imaging plane adjustment. Off-line cutplane optimization, feasible in three-dimensional datasets, improves measurement accuracy and reproducibility by elimination of errors related to inappropriate viewing plane selection.

References

1.   Bednarz JE, Krauss D, Lang RM. An echocardiographic approach to the assessment of aortic stenosis. J Am Soc Echocardiogr 1996;9:286-94.

2.   Hoffmann R, Flachskampf FA, Hanrath P. Planimetry of orifice area in aortic stenosis using multiplane transesophageal echocardiography. J Am Coll Cardiol 1993;22:529-34.

3.   Hofmann T, Kasper W, Meinertz T, Spillner G, Schlosser V, Just H. Determination of aortic valve orifice area in aortic valve stenosis by two-dimensional transesophageal echocardiography. Am J Cardiol 1987;59:330-5.

4.   Stoddard MF, Arce J, Liddell NE, Peters G, Dillon S, Kupersmith J. Two-dimensional transesophageal echocardiographic determination of aortic valve area in adults with aortic stenosis. Am Heart J 1991;122:1415-22.

5. Tribouilloy C, Shen WF, Peltier M, Mirode A, Rey JL, Lesbre JP. Quantitation of aortic valve area in aortic stenosis with multiplane transesophageal echocardiography: comparison with monoplane transesophageal approach. Am Heart J 1994;128:526-32.

6. Kim CJ, Berglund H, Nishioka T, Luo H, Siegel RJ. Correspondence of aortic valve area determination from transesophageal echocardiography, transthoracic echocardiography and cardiac catheterization. Am Heart J 1996;132:1163-72.

7. Pandian NG, Roelandt J, Nanda NC, Sugeng L, Cao Q, Azevedo J et al.   Dynamic three-dimensional echocardiography: methods and clinical potential. Echocardiography 1994;11:237-59.

8. Roelandt JRTC, Ten Cate FJ, Vletter WB, Taams MA. Ultrasonic dynamic three-dimensional visualization of the heart with a multiplane transesophageal imaging transducer. J Am Soc Echocardiogr 1994;7:217-29.

9. Belohlavek M, Foley DA, Gerber TC, Kinter TM, Greenleaf JF, Seward JB.   Three- and four-dimensional cardiovascular imaging: a new era for echocardiography. Mayo Clin Proc 1993;68:221-40.

10. Salustri A, Roelandt JRTC. Ultrasonic three-dimensional reconstruction of the heart. Ultr Med Biol 1995;21:281-93.

11. Nanda NC, Roychoudhury D, Chung SM, Kim KS, Ostlund V, Klas B. Quantitative assessment of normal and stenotic aortic valve using transesophageal three-dimensional echocardiography. Echocardiography, 1994;11:617-25.

12. Kasprzak JD, Salustri A, Roelandt JRTC, Ten Cate FJ. Three-dimensional echocardiography of the aortic valve: feasibility, clinical utility and limitations. Echocardiography, in press.

13. Roelandt JRTC, Thomson IR, Vletter WB, Brommersma P, Bom N, Linker DT. Multiplane transesophageal echocardiography: latest evolution in an imaging revolution. J Am Soc Echocardiogr 1992;5:361-7.

14. Bland JM, Altman DG. Statistical methods for assessing agreement between two methods of clinical measurement. Lancet 1986;1:307-10.

15. Gorlin R, Gorlin S. Hydraulic formula for calculation of the area of the stenotic mitral valve, other cardiac valves and central circulatory shunts. Am Heart J 1951;41:1-45.

16. Cannon SR, Richards KL, Crawford M. Hydraulic estimation of stenotic orifice area: a correction of the Gorlin formula. Circulation 1985;71:1170-8.

17. Foster GP, Weissman NJ, Picard MH, Fitzpatrick PJ, Shubrooks Jr. SJ, Zarich SW. Determination of aortic valve area in valvular aortic stenosis by direct measurement using intracardiac echocardiography: a comparison with the Gorlin and continuity equations. J Am Coll Cardiol 1996;27:392-8.

18. Jiang L, de Prada JAV, Lee MY, He J, Padial LR, Fallon JT et al. Quantitative assessment of stenotic aortic valve area by using intracardiac echocardiography: in vitro validation and initial in vivo illustration. Am Heart J 1996;132:137-44.

19. Akasaka T, Yamamuro A, Morioka S. Noninvasive assessment of aortic valve area in patients with valvular aortic stenosis using planimetry by transthoracic two-dimensional echocardiographic approach. Circulation 1996;94 (Suppl. I):I-616.

20. Stoddard MF, Hammons RT, Longaker RA. Doppler transesophageal echocardiographic determination of aortic valve area in adults with aortic stenosis. Am Heart J 1996;132:337-42.

21. Kim KS, Maxted W, Nanda NC, Coggins K, Roychoudhry D, Espinal M et al. Comparison in multiplane and biplane transesophageal echocardiography in the assessment of aortic stenosis. Am J Cardiol 1997;79:436-41.

22. Schwartz SL, Cao QL, Azevedo J, Pandian NG. Simulation of intraoperative visualization of cardiac structures and study of dynamic surgical anatomy with real-time three-dimensional echocardiography. Am J Cardiol 1994;73:501-7.

23. Belohlavek M, Foley DA, Seward JB, Greenleaf JF. Diagnostic performance of two-dimensional versus three-dimensional transesophageal echocardiographic images of selected pathologies evaluated by receiver operating characteristic analysis. Echocardiography 1994;11:635-45.

24. Kasprzak JD, Salustri A, Roelandt JRTC, Ten Cate FJ. Comprehensive analysis of aortic valve vegetation with anyplane, paraplane and three-dimensional echocardiography. Eur Heart J 1996;17:317-8.

25. Hsu TL, Ho SJ, Lai ST, Yu TJ, Chang Y, Shih CC et al. Enhanced diagnostic accuracy of aortic and mitral valvular perforation by three-dimensional echocardiography. J Am Coll Cardiol 1997;29:173A.

26. Menzel T, Mohr-Kahaly S, Koelsch B, Kupferwasser I, Kopp H, Spiecker M, et al. Quantitative assessment of aortic stenosis by three-dimensional echocardiography. J Am Soc Echocardiogr 1997;10:215-23.

27. Ge S, Warner JG, Abraham TP, Kon ND, Brooker RF, Nomeir AM et al. Three-dimensional transesophageal echocardiography for determining aortic valve area in valvular aortic stenosis: a prospective clinical study. J Am Coll Cardiol 1997;29:Suppl. A:4A.

28. Srivastava S, Kanoija A, Mittal S, Kasliwal R, Bapna R, Trehan N et al. How accurate is three-dimensional echocardiographic determination of aortic valve area in patients with aortic stenosis? - comparison with direct anatomic aortic valve area measurement at surgery. J Am Coll Cardiol 1997;29(Suppl. A):173A.

CHAPTER 10

CONCLUSIONS

The studies presented in this thesis were designed to assess the feasibility and the accuracy of 3D echocardiography in the assessment of the most frequently occurring congenital cardiac anomalies undergoing cardiac surgery. From our results we conclude that 3D echocardiography offers advantages and *potentially* increases the diagnostic assessment in congenital heart disease.

First of all 3D echocardiography gives a realistic representation of the different cardiac anomalies and renders in one single view the anatomy of the lesions and their spatial relationships.

3D echocardiography is able to visualise a lesion from any point of view. It can reproduce the surgical perspective and furthermore create a multitude of views with the potential to add more information.

3D echocardiography is also an accurate and reproducible quantitative technique enabling to measure the true dimensions of a lesion, without the need of geometrical assumptions.

3D echocardiography in the assessment of the atrial septal defect

3D echocardiography has the advantage to create an *"en face"* image of the interatrial septum. The atrial septal defect is a distinct entity, which varies in shape and extension in the septum and has a more complex anatomy on the right side. 3D echocardiography creates images of the secundum atrial defect with good anatomical accuracy and in 9% of our population it gives additional information in comparison with 2D echocardiography.

Moreover, 3D echocardiography allows to measure the area and both the antero-posterior and the infero-superior diameters of the atrial septal defect in one single image with good intra- and interobserver variability.

It appears that the secundum atrial septal defect is a dynamic 3D structure, which is relevant when closure of the defect with a catheter-based technique is considered. 30-40% of patients with a secundum atrial septal defect are candidates for catheter closure.

An adequate image quality for qualitative and quantitative analysis of the atrial septum defect is obtained using up to 8 degrees rotational interval. This implies a shorter acquisition time and reduces motion artefacts, which is important for using 3D echocardiography during the catheter-based device closure procedure.

3D echocardiography in the assessment of ventricular septal defects

3D echocardiography provides an accurate view on the anatomy of the VSD when visualised from a right ventricular perspective. The location, size and spatial relation of the common VSDs are adequately identified. Moreover, 3D reconstruction gives additional information in 21% of the patients. The agreement on anatomy between 3D reconstructions and intraoperative findings is good in all patients. The *"en face"* view of the VSD allows to measure the diameters of the defect with a good intra- and interobserver variability.

3D echocardiography in the quantification of Right Ventricular Volume

In this study we demonstrate that transthoracic 3D acquisition and reconstruction of the right ventricle are feasible. The right ventricle of patients with different conditions and malformations are acquired using transthoracic approach.

3D measurements of right ventricular volume and function are accurate and reproducible. Paraplane and omniplane methods have comparable measurement accuracy and are more reproducible in comparison to the biplane approach for volume calculation.

3D echocardiography in the assessment of obstructive lesions of the right and left ventricular outflow tract

3D reconstruction of both left and right ventricular outflow tract, at any level, is feasible, either by the transthoracic as well as by the transesophageal approach, and may offer advantages by providing more realistic information with depth perception.

3D echocardiography can display the shape, the extent, and the anatomical nature of obstruction at subvalvular level. Volume-rendered reconstructions of subaortic obstruction turn out to be more informative than those at subpulmonary level.

3D echocardiography gives a good delineation of the aortic and pulmonary valves anatomy, on the number of cusps, on their anomalies and on their motion pattern. For the first time, horizontal cross-sections of pulmonary valves are represented.

The analysis of supravalvular anomalies is also feasible. However, imaging of lesions at suprapulmonary level is limited at the first 2-3 cm, due to scarce lateral resolution and limited acoustic window.

Furthermore, 3D echocardiography allows the measurement of the degree and extension of obstruction at subvalvular level, which gives a better characterisation of the anomaly. Parallel scanning throughout the valve level allows the measurement of both aortic and pulmonary valve annulus.

3D echocardiography in the assessment of tetralogy of Fallot

3D echocardiography can be used for the analysis of more complex anomalies such as tetralogy of Fallot. It enables to assess the most important features of this entity.

3D imaging of the right sided surface of the ventricular septal defect allows to identify all the margins and consequently to categorise the defect and to assess the anatomy with regard to the conduction system.

The obstruction of the right ventricular outflow tract can be displayed at any level. Its nature, extension and the degree of the narrowing is evaluated on horizontal cross-sections, the pulmonary valves are visualised in their short-axis and the pulmonary trunk can be followed over a limited distance.

The degree of overriding of the aorta is displayed and estimated in the same way as in the intraoperative exposure. However, reconstruction of the coronary arteries was not successful most probably due to limitations in resolution of the 3D data sets.

LIMITATIONS AND FUTURE DIRECTIONS

Despite the accuracy and the advantages in the representation of simple as well more complex congenital heart disease, the actual 3D echocardiographic technique has some limitations, which currently constrain a widespread and routinely use in the clinical setting.

The acquisition of the data set is relatively long. It requires 3 to 5 minutes per rotation, depending on the respiratory and cardiac frequency triggering, in addition to the time needed for the routine 2D echocardiography. The patient should not move during the procedure, in order to avoid artefacts. The latter is difficult to obtain in children especially when very small. Therefore sedation of the young patients is obligatory.

Processing and reconstruction are still off-line procedures and require a special 3D workstation. The time needed to process and reconstruct 3D images is considered one of the major limitations of the technique. However, in the last years new software versions have appeared in which the time requested for processing has diminished from 30-40 to 5-10 minutes regardless of the size of the 3D data set. Also the final creation of 3D images, so called *volume rendered* images, has become faster. The effective time for displaying such image has been reduced from 5 to less than 1 minute.

In addition, profound knowledge of normal and pathological anatomy and a possibly long learning curve are indispensable for correct orientation, reconstruction and final interpretation of the images.

Drawbacks present on 2D echocardiography will persist and sometimes be enhanced in the 3D reconstructions. Resolution decreases during transfer of the original ultrasound data from the 2D equipment to the 3D-acquisition system as a result of the resampling and segmentation process. This is especially true for thin structures such as the Eustachian valve and the Chiari network or a fenestrated valvula foramina ovalis. These structures are sometimes lost also due to their fast motion. The resolution is also differently distributed in the 3D dataset. Furthermore the location of a defect may hamper to include the region of interest in the conical dataset.

The awareness of these limitations is important for the correct interpretation of the images in order to avoid diagnostic mistakes.

In the last few years further technical improvement has rapidly occurred. 3D acquisition procedure can now be performed with special programs implemented in the routinely used 2D echocardiographic equipment. Special ultrasound probes with incorporated miniaturised rotational motor for both transthoracic and transesophageal 3D data acquisition

have been developed. In this way mechanical problems due to the external motor which was interfacing the probe and the computer acquisition system are avoided. The new transthoracic probe has also become more user friendly and allows to receive images from any window with much more freedom in angulating the probe position. The use on the chest of very small babies looks "less traumatic".

Acquisition of Color-Doppler imaging has also become a reality, however further technical improvement and clinical studies to define its role are necessary.

CHAPTER 11

SUMMARY

Chapter 1 provides an introduction to the thesis. The clinical and scientific background, the methodology and an outline of the thesis are brought to attention.

Chapter 2 gives an overview of the potential application of 3D echocardiography in different congenital anomalies. The various anomalies are presented following the sequential approach and their 3D aspects are described.

Chapter 3 is an evaluation of the diagnostic relevance of 3D echocardiography in the assessment of secundum atrial septum defect. Qualitative and quantitative characteristics were analyzed and compared with surgical findings. Intra- and interobserver variability was assessed. 3D reconstruction of the secundum atrial septum defect was feasible in all the acquired data sets. The gross anatomy of the atrial septum defect was confirmed by the intraoperative findings in 91% of the cases. However the presence of membranous or fenestrated remnants of the valvula foramina ovalis in the defect was not optimally visualised in 30% of the reconstructed septal defects. 3D echocardiography could provide additional information in comparison with 2D echocardiography in 9% of the patients. Regarding the location of the septal defect anatomical agreement lacked in 9% of the cases. On 3D echocardiography the relation of the septal defect with the tricuspid valve could be assessed in 91% of the patients, with the superior caval vein in 61%, with the inferior caval vein in 4% and with the coronary sinus in 52% of the patients.

Both the antero-posterior and the supero-inferior diameters were measured with good intra-
(r=0.95, r=0.92) and interobserver (r= 0.96, r=0.94) variability. Moreover, 3D images
displayed in motion showed that throughout the cardiac cycle there was a reduction in size of
both diameters of about 30%.

Chapter 4 is an evaluation of the largest rotational acquisition interval able to assess
rapidly and accurately the morphology and the dimensions of secundum atrial septum defect.
Patients with a secundum atrium defect underwent 3D echocardiography acquisition with 2°
rotational interval. The images were processed to result in data sets containing images at 2°,
4°, 8° and 16° intervals by excluding interadjacent images. Volume-rendered "*en face*" views
of atrial septal defects were created and their morphological aspects as their area and
diameters were measured, by 2 independent observers. Volume-rendered secundum atrium
septum defect "*en face*" views obtained from 3D data sets with original images up to 8°
rotational intervals were of adequate qualitative and quantitative quality. The interobserver
variability was close with original images at 2°, 4°, 8° intervals than with 16°. The use of 8°
rotational interval for the acquisition of secundum atrium septal defect diminishes the
acquisition time from 5 to 1 minutes. In this way the acquisition artefacts can be avoided and
also the processing and reconstruction time can be faster.

Chapter 5 defines the clinical utility of 3D echocardiography in the assessment of
ventricular septal defects. It evaluates whether 3D echocardiography can accurately identify
and characterise, in patients undergoing surgery, the morphology of the ventricular septal
defect and assess its geometry and size. The results were compared with 2D
echocardiography and with the intraoperative findings. There was a complete agreement on

morphology of the ventricular septal defect between 2D and 3D echocardiography. 3D reconstructions were of additional value compared with 2D echocardiography in 21% of the patients. The agreement on anatomy between 3D reconstructions and intra-operative findings was complete in all patients. Both antero-posterior and supero-inferior diameters of the ventricular septal defects could be measured with a good intra- (r=0.9, r=0.7) and interobserver (r=0.9, r=0.9) variability. When the antero-posterior diameter measured on 3D echocardiography was compared with those measured on 2D echocardiography the correlation was modest (r=0.6).

Chapter 6 evaluates the feasibility of right ventricular volume measurements by 3D echocardiography. Three different methods (biplane modified Simpson, omniplane and Simpson's methods) were applied and the results were compared with magnetic resonance as the reference method. Finally there were no significant differences between measurement of right ventricular volumes and ejection fraction obtained from magnetic resonance and from 3D echocardiography. However, closer limits of agreement were found between magnetic resonance measurements and both 3D Simpson's and omniplane methods for end-diastolic and end-systolic right ventricular volume and ejection fraction respectively. Intraobserver and interobserver variability was good (r=0.90 and 0.99 respectively). Paraplane (or Simpson's method) and omniplane analysis provides more accurate and reproducible measurements of the right ventricular volume and ejection fraction than the biplane modified Simpson method.

Chapter 7 is a comprehensive assessment with 3D echocardiography of the left and right ventricular outflow tracts at all levels. 3D reconstructions were suitable for analysis in 100% of subvalvular- and supravalvular obstruction and in 77% valvular obstructions of the

left ventricular outflow tract. 3D reconstructions were suitable for analysis in 100% of sub-valvular obstruction of the right ventricular outflow tract and in 50% of the valvular and supravalvular level. Volume-rendering reconstructions were compared with surgical findings and anatomical accuracy was ranging between 90 to 100%. Using 2D computer-generated images extension and degree of subvalvular obstructions was determined.

Chapter 8 is an assessment with 3D dimensional echocardiography of the most important features of tetralogy of Fallot. The ventricular septal defects were spatially located and could be classified as perimembraneus type. The anatomical accuracy was confirmed in all cases. From computer-generated short-axis view could be defined the degree of overriding of the aorta, which was between 15 and 95%. Visualisation of the coronary arteries was difficult: the left coronary artery could be visualised only in 13% of the patients, while the right coronary artery could not be seen at all.

Adequate reconstruction of the right ventricular outflow tract at subvalvular and valvular level could be obtained in around 90% of the patients with good anatomical accuracy when compared with intraoperative findings. Using modified computer-generated cross-sections the mean smallest area of obstruction could be measured (0.7 cm^2). The pulmonary area was reconstructed in 81% of the cases. The number of leaflets could be determined in 89% and their anatomical accuracy was of 100%. The pulmonary trunk could be imaged for maximally 2-3 cm in 10% of the cases.

Chapter 9 is a study designed to determine the feasibility of 3D echocardiographic aortic valve area planimetry and to evaluate potential errors resulting from suboptimal imaging plane position. Orifice area was similar in 2D and in 3D studies. The limits of

agreement are close and their correlation is high (r=0.98). Significant overestimation was observed with cut-planes angulation by 10 to 30 degrees or parallel shift by 1.5 to 7.5 mm. Three-dimensional echocardiographic measurement variability was very low (coefficient of variation: intraobserver 3.9%, interobserver 5.3%) and compared favourable against that of two-dimensional echocardiography (coefficient of variation: intraobserver 4.8%, interobserver 10%).

Chapter 10 provides the conclusions of the project. The limitations and the future directions of 3D echocardiography are discussed.

SAMENVATTING

Hoofdstuk 1 geeft een introductie van het proefschrift. De klinische en wetenschappelijke achtergronden en de methodologie worden besproken en een kort overzicht wordt gegeven.

Hoofdstuk 2 geeft een algemeen overzicht over de potentiële toepassing van 3D echocardiografie in verschillende aangeboren afwijkingen. De verschillende afwijkingen zijn geanalyseerd volgens de sequentiële benadering en hun 3D aspecten zijn beschreven.

Hoofdstuk 3 is een evaluatie van de diagnostische rol van 3D echocardiografie in het onderzoek van het secundum atrium septum defect. Kwalitatieve en kwantitatieve kenmerken worden geanalyseerd en vergeleken met de intraoperatieve bevindingen. "Intra- en interobserver" variabiliteit worden ook onderzocht. 3D reconstructie van het secundum atrium septum defect was mogelijk in alle opgenomen data sets. De anatomie van het secundum atrium septum defect werd intraoperatief bevestigd bij 91% van de patiënten. Het bestaan van membraneuze of gefenestreerde resten van de valvula foramina ovalis in het defect kon echter niet goed vastgesteld worden bij 30% van de gereconstrueerde defecten. 3D echocardiografie kon bij 9% van de patiënten extra informatie geven in vergelijking met 2D echocardiografie. De locatie van het defect kon bij 9% van de patiënten niet volledig juist gediagnostiseerd worden. Met 3D echocardiografie kon de relatie met de tricuspidalis klep bevestigd worden bij 91% van de patiënten, met de vena cava superior bij 61%, met de vena cava inferior bij 4% en met de sinus coronarius bij 52% van de patiënten.

Zowel de antero-posterior als de supero-inferior diameter konden worden gemeten met een goede "intra-" (r=0.95, r=0.92) en "interobserver" (r=0.96, r=0.94) variabiliteit.

De dynamische 3D beelden tonen aan dat tijdens de hart cyclus er een vermindering van 30% van de defect grootte optreedt.

Hoofdstuk 4 bepaalt welke de grootste rotatie interval is, dat toch nog een nauwkeurige reconstructie van het secundum atrium septum defect mogelijk maakt.

Patiënten met een secundum atrium septum defect ondergingen een 3D echocardiografisch onderzoek met een rotatie interval van 2°. Tijdens het verwerken van de data zijn data sets gecreëerd met beelden op 2°, 4°, 8° en 16° afstand door de tussenliggende data weg te laten. *"En face"* beelden van het atrium septum defect werden gecreëerd en zowel morfologische aspecten als oppervlak en diameters werden beoordeeld door twee onderzoekers. Reconstructie van het atrium septum defect in data sets met beelden tot 8° rotatie intervallen waren geschikt voor morfologische en voor kwantitatieve metingen. De "interobserver" variabiliteit was kleiner met 2°, 4° en 8° beelden dan met 16°. Met het gebruiken van maximaal 8° rotatie intervallen voor de acquisitie van een atrium septum defect werd de acquisitie tijd van 5 minuten naar 1 minuut verminderd. Op deze manier kunnen acquisitie artefacten worden vermeden en ook de bewerking en de reconstructie tijd worden versneld.

Hoofdstuk 5 beschrijft de preoperatieve diagnostische bruikbaarheid van 3D echocardiografie in het onderzoek van ventrikel septum defecten. Het evalueert of 3D echocardiografie in patiënten die een chirurgische correctie ondergaan, met nauwkeurigheid de morfologie van het ventrikel septum defect kan beschrijven en zijn diameters meten. De resultaten werden vergeleken met 2D echocardiografie en met de intraoperatieve

bevindingen. Er was een goede overeenkomst in morfologie tussen 2D en 3D echocardiografie. 3D reconstructie was van extra waarde vergeleken met 2D echocardiografie in 21% van de patiënten. De anatomische overeenkomst tussen 3D echocardiografie en de intraoperatieve bevindingen was 100%. Zowel de antero-posterior als de supero-inferior diameter van het ventrikel septum defect waren goed te meten met een goede "intra-" (r=0.9, r=0.7) en "interobserver" (r=0.9, r=0.9) variabiliteit. De correlatie van de gemeten antero-posterior diameter tussen 3D en 2D echocardiografie was matig (r=0.6).

Hoofdstuk 6 onderzoekt de geschiktheid van 3D echocardiografie voor metingen van het volume van de rechter ventrikel. Drie verschillende methoden (biplane modified Simpson, omniplane and Simpson's methode) werden gebruikt en de resultaten zijn vergeleken met magnetische resonantie als referentie methode. Uiteindelijk was er geen verschil tussen metingen van het rechter ventrikel volume en de ejectie fractie wanneer magnetische resonantie met 3D echocardiografie werd vergeleken. Een betere overeenkomst van eind-diastolisch en eind-systolisch rechter ventrikel volume en ejectie fractie werden gevonden tussen magnetische resonantie en zowel 3D Simpson's als de omniplane methode. "Intra- en interobserver" variabiliteit waren goed (r=0.90 en 0.99, respectievelijk). Paraplane (of Simpson's methode) en omniplane analyse geven een meer nauwkeurige en beter reproduceerbare meting van het rechter ventrikel volume dan de biplane modified Simpson's methode.

Hoofdstuk 7 geeft een overzicht van de toepassing van 3D echocardiografie in het onderzoek van de uitstroombaan van de linker en rechter ventrikel. 3D reconstructie was geschikt voor analyse bij 100% van de obstructies onder en boven het niveau van de klep en

bij 77% van de valvulaire vernauwingen van de linker ventrikel uitstroombaan. 3D

reconstructie was geschikt voor analyse bij 100% van de obstructie van de rechter ventrikel

uitstroombaan en bij 50% op niveau van de pulmonaal klep en boven de klep. Reconstructie

werd vergeleken met de chirurgische bevindingen en de anatomische nauwkeurigheid was

tussen 90 en 100%. De lengte in de stenose en de mate van obstructie werden gemeten.

Hoofdstuk 8 beschrijft de belangrijkste kenmerken van de tetralogie van Fallot

onderzocht met 3D echocardiografie. Het ventrikel septum defect werd gelokaliseerd en kon

als perimembraneus geclassificeerd worden met een nauwkeurigheid van 100%. Door middel

van de "computer-generated" korte as was het mogelijk de graad van "overriding" van de

aorta te meten. De data sets waren onvoldoende om de kransslagaders in beeld te brengen. De

linker kransslagader werd gezien bij 13% van de patiënten, terwijl de rechter kransslagader

niet gezien werd.

Reconstructie van de rechter ventrikel uitstroombaan op het subvalvulaire en valvulaire

niveau was geschikt bij 90% van de patiënten met goede anatomische nauwkeurigheid. Met

gebruik van gemodificeerde "computer-generated" doorsnedes werd het kleinste oppervlak

van de obstructie gemeten (0.7 cm^2). De oppervlak van de pulmonaal klep kon bij 81%

gereconstrueerd worden. Bij 89% van de kleppen was het mogelijk het aantal klep bladen te

zien, met een 100% van nauwkeurigheid. De pulmonaal takken werden in beeld gekregen bij

slechts 10% van de patiënten.

Hoofdstuk 9 onderzocht de geschiktheid van 3D echocardiografie bij het meten van

het aorta klep oppervlak en de mogelijke fouten die kunnen optreden met een niet optimale

positie van het beeld. Het oppervlak van de aorta klep opening was gelijk in 2D en 3D

onderzoeken. De mate van overeenstemming is groot en hun correlatie is hoog (r=0.98). Een overschatting werd geobserveerd bij een "doorsnij hoek" van 10 tot 30 graden of bij een parallel verschuiving van 1.5 tot 7.5 mm.

De variabiliteit van de 3D echocardiografische metingen was zeer laag ("intraobserver" variabiliteit = 3.9%, "interobserver" variabiliteit = 5.3%) en was beter in vergelijking met 2D echocardiografie ("intraobserver" variabiliteit = 4.8%, "interobserver" variabiliteit = 10%).

Hoofdstuk 10 beschrijft de conclusies van het verrichte onderzoek. De huidige beperkingen en de toekomst van 3D echocardiografie zijn besproken.

ACKNOWLEDGMENT

My staying at the Thoraxcenter and the preparation of this thesis have been an important step of my life. It has been for me a new, exciting, and sometimes unpredictable, journey in the field of experimental research in one of the new branches of cardiology. Not only this, but it has also been an incomparable, rich experience in my personal development as a young woman with regard to my career and being abroad.

First of all, I would like to thank Prof. AJJC Bogers, today here as my Promotor. I thank him for finding me a position as researcher at the Erasmus Medical Faculty, which allowed me to stay in the Netherlands and to continue the research after the preliminary studies. Since the very beginning he demonstrated interest and curiosity for this new technique and its potential application in the operative field. His expertise in cardiac anatomy and spatial orientation was very helpful for the progress of the research, especially in the early beginning when we were struggling trying to understand "something or anything". He did not only closely followed the progress of the studies, but he also helped in the review of all my articles, in solving problems and sustaining motivation despite the many technical and organising problems which we were encountering. Although man of few words, he was there to encourage me during my deepest moments. Thank you!

Second, but not less important, I would like to show my appreciation to Prof. JRTC Roelandt, also my Promotor. His interest in 3D echocardiography and his futuristic ideas stimulated my research. I thank him for allowing me to be guest in the laboratory of Echocardiography and for his special final touch in the correction of the manuscripts. I could find in him not only the scientist but also a man with broad culture.

I am particularly grateful to Mrs. Jackie McGhie, echocardiographist specialised in congenital heart disease. Together, we started this experience and shared dreams and nightmares. Her scottish humour was keeping us alive during the long hours in front of the monitor trying to understand these new images. How big was our disappointment when by loading our best reconstruction the computer was suddenly crashing and all the work had to

for research; Dr. LA Van Herwerden, thoracic surgeon, with whom I had the pleasure to write my first article.

I would like to thank for their co-operation all the technicians of the Echocardiography Laboratory (Veronica, Mike, Susan, Elly, Marion, Debby); the anaesthetists, nurses and perfusionists of the operation rooms and the secretaries of the Department of Thoraxsurgery (Saskia, Ria, Annette, Ria, Jacqueline, Marijke) who always welcome me and made me feel comfortable.

I won't forget Rene Frowijn, computer technician in the Echocardiography Laboratory, from whom I got always help and advise in the use of the computer programs and on whom I could rely in the last minutes, while preparing a presentation or a poster. He also demonstrated to be a good friend.

During my fellowship I had the opportunity to know a lot of colleagues from all over the world, with the same dreams and the same courage. It has been for me a unique experience to know them and have the opportunity to share my ideas and my time with them. They include: Y. Nosir (Egypt), A. El Hendy (Egypt), Q. Chen (China), O. Franzen (Germany), Aiazian (Russia), J. Kasprzak (Poland), M. Conceiçao (Portugal), Y. Osaki (Japan), C. van Birgelen (Germany), E. Camenzin (Switzerland), C. Di Mario (Italy), A. Salustri (Italy), M.T. Mallus (Italy), A. Nicosia (Italy), R. Rambaldi (Italy), E. Fiuza (Portugal), J. Winkelman (USA), V. Lajos (Hungary), J. Yao (China), L. Koroleva (Russia), S. Carlier (Belgium), B. Paelinck (Belgium), G. Rocchi (Italy), A. Menozzi (Italy), G. Diricatti (Italy), F. Sozzi (Italy), S. Boito (Italy), J. Del Diego (Spain), E. Vourvouri (Greece), G. Sianos (Greece), J. de Sutter (Belgium), E. Regar (Germany), L. Diamantopoulos (Greece) and many others...

Finally, but not last, I'd like to thank my family and especially my mother, who always supported me in my decisions, who listened and comforted me when things were not going well. I know that she suffered a lot for my absence from home, but I hope that she will be happy for me and with me today. I would like to thank my father on whom I always could rely. And I would also like to remind my sisters (Afra and Alina), who are my best friends.

CURRICULUM VITAE

Name:	Anita Dall'Agata
Born:	18 November 1965
	Basel, Switzerland
Nationality:	Italian

Education

1979-84	Lyceum-Gymnasium "M. Flaminio" Vittorio Veneto (Treviso) – Italy
1984-91	Faculty of Medicine, Padova, Italy
1992-1996	Resident of Cardiology, Cardiology Department, Academical Hospital, Padova-Italy
5/1995-1998	Research Fellow Department of Echocardiography, Thoraxcentrum, Erasmus Medical Center, Rotterdam (NL)
1999-2000	Clinical Fellow Department of Cardiology, Thoraxcentrum, Erasmus Medical Center, Rotterdam (NL)

Memberships

1996	Working Group of the European Society of Cardiology in Grown-up Congenital Heart Disease
1997	Working group of the European Society of Echocardiography in Three-dimensional Echocardiography
5/1999	Dutch registration as Cardiologist

PUBLICATION LIST and LECTURES

Manuscripts and book chapters

1. Casiglia, MS. Baccillieri, G. Bergamo, A. Camarotto, G. Colangeli, **A. Dall'Agata**, C. Daskalakis, I. El Asmar, A. Incognito, G. Maniati, L. Mario, M. Michieletto, L. Pavan, A. Pasinato, S. Petucco, A. Sapontzakis, D. Terranova, E. Zugno. *Ritmo circadiano delle resistenze periferiche agli arti inferiori.* Cuore e Vasi 1991, 11:6

2. Razzolini, A. Ramondo, G. Isabella, F. Campisi, P. Cardaioli, MC. Marchiori, P. Ostan, D. Sarandria, **A. Dall'Agata**, G. Grassi, R. Chioin. *Variazioni emodinamiche acute in corso di valvuloplastica mitralica.* in Cardiomiopatia Ipertrofica, Riunione Triveneta di Cardiologia, Rovigo 7 Nov 1992

3. Palatini, G. Scannavacca, S. Bongiovi', **A. Dall'Agata**, G. Maraglino, P. Mormino, AC. Pessina. *Prognostic significance of ventricular extrasystoles in healthy professional athletes: result of a 5-year follow-up.* Cardiology 1993;82:286-293

4. R Rambaldi, A˙ **Dall'Agata**, M Gellijnse, PM Fioretti. *Stratificazione del rischio nell'Angina Instabile.* In Atti Cardiologici, Settembre 1996

5. **Dall'Agata**, MA Taams, PM Fioretti, JRCT Roelandt, LA Van Herwerden. *Cosgrove-Edwards mitral ring dynamics using transesophageal three-dimensional echocardiography.* Ann Thorac Surg. J 1998;65:485-90

6. JD Kasprzak, YFM Nosir, **A. Dall'Agata**, A Elhendy, M Taams, FJ Ten Cate, JRTC Roelandt. *Quantification of the aortic valve area in three-dimensional echocardiographic datasets:analysis of orifice overestimation resulting from suboptimal cutplane selection.* Am Heart J 1998;135:995-1003

7. J Yao, MRHM van Sambeek, **A Dall'Agata**, LC van Dijk, M Kozakova, PJ Koudstaal, JRTC Roelandt. *Three-dimensional ultrasound study of carotid arteries before and after endarterectomy: analysis of stenotic lesion and surgical impact on the vessel.* Stroke 1998;29:2026-31

8. WRM Hermans, **A Dall' Agata**, RJ van Geuns, C Breburda, JRTC Roelandt.*Atrial myxoma.* The Thoraxcentre Journal 1998;10:24

9. **Dall'Agata**, J. Mc Ghie, MA Taams, AH Cromme-Dijkhuis, S Spitaels, CSM Breburda, JRTC Roelandt, AJJC Bogers. *The atrial septal defect is a dynamic three-dimensional entity.* Am Heart J 1999;137:1075-81

10. YFM Nosir, J Stoker, JD Kasprzak, MH Lequin, **A. Dall'Agata**, FJ Ten Cate, JRTC Roelandt. *Paraplane analysis from precordial three-dimensional echocardiographic data*

sets for rapid and accurate quantification of left ventricular volume and function: a comparison with Magnetic Resonance Imaging. Am Heart J 1999

11. J Yao, **A Dall'Agata**, Q-L Cao, JD Kasprzak, L Sugeng, NG Pandian, JRTC Roelandt. *Evaluation of abnormal masses in the cardiovascular system by three-dimensional echocardiography.* Submitted.

12. **A Dall'Agata**, AH Cromme-Dijkhuis, FJ Meiboom, JS McGhie, G. Bol-Raap, YFM Nosir, JRTC Roelandt, AJJC Bogers. *Three-dimensional echocardiography enhances the assessment of ventricular septal defect.* Am J Cardiol 1999;83:1576-9

13. **A Dall'Agata**, AH Cromme-Dijkhuis, FJ Meijboom, SEC Spitaels, JS McGhie, JRTC Roelandt, AJJC Bogers. *Use f three-dimensional echocardiography for analysis of outflow obstruction in congenital heart disease.* Am J Cardiol 1999:83:921-5

14. **Dall'Agata**, JS McGhie, F Meijboom, JRTC Roelandt, AJJC Bogers. *Preoperative assessment of Tetralogy of Fallot by three-dimensional echocardiography* Cardiovascular Engineering 2000;5:21-5

15. YFM Nosir, MH Lequin, **A Dall'Agata**, JD Kasprzak, JRTC Roelandt. *Biplane, Omniplane and Paraplane echocardiographic analysis for accurate right ventricular volume measurement: a comparison with Magnetic Resonance Imaging.* Submitted

16. **A Dall'Agata**, JRTC Roelandt, AJJC Bogers. *Congenital heart disease.* In: JRTC Roelandt. Three-dimensional echocardiography of the heart and the coronary arteries. Van Zuiden Communications BV, Alphen aan de Rijn, 153-69

17. **A Dall'Agata**, JRTC Roelandt. *Miscellaneous conditions.* In: JRTC Roelandt. Three-dimensional echocardiography of the heart and the coronary arteries. Van Zuiden Communications BV, Alphen aan de Rijn, 171-8

18. YFM Nosir, **A Dall'Agata**, RT van Domburg, AJJC Bogers, JRTC Roelandt. Three-dimensional echocardiographic acquisition at 8 degree rotational intervals adequate morphological and accurate quantitative assessment of atrial septal defects. Submitted

19. GP Kimman, DAMJ Theuns, P Vantrimpont, **A Dall' Agata**, LJLM Jordaens. Een aanhoudende linker kamer tachycardie en een gedilateerde cardiomyopathie: een kwestie van de kip of het ei?. Submitted

20. Eleni C Vourvouri, Johan De Sutter, Don Poldermans, Paolo Izzo, **Anita Dall' Agata**, Fabiola Sozzi, Georgios Parcharides, Georgios Louridas, Jos RTC Roelandt. *Experience with an ultrasound stethoscope.* Submitted

21. **A Dall'Agata**, P Vranckx, J De Sutter, EC Vourvouri, JRTC Roelandt. *Focused echocardiography with a new portable system in acute coronary setting.* Submitted.

...and various abstracts at international meetings.

Invited lecturer in:

1. How to use three-dimensional echocardiography. In *How to do Session*, 4th Alpe Adria Cardiology Meeting, Grado (Italy), May 1996

2. Motion and shape of annuloplasty mitral rings: three-dimensional echocardiographic study. In *New choices in mitral and tricuspid valve repair*, Bruxells (Belgium), September 1996

3. Ecocardiografia tridimensionale: passato, presente e futuro. In *Giornata del Dipartimento*, Padova (Italy), March 2000

...and at various local meetings.